(NASA-CR-114701) PRELIMINARY DESIGN REPORT, LARGE SPACE TELESCOPE OTA/SI PHASE B STUDY: HIGH SPEED AREA PHOTOMETER (Martin Marietta Corp.) 159 p HC $6.75 CSCL 20F

N76-14991

Unclas
G3/89 07173

Itek Subcontract
PO 8237-A-0003
MCR-75-298

Preliminary
Design
Report

15 August 1975

Large Space Telescope OTA/SI Phase B Study

High Speed Area Photometer

MARTIN MARIETTA

NATIONAL AERONAUTICS AND SPACE ADMINISTRATION
GODDARD SPACE FLIGHT CENTER
GREENBELT, MARYLAND 20771

2 December 1975

PREAMBLE

The following report was generated by the Martin Marietta Corporation, Denver Division, acting as a subcontractor to the Itek Corporation, which was a prime Phase B contractor on the Large Space Telescope (LST) project.

During the Phase B study period, the number of instrument concepts investigated exceeded the number of instruments that could be accomodated in the first payload on the LST. In July of 1975 it was decided on the basis of various arguments that a High Speed Area Photometer (HSAP) should not be considered as a candidate instrument for the first launch. The consequence of this decision was to terminate work on the conceptual design of the HSAP, with the exception that a preliminary design report should be forwarded as was required for all the instruments under study. Therefore, this discussion presents only the results of a truncated investigation. However, a review of this report convinced us that even though it describes a constrained result and one that could be improved, it is a report of superior merit. Therefore, as the report advances a thoughtful design discussion of a generic type of spaceborne instrumentation that could perform vital astronomical observations, we decided it would be a benefit if the report were released for public distribution.

George M. Levin
LST Study Manager

DRAFT

PRELIMINARY DESIGN REPORT
LARGE SPACE TELESCOPE OTA/SI PHASE B STUDY

HIGH SPEED AREA PHOTOMETER

15 AUGUST 1975

MARTIN MARIETTA CORPORATION
DENVER DIVISION
DENVER, COLORADO

FOREWORD

This document is submitted in accordance with the requirements of Exhibit A, Paragraph 4.6.4.3 (Delivery) of Contract Statement of Work - Contract 8237-A-0003.

TABLE OF CONTENTS

LIST OF FIGURES

LIST OF FIGURES (Continued)

LIST OF FIGURES (Concluded)

LIST OF TABLES

Abbreviations and Acronyms

ALU	Arithmetic Logic Unit
A/D	Analog-to-digital Converter
CCD	Charge Coupled Device
Cres	Corrosion resistant steel
C&DH	Command and Data Handling
C.G.	Center of Gravity
Dia	Diameter
DIU	Data Interface Unit
EMC	Electro-Magnetic Compatibility
FET	Field Effect Transistor
FGS	Fine Guidance System
FPA	Focal Plan Assembly
f/	f-number or focal ratio
GSE	Ground Support Equipment
ICCD	Intensified Charge Coupled Device
I/O	Input/Output
HSAP	High Speed Point/Area Photometer
LST	Large Space Telescope
Mbps	Megabits per second
mtf	modulation transfer function
N-MOS	N-channel metal oxide semiconductor
OTA	Optical Telescope Assembly
Pixel	Picture Element
pps	pulses per second
PROM	Programmable Read-Only Memory
psf	point spread function
P&CS	Pointing and Control System
RAM	Random Access Memory
SI	Scientific Instrument
SNR	Signal-to-Noise Ratio
SSE	Space Support Equipment

SSM	Support System Module
Sta	Station
ULE	Ultra Low Expansion Glass
wfe	wavefronterror
α	Thermal Coefficient of Linear Expansion
λ	Wavelength
ν	Spatial Frequency
ξ	Spatial Frequency

1.0 INTRODUCTION

The LST Photometer will have the highest sensitivity and radiometric precision of all ultraviolet and visible instruments used on the LST and will provide a vast improvement over ground based photometry. Advantages of orbital operation that can be exploited by the Photometer are accessibility of the UV wavelengths which are absorbed by the atmosphere, great reduction in the veiling effects of airglow and auroras, and freedom from spurious intensity and position modulation by inconstancies in the atmosphere.

Orbital use, in general, makes an instrument inaccessible and places it in a harsh environment. Both factors require a highly reliable and tough instrument. The use of the shuttle makes possible recovery of a malfunctioning or obsolete instrument but such recovery and replacement is expensive and does not relieve the photometer design from the necessity of meeting environmental challenges and performing well over a great length of time with no maintenance.

The Photometer basically requires only an extension of existing technology and the combination of several features from separate instruments into a single package.

The design presented here has both point and area photometry capability with provision for inserting filters to provide spectral discrimination. The electronics provide for photon counting mode for the point detectors and both photon counting and analog modes for the area detector. The area detector also serves as a target locating device for the point detectors.

The design presented here originally had provision to analyze the state of polarization. The elements to provide this have been removed from the optical train. However, if it should again be desired, the design is such that these elements could easily be included.

2.0 PERFORMANCE REQUIREMENTS

This set of performance requirements is extracted from the Final Instrument Definition, the LST Working Group Consensus Statement, various Goddard Space Flight Center contractor directives and our own work in cases where we felt out design would be expedited by generating our own working requirements.

The basic performance requirements imposed on the Photometer are as follows:

1. Wavelength coverage from 115 to 650 nm.

2. Wavelength resolution will be defined by selectable absorbing filters and/or by the intrinsic sensitivity of the detectors.

3. Fields-of-view will be selected with a set of ten apertures. The aperture set will include circles which have nominal fields-of-view corresponding to two Airy disk diameters to 128 Airy disk diameters, two long narrow slits, and one or two rectangles, and a dark "aperture".

4. Angular resolution of the aerial (light) image incident on the area detector will be nearly diffraction limited.

5. Exposure durations will be selectable from 0.1 msec to 18 ksec (5 hours).

6. Exposure durations will be controlled to better than $\pm$ 0.1%.

7. Photometric accuracy relative to standard stars will be 0.1% (goal) for point photometry and 1% (goal) for area photometry.

8. Object radiances will be measurable from magnitude 7.5 with a coincidence loss of 10% to the system noise limit.

9. Area imagery will be accomplished at either f/24 or f/96 as desired.

10. Lifetime without maintenance will be 2.5 years, probable.

There are other requirements imposed on the design of the instrument. Those are discussed in appropriate sections below.

3.0 DETAILS OF PHOTOMETER PRELIMINARY DESIGN

The material below presents our preliminary design. The design meets the requirements but a final design would need further analyses in the areas of optical design, thermal analysis, electronic circuit design and others. We have generated numerical values for design parameters wherever feasible to serve as points of departure for the final design and to facilitate performance prediction.

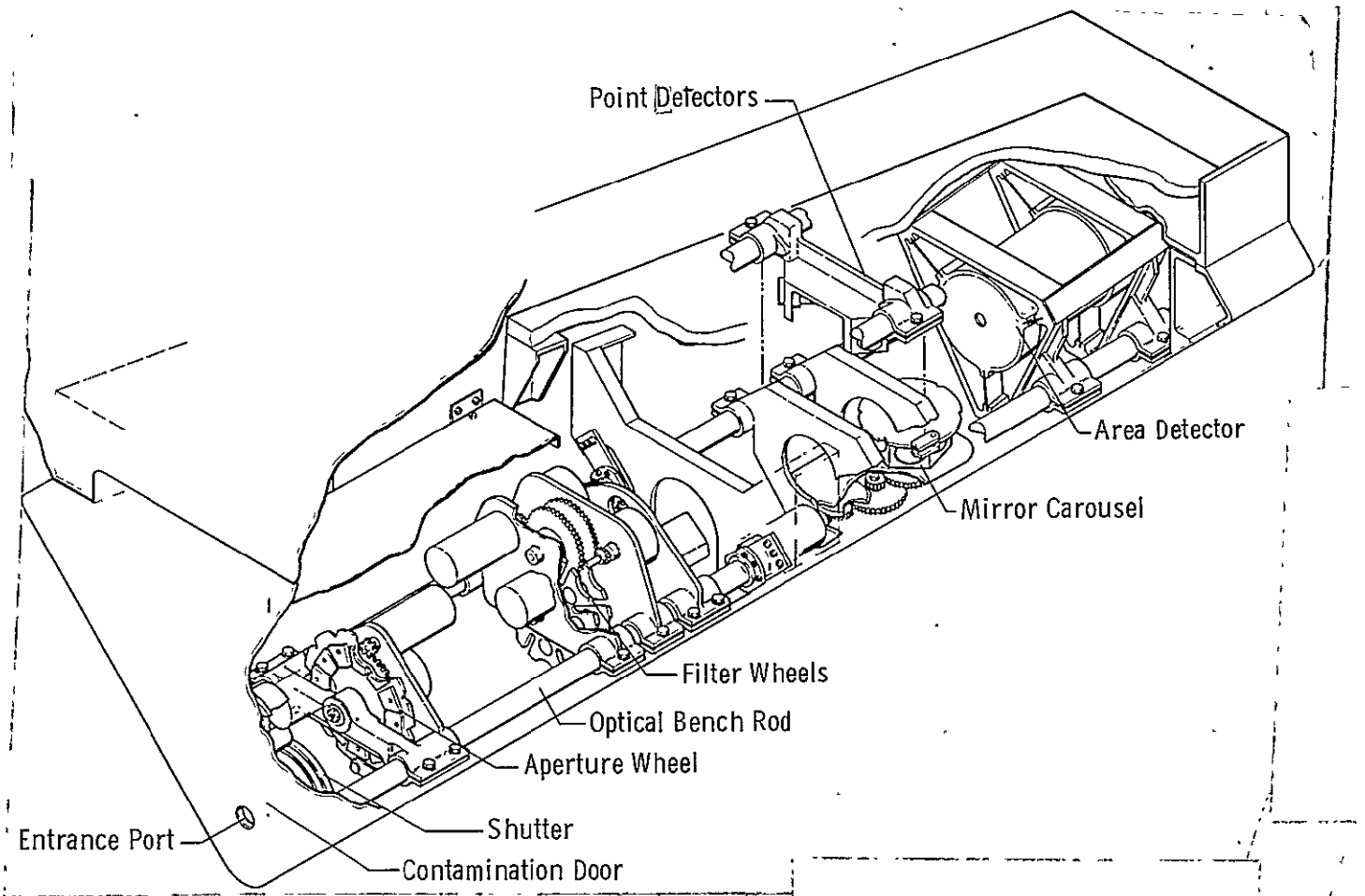

Figure 3.0-1 General Arrangement of Optical Elements and Mechanisms in the Opto-mechanical Submodule

3.1 OPTICAL SYSTEM

The optical design requirements imposed on the Photometer are that it have:

1) A set of selectable apertures used as field stops

2) A set of selectable absorptive filters used for spectral discrimination

3) A pair of internal reimaging relays used to allow images to be formed at f/24 and f/96 for area detection modes

4) Sensitivity over the wavelength range from 115 to 650 nm

5) Nearly diffraction limited images (for area detection modes)

6) The highest possible optical throughput and lowest possible stray-light for high signal-to-noise ratio

7) No single point failures that can render a substantial portion of the instrument functions unusable

8) A set of two point detectors with no imaging capability

9) The capability of applying spectral filtration with either point or area detectors.

There has been a requirement for polarization analysis as well. The requirement is not now in effect. A polarimetry feature has been the subject of preliminary design and the existing design of the Photometer can accommodate a polarimetry apparatus without major revision. Section II discusses the polarimetry option in more detail.

3.1.1 General Arrangement

The Photometer consists optically of two conventional photometers and two imaging photometers which resemble cameras. Each optical configuration has its own optics.

The original optical design approach was to use a single mirror as a Fabry mirror for the point detectors and as a primary mirror for both f/24 and f/96 relay systems. Analyses showed that the resultant optical formulas were so highly constrained that there was no hope of achieving adequate image quality for more than one configuration. Furthermore the single Fabry/relay mirror approach inevitably required point detectors with large (about 10 mm diameter) photocathodes which were expected to be intolerably noisy in the space radiation environment.

Separate Fabry mirrors were then incorporated for each of the two point detection modes and separate relay primary mirrors for each area detection magnification. The resultant deconstrained optical problem permitted solutions for each optical function while adhering to the geometric constraints.

3.1.1 (Continued)

The first optical element encountered by the light in the Photometer is a set of entrance apertures which serve as field stops to select the portion of the sky whose brightness is to be measured or which is to be imaged. There are a set of circular, slit, and rectangular apertures. The OTA image falls on the apertures. The light then diverges from focus until it encounters a set of spectral filters (or open filter wheel positions). If polarimetry were to be performed by the Photometer, the required waveplates and linear polarizer would precede the filters. Next the light strikes one of the Fabry or relay mirrors. If the mirror is a Fabry mirror the light is reflected to a point detector. An image of the telescope's exit pupil is formed on the point detector photocathode. If the mirror is either of the relay primaries the light is reflected to a secondary mirror and then to the area detector. Figures 3.1-1 and 3.1-2 show cross-sections of the opto-mechanical submodule and its contents.

The Fabry and relay mirrors are about 505 mm from the aperture wheel. The aperture wheel is about 95 mm from the front surface of the axial bay module. The entire optics assembly uses less than a meter of the approximately two meter length of the axial bay module. There does not appear to be any optical reason for using the extra volume but it is available. The optical design can accommodate at least one additional point detector by modifying only the point detector mounting assembly and by adding another Fabry mirror to a mirror carousel spare position. Similarly, there is room for growth of the area detector in both length and diameter.

One of the more serious constraints on the general optical arrangement was the need to safisfy two conflicting requirements: the need to be close to the telescope's optical axis and the need to fit optics and mechanisms into the corner of the allowed axial bay envelope. Naturally there were other constraints but packaging the opto-mechanical portion of the Photometer was the most inflexible. The closest we could place the entrance aperture to the OTA axis was 75 mm which left a little room for thermal insulation, a growth allowance, and rattle room. The mechanical design fits the available volume as closely as possible and still allows access to the interior of the instrument for alignment, checkout, installation and removal of components.

The Photometer inherently has little susceptibility to stray light because of the relatively small size of the entrance aperture. Nevertheless the inside of the Photometer will be blackened and bulkheads and other structures used to prevent propagation of stray light.

3.1.2 Transmissive Optics

The Photometer can make spectral discrimination of the incoming light in either point or imaging modes. The spectral discrimination is accomplished by placing one or two filters from the two sets available into the light path. The filters need not be in the beam but when they are in place they are between the entrance apertures and the Fabry/relay mirror set.

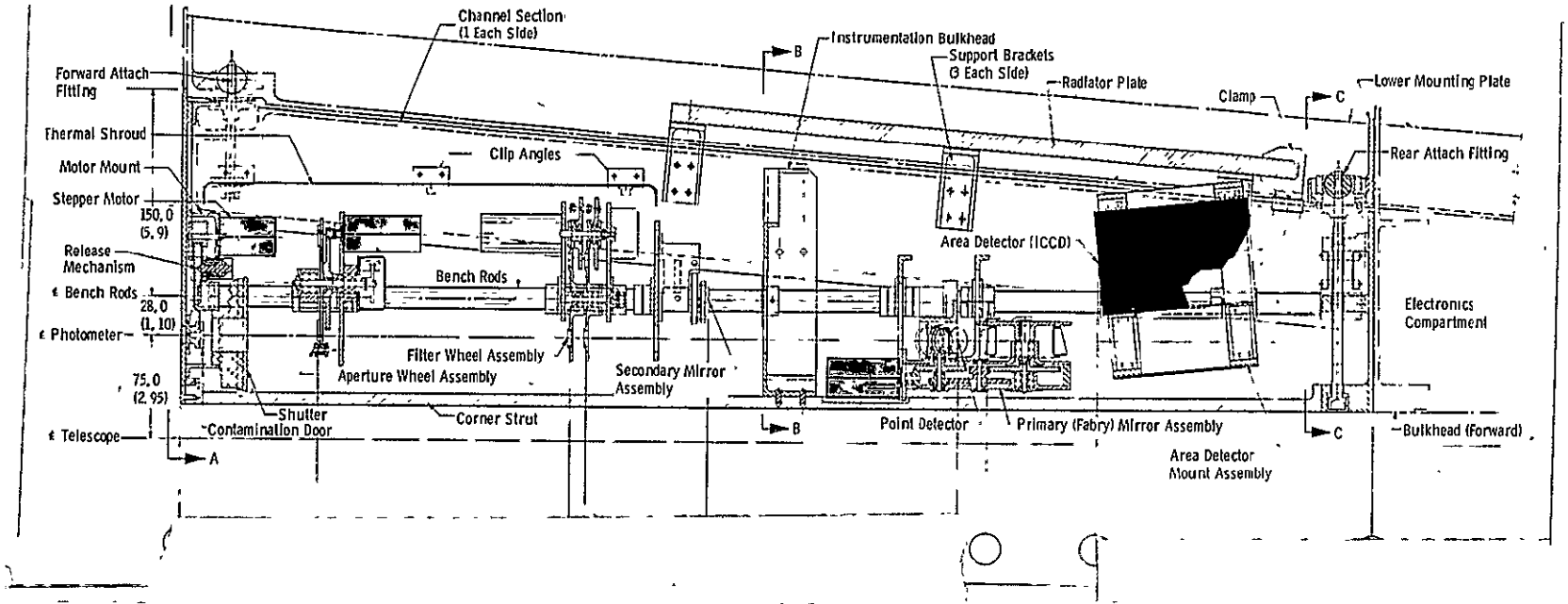

All the optical elements and their associated drive mechanisms are located in the opto-mechanical submodule. Light enters from the left through a port protected by a contamination door. The light can then be intercepted by a shutter for dark count calibrations. The image from the OTA falls on the selected aperture and then diverges again. Light passes through the two filters and is collected by either Fabry or relay mirrors on a carousel. The light beam then travels one of four possible paths: two go to point detectors and two go to small secondary mirrors. The light from either secondary mirror is imaged into the area detector. There is room between the aperture wheel assembly and the filter wheel assembly for polarization analysis optics. All components are mounted on a pair of optical bench rods which run the length of the submodule. Other explanation of the design is contained in the text.

Figure 3.1-1 Opto-mechanical Submodule Elevation

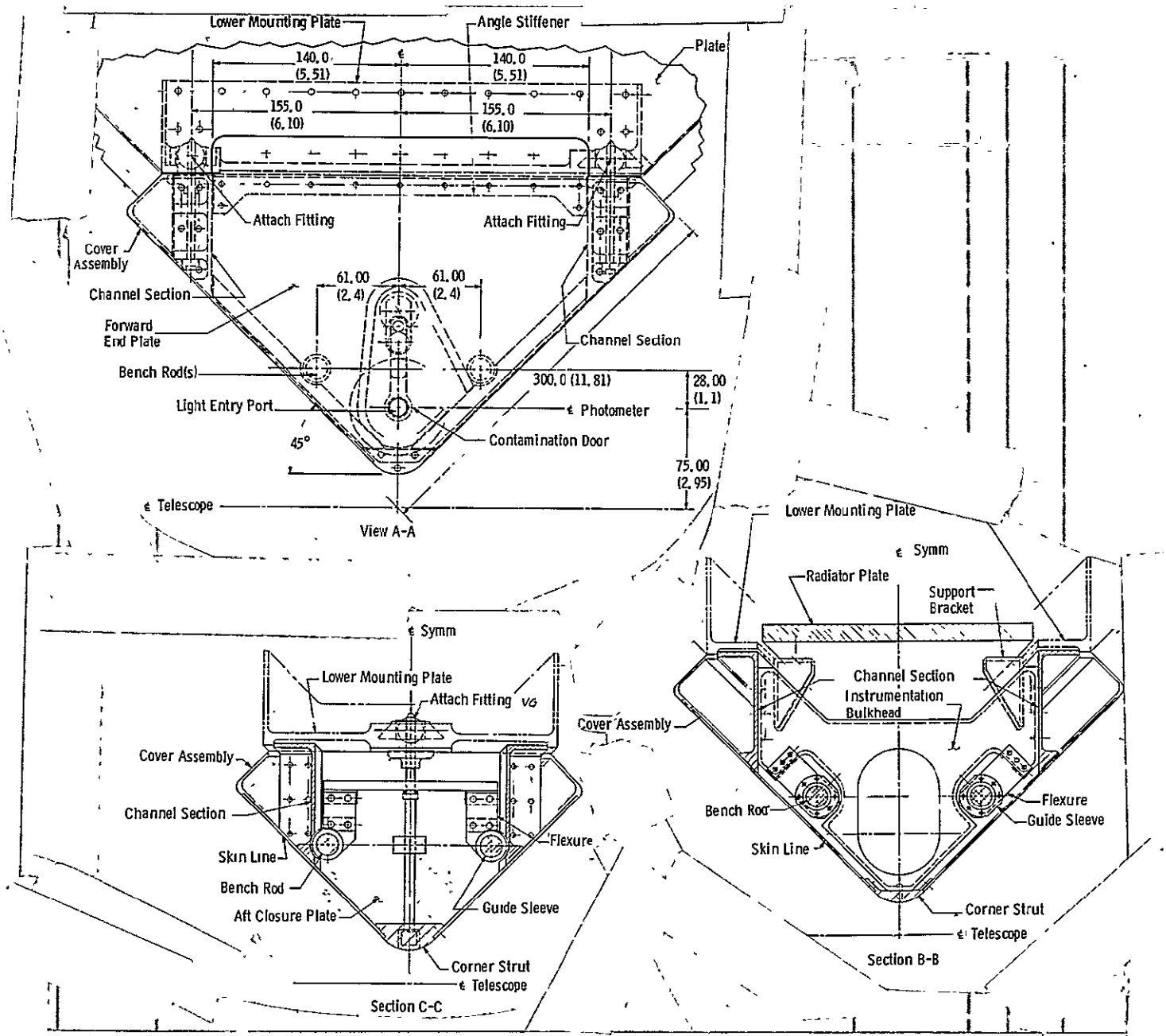

Several sections referred to in Figure 3.1-1 are shown. View A-A shows the forward invar plate of the submodule. The bench rods are pinned to this plate. The plate also holds the contamination door assembly. The view also shows two of the three fittings which attach the opto-mechanical submodule to the structural housing. They are designed to provide a statically determinant attachment which precludes introduction of strains into the optical bench. Sections B-B and C-C show that the optical bench rods are restrained by flexures which allow longitudinal motion of the submodule sturucture relative to the virtually inextensible rods without inducing strains. The flexures are stiff in the plane of the paper to maintain correct spacing and parallelism of the rods. The structural concepts are discussed more thoroughly in Section 3.2.2.

Figure 3.1-2 Opto-mechanical Submodule Sections

3.1.2 (Continued)

The filter elements are placed more than 200 mm from the entrance aperture to allow the beam to diverge enough to cover an area of 60 mm^2 or so, in order to average any nonuniformities in transmittances and so that positional repeatability is not critical.

3.1.2.1 Filter Wheel Assemblies

There are two sets of mechanically independent filters in tandem. The filter sets are used to define a broadband photometric system and to select various spectral regions which may be of interest for particular specialized investigations. Each filter wheel has eight positions for filters at least one of which shall be an open hole.

The filter substrates are made as thin as possible to avoid unwanted bulk absorption and to minimize focus shifts within the optics due to optical path length changes. The substrate surfaces need to be accurately parallel to prevent image motions (for area detection mode) when they are put in the light path. Good optical finish is also required to prevent degradation of the images from either induced wavefront error or from scattering. Substrate material is chosen with regard to susceptibility to potential damage from radiation.

The appropriate clear aperture for the filters depends on their distance from the entrance aperture and the size of the largest aperture. We designed all filters to be at least twenty percent larger than the calculated beam size to prevent vignetting even in the presence of filters being somewhat out of their nominal positions. Filter diameters are about 16 mm. The filter substrates are made large enough to permit retention in their mounts on the filter wheels.

Filter characteristics have not been specified because the ultimate decision will be made by the investigators in accordance with the particular observations they wish to make.

3.1.33 Point Photometry

Point photometry is the conventional form of photometry. Light from a portion of the OTA image is selected by one of the apertures. The light diverging from the OTA focus shines on a concave Fabry mirror which images the exit pupil of the telescope onto a detector. All the light which passes through the entrance aperture is collected onto the detector. To the first order, motion of the image within the aperture has no effect. Strictly speaking, of course, the image of even a star has an infinite extent. Most of the image power, however, is concentrated near the center of the image (82% falls inside the so-called Airy disk for a perfect circular lens) so that unless the aperture size is on the order of the Airy disk diameter or less, motion of the image has only a very small effect on the light irradiance entering the Photometer. In our design the smallest aperture is 72 μm in diameter. The Airy disk diameter from the OTA at a wavelength of 632.8 nm is about 37 μm. The actual point spread function is somewhat larger because of the astigmatism inherent in the OTA design. Most of the image light should enter the aperture even in the

3.1.3 (Continued)

presence of some misalignment of the image. At shorter wavelengths the diffraction spot is smaller so that the size of the entrance aperture is even larger relative to the point spread function. The photometer apertures are all large enough that the transmitted irradiance will not be strongly influenced by image motion. Figure 3.1-3 shows the relationship between the OTA predicted geometric image, the Airy disk, and the smallest Photometer entrance aperture.

3.1.3.1 Optics

The optics for point photometry are quite simple. A Fabry concave mirror forms an image of the OTA exit pupil on the selected detector. Each concave Fabry mirror is a rather severely curved ellipsoid. The optics are illustrated in Figure 3.1-4. The point detectors are small and thus must be illuminated with a short focal length Fabry mirror. The detectors must also be placed off the axis of the Photometer to avoid obstructing the incoming light. A ray from the center of the Photometer entrance aperture to the center of the Fabry mirror and then to the center of the point detector is reflected through an angle of 135^{o} (or 180^{o} -445^{o}). Fortunately imaging quality is of no great importance in this configuration so long as all the image light is captured by the detector photocathode.

A separate Fabry mirror is used for each of the two point detectors. The mirrors are identical except for their orientations on the Fabry/relay mirror changer carousel. The radii of curvature of the mirrors are 60.47 mm and 70.85 mm. The conjugates are 504 mm on the object side and 35 mm image side.

The Fabry mirrors are used in the vacuum ultraviolet so that they have coatings similar to those for the OTA mirrors. At this time the coating is expected to be aluminum overcoated with magnesium fluoride. The mirror substrate is of low expansion material such as Cer-Vit or ULE.

3.1.3.2 Point Detectors

Point detectors are used in the conventional photometer fashion: a Fabry mirror provides an image of the exit pupil of the telescope to illuminate the photocathode more or less uniformly. The image is, to the first order, independent of line-of-sight motion and motions of other optical elements. Photocathode response is, in general, nonuniform so the goal of optical design is to provide an image which does not move in response to residual telescope line-of-sight motion.

The design allows space for three point detectors although only two are required at present. The design would not be changed significantly by permitting just two point detector positions, so a spare position is provided. The third position could be used for a tube with different spectral sensitivity, a spare duplicate of one of the two active positions, or for monitoring dark counts due to radiation.

An external envelope 20 mm in diameter and 50 mm long is provided for each point detector. The actual sensitive area is 1.4 mm in diameter and has an area of 1.5 mm^2. There are several possible kinds of detectors. Our

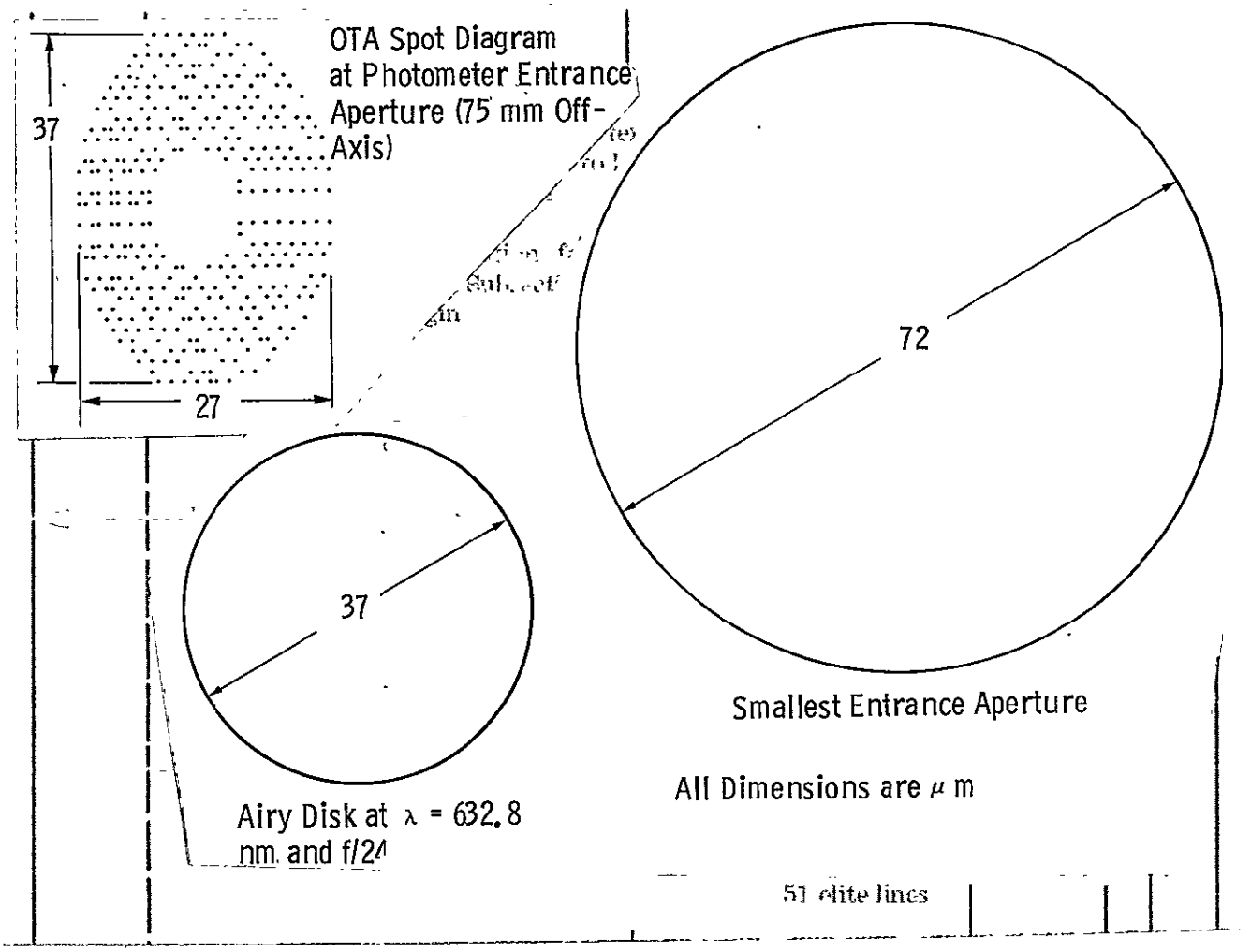

The OTA design has inherent astigmatism and focal surface curvature which vary quadratically with field angle. We traced rays through the OTA for the field position corresponding to the entrance aperture of the Photometer. At that point 75 mm off the OTA axis the rays form a spot at best focus which is about the size of the Airy disk (at λ = 632.8 nm). The OTA image is not "near diffraction limited" at the entrance aperture of the Photometer.

The imaging relays in the Photometer have been designed to compensate for the OTA's inherent aberrations.

Note that the actual point spread function is determined both by the diffraction and the geometric raytrace results. At the Photometer location 75 mm off axis the point spread function "width" is approximately twice the size of the Airy disk. Thus, most of the image light passes through the smallest aperture if the whole system is properly aligned. A significantly smaller entrance aperture would block a substantial amount of the incoming OTA image light.

Figure 3.1-3 OTA Image at the Photometer Entrance Aperture

The two Fabry mirrors are both eccentric portions of oblate spheroids (or ellipsoids). The ellipsoids have major axes of 432.34 mm and eccentricities of 0.9314. The glass of the mirrors has a clear diameter of 38 mm. Numbers in parentheses are optical path lengths.

Figure 3.1-4. Fabry Mirror

3.1.3.2 (Continued)

choice at this time is a photomultiplier tube using a channel electron multiplier rather than the more common dynode chain multiplier section. The principal reason is compactness. Figure 3.1-5 illustrates a commercially available channel electron multiplier tube.

There is a requirement for small photocathode size to reduce tube noise and a resultant geometric constraint on the overall dimensions of the detector. The noise is induced by particulate radiation, and susceptibility is proportional to photocathode area so that small photocathodes are clearly beneficial. It is not known at present if shielding is beneficial. We assume that operation during passage through the South Atlantic Anomoly and during solar flare events will not be attempted. Other observational constraints have not been identified.

The two point detectors identified now are similar to off-the-shelf channel electron multiplier tubes available from several suppliers. One tube has a CsI photocathode on a MgF_2 window. The CsI tube spectral response is confined to the far ultraviolet. The other tube has a bi-alkali photocathode on a MgF_2 window. The bialkali tube's response is from ultraviolet through virtually all of the visible spectrum. In each case probable peak quantum efficiencies will be on the order of 0.3 and the dark count rate at room temperature will be a few counts per second. Spectral sensitivities of the two detectors are shown in Figures 3.1-6 and 3.1-7.

Both detectors are mounted onto a carrier which attaches to the optical bench rods. The detectors can be moved independently through a small range to permit fine alignment. The mounts are designed to facilitate replacement of detector modules (on the ground) with minimal disassembly and disturbance of the rest of the Photometer.

3.1.4 Area Photometry

Area photometry is performed by optical systems which resemble cameras. There are two optical systems which accept the astigmatic off-axis image from the telescope and reimage the light onto an ICCD at either f/24 or f/96. The reimagining not only adjusts the plate scale of the image it also removes virtually all of the telescope's image aberration.

The ICCD is being developed separately from the Photometer and is expected to be furnished by the government. It will be carefully calibrated to determine its threshold modulation, noise equivalent input irradiance, and gain so that output images will contain precise photometric data. The geometric performance of the light and electron optics will also be calibrated.

3.1.4.1 Reflective Optics for f/24 and f/96

All the image forming optics in the Photometer are reflective. The number of reflections in any optical path is two to minimize light losses, especially at the short wavelengths. Figure 3.1-7 shows the estimated OTA and Photometer combined transmittance as a function of wavelength. All mirrors were assumed to be uncontaminated aluminum overcoated with magnesium fluoride.

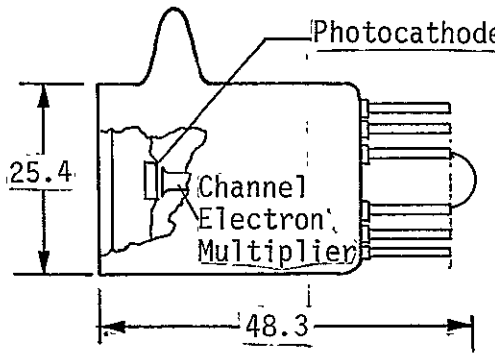

The sketch represents a commercially available tube which approximately meets the requirements for the Photometer point detector. The photocathode is deposited on a magnesium fluoride faceplate. The photoelectrons are multiplied by a channel electron multiplier. The two tubes in the Photometer are mechanically the same. One has a CsI photocathode and the other a bi-alkali photocathode. Some construction features such as the bonding of a magnesium fluoride window to the tube must be further developed by vendors and the Photometer would also benefit from a tube with a somewhat smaller envelope.

Figure 3.1-5 Point Detector

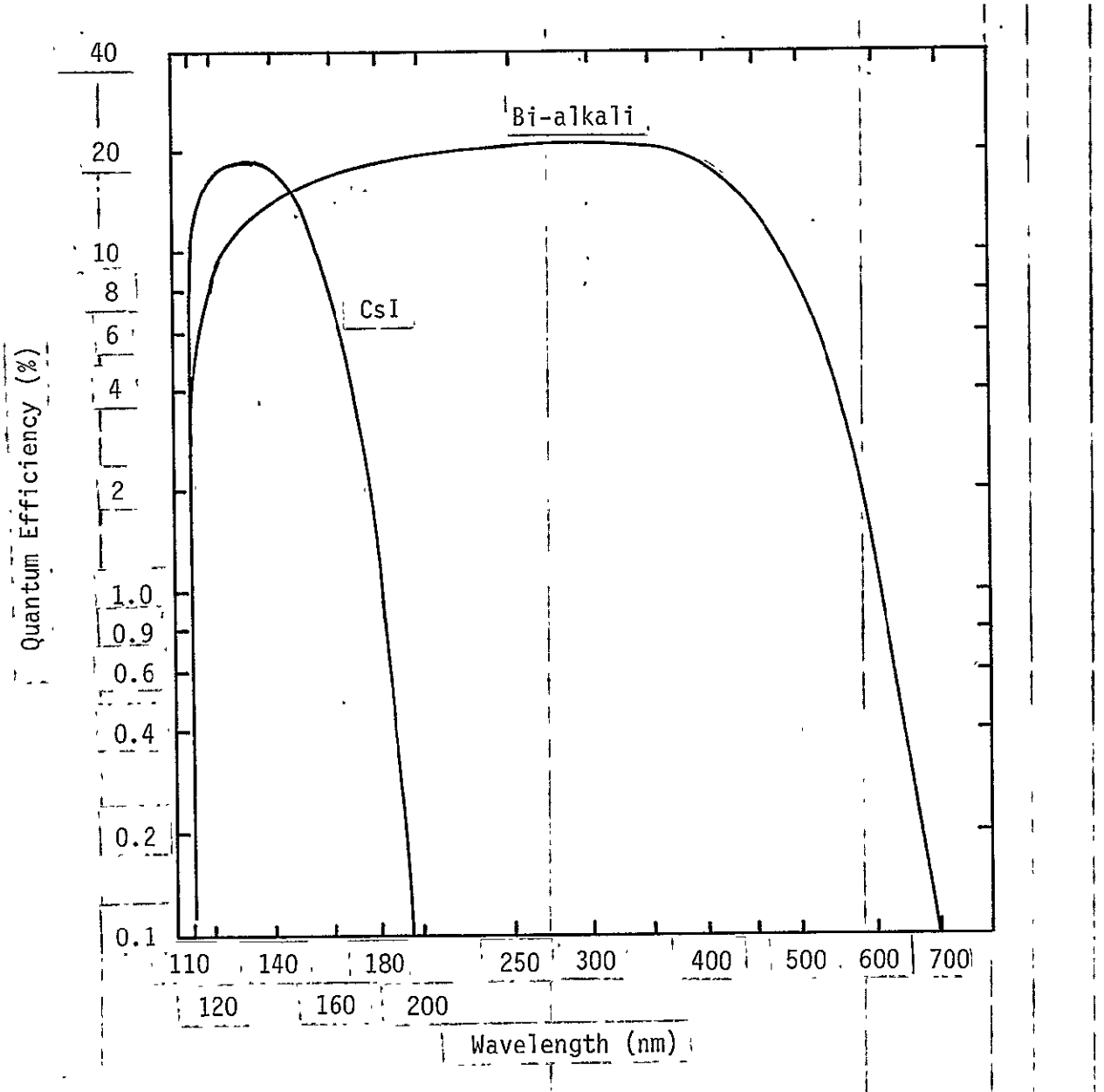

The illustrated spectral responses are conservative. Selection of particular tubes could lead to higher operation efficiencies, say, peaking at 30% rather than the 20% shown. In both tubes the precipitous fall-off at short wavelengths is due to absorption in the magnesium fluoride faceplates.

Figure 3.1-6 Typical Spectral Response of CsI and Bi-alkali Photocathodes

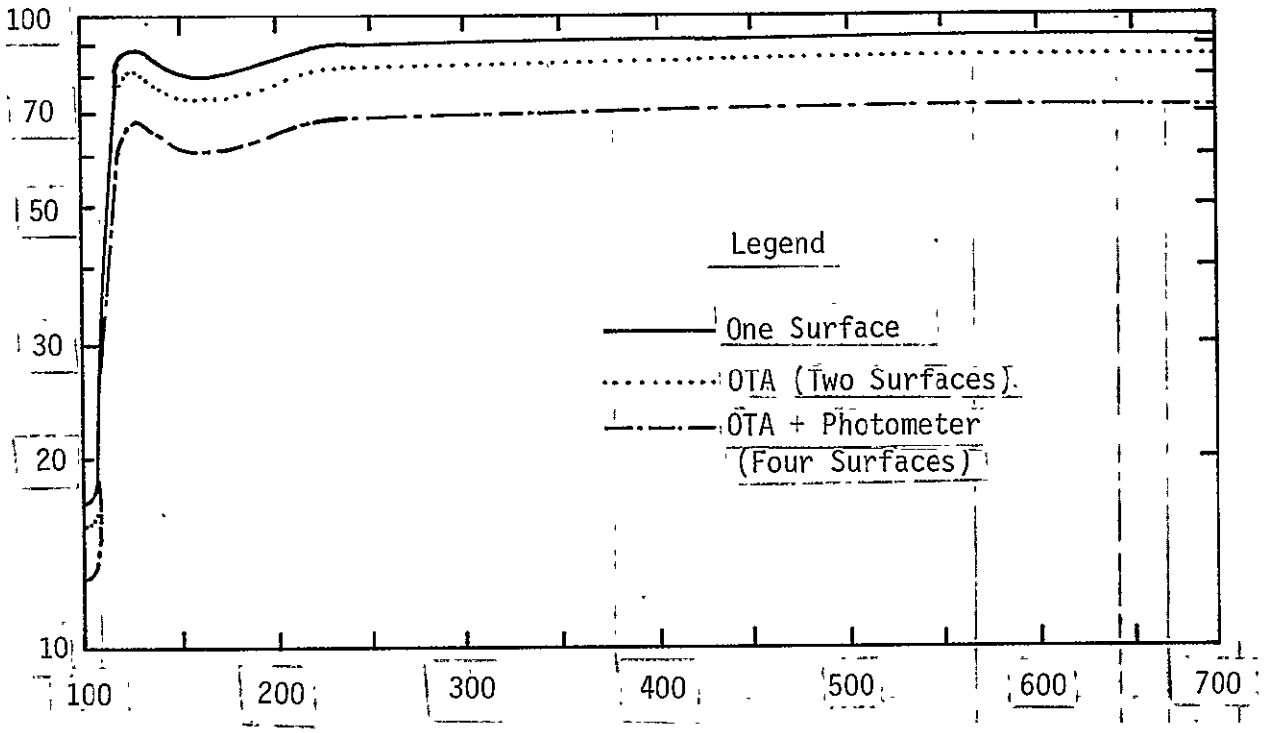

We assumed that the photometer mirrors are all coated with the same reflective surface as the OTA mirrors. The coatings are about 50 nm of aluminum overcoated with 25 nm of magnesium fluoride. Even for a total of four surfaces the system transmittance is quite high down to a wavelength of 120 nm. It falls to about 15% at the 115 nm shortest design wavelength.

Figure 3.1-7 Transmittance of Photometer and OTA as a Function of Wavelength

3.1.4.1 (Continued)

Separate optical systems were designed for the two area detector magnifications at f/24 and f/96 to allow optimization of the optical surfaces for one function at a time. This is important because only two surfaces are used within the photometer for any imaging operation. In general, the optical design possibilities for good quality imaging are quite limited with only two surfaces. We have thus chosen not to degrade performance by forcing the same optics to operate in two modes. There are primary and secondary relay mirrors for f/24 and separate primary and secondary relay morrors for f/96.

The f/24 and f/96 primary mirrors are mounted on a hexagonal rotating carousel which places the desired mirror in the light path. The Fabry mirrors for point detection are also mounted on the same carousel. Both f/24 and f/96 secondary mirrors are in fixed positions because of their critical alignment, to avoid the complexity of another mechanism, and because the optical designs are more efficient this way.

At f/24 the system image resolution is limited almost equally by optical image quality and by inherent detector resolution depending on the wavelength. At f/96 the system image resolution is limited by the optical image quality which in turn is limited by diffraction. The f/96 pictures are expected to contain nearly all of the image information possible from a 2.4m telescope. The high resolution of f/96 is obtained at a price, of course. The image irradiance is less than that at the f/24 OTA image by a factor of at least sixteen. For many astronomical objects the obtainable resolution will be limited by photon statistical fluctuations.

3.1.4.1.1 f/24 Relay System

The f/24 relay optics reimage the OTA Cassegrain focus image onto the area detector after the light has been spectrally filtered. The relay has been designed to correct the OTA image aberrations which are inherent in the Ritchey-Chretien OTA design at off-axis image positions. The design was constrained to fit into the existing instrument geometry and to provide the area detector with nearly diffraction limited images over its entire format. Magnification of the relay is unity. The geometric relationship of the Photometer to the OTA was determined primarily by the geometry of the Scientific Instrument Ensemble and is shown schematically in Figure 3.1-8. It is worth noting that the Photometer optical axis must be both displaced laterally and angularly from the OTA axis. The angular tilt of the Photometer is used to introduce compensating aberrations which partially nullify the OTA off-axis aberrations.

The f/24 design can be considered nearly diffraction limited because raytracing has shown geometric spot diagrams which are substantially smaller than the Airy disk size expected from diffraction alone. The Airy disk diameter at the test wavelength of 632.8nm is about 37 μm; the geometric spot size is about 9 μm. The high quality images are obtained everywhere on the area detector format. For the most part the design process was executed using geometric raytracing. The designs which exhibited geometric spots smaller

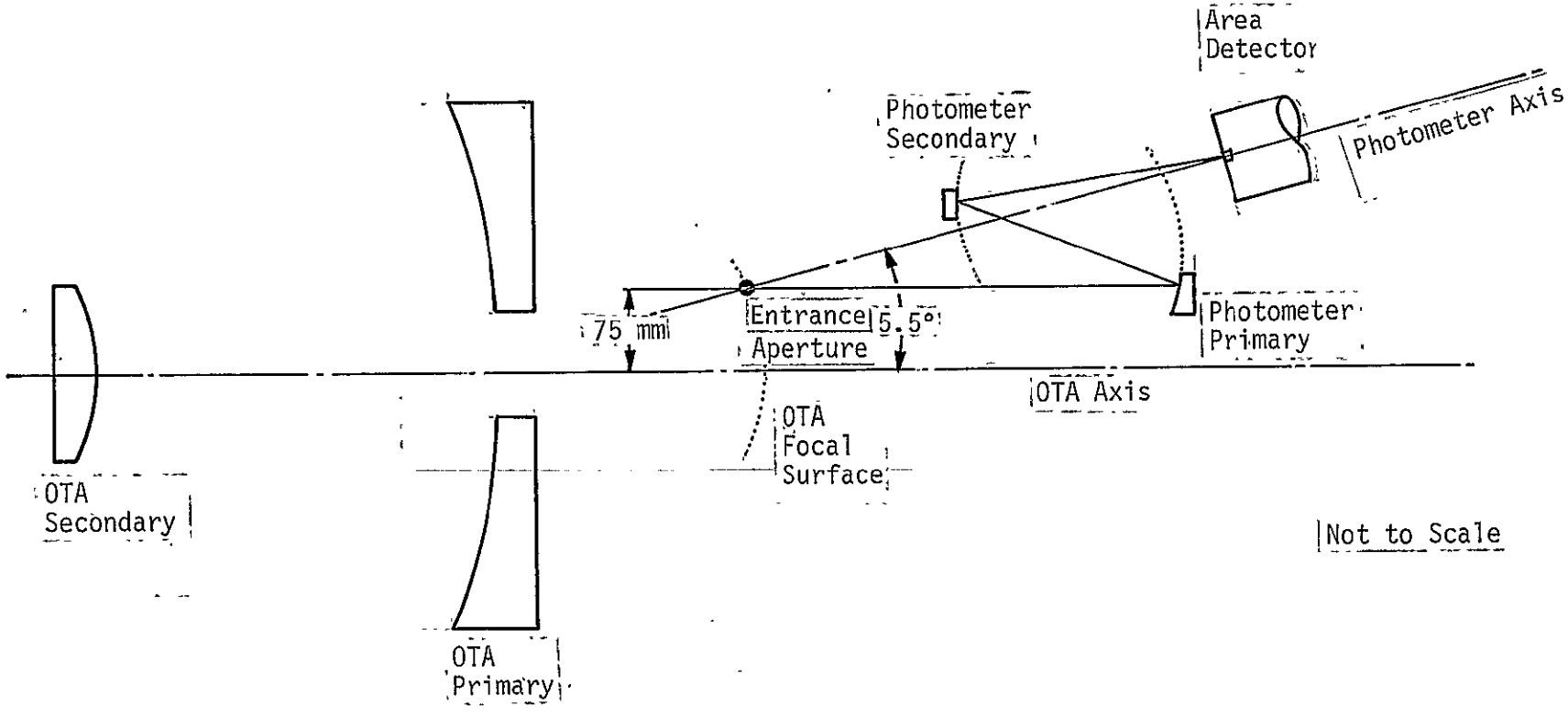

The Photometer entrance aperture is 75 mm from the optical axis of the telescope. The Photometer's optical axes for both f/24 and f/96 are tilted around the entrance aperture about 5.5° in the meridional plane of the telescope.

Figure 3.1-8 Schematic Relationship of the Photometer to the OTA.

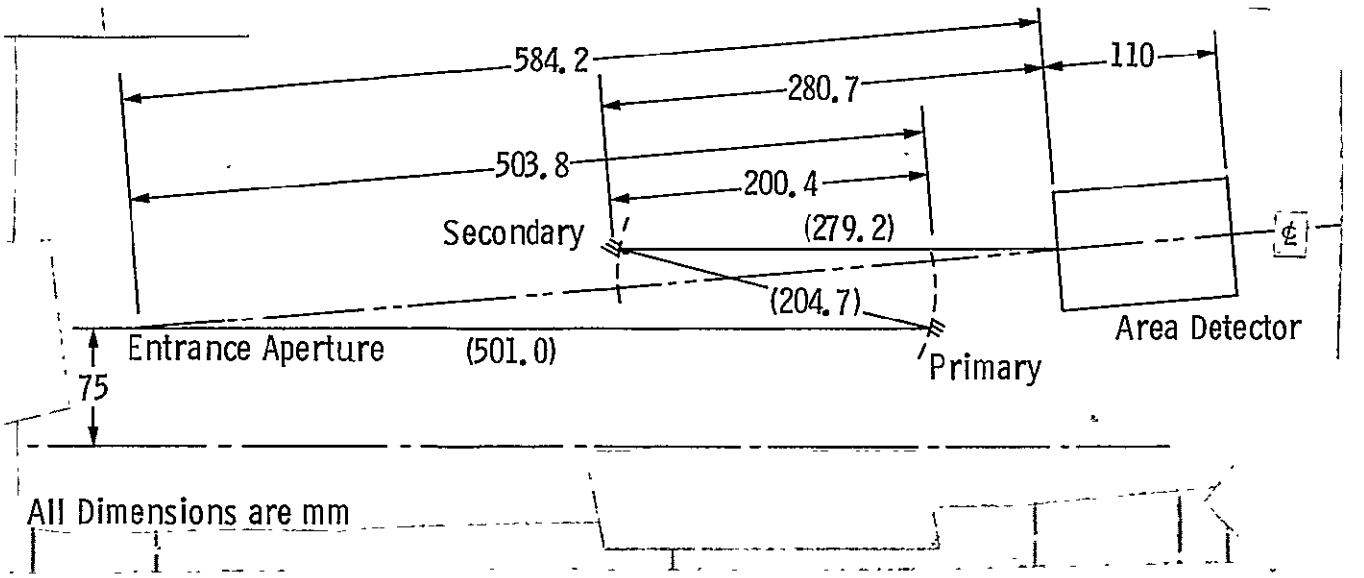

Dashed curves represent cross sections of the optical formula surfaces. The optical elements (Primary and Secondary mirrors) are off-axis parts of those surfaces. Numbers in parentheses are optical path lengths along a ray from the center of the entrance aperture to the center of the area detector. The line indicated ℄ is the axis of the optical formula: it goes from the entrance aperture directly to the area detector.

Figure 3.1-9 Optical Layout of f/24 Imaging Relay

than the Airy disk were further analyzed by computations which included diffraction effects. Those computations generated point spread functions (i.e. the predicted irradiance distribution in a star image), two dimensional modulation transfer functions, and wavefront error maps.

Point spread functions (psf's) are most indicative of what the Photometer image will look like while the modulation transfer function is perhaps the most useful starting point for computing merit functions such as spatial resolution. The wavefront error (wfe) map is of some use to the designer in that it indicates what kind of surface shapes on the mirrors may be useful in achieving good imagery. Some results of analysis of the f/24 design are shown in figures. Figure 3.1-10 is a set of geometric spot diagrams which are relatively easy and economical to generate. The spot diagrams show the uniformity of the images over the field. A typical field point was selected for computation of the psf shown in Figure 3.1-11. The psf is compared with the psf that would be generated by an aberration-free system with a central obstruction like the OTA's. A wfe map is presented in Figure 3.1-12. The wavefront looks somewhat comatic which is consistent with the shape of the spot diagrams. Most important is that the wfe map does not appear visually to have an astigmatic component which could be corrected by a toric surface component on the relay's mirrors. The use of torics was abandoned early in the design process because the possible improvement was not judged to be sufficient to justify the increased costs of the complex surface.

The position of the Photometer off the OTA axis led to initial attempts to specify only the locations of the relay mirrors and then to use tilted toric surfaces. Raytracing showed such a design approach to work well for a perfect (i.e. point) OTA input. If the Photometer were on the OTA optical axis where the input is perfect the toric solution would suffice. Raytracing for the actual Photometer location showed, however, that the toric design could not cover a flat field even though the field angles in object space are only seventy microradians or less.

Another design start was made using an eccentric pupil Gregorian microscope objective as a first order solution. The entrance aperture and center of the area detector were chosen as two points to define the optical axis of the relay. Several tilt increments of the Photometer axis were tried subject to the constraints that there a) be room for the mechanical envelope of the area detector with some room for growth, b) be no vignetting of the light beams, and c) that the tilt be as small as possible. The resultant optical formula is a conventional rotationally symmetric design, but the actual mirror surfaces are eccentric sections. The Photometer axis is tilted about 5.5° away from the OTA axis.

The optical design program was allowed to use conic constants and higher order aspheric terms to give uniformly good image quality of all points on the area detector. The program converged rapidly to a very good solution. The optical formula was then analyzed by two different programs which confirmed the adequacy of the eccentric Gregorian design. The program used only one higher order aspheric coefficient so the mirrors promise to be manufacturable by ordinary fabrication and testing techniques. The relative mildness of the surfaces allows them to be tested with simple test setups probably including a null lens in a

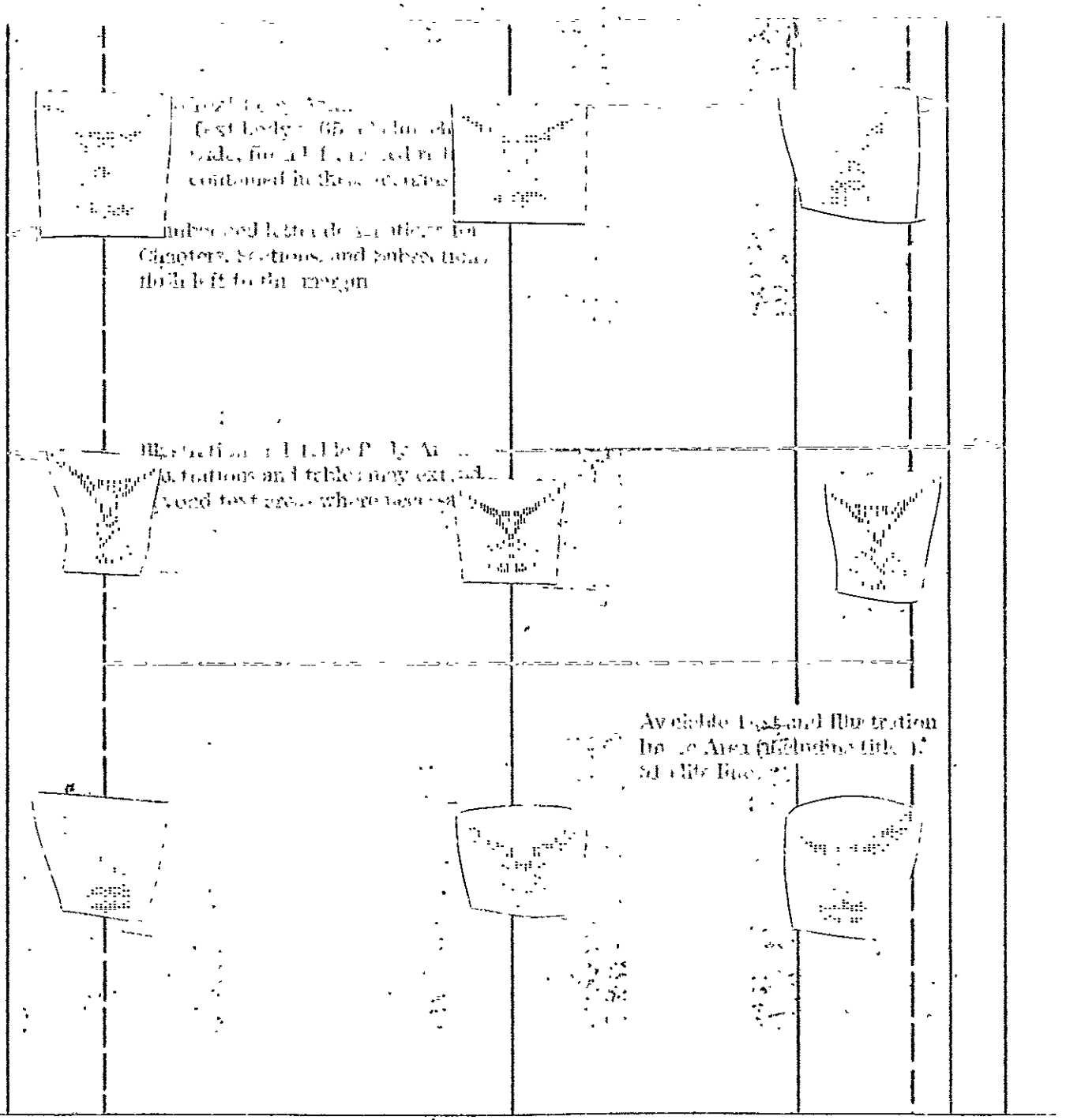

The spots indicated in the figure are geometric predictions derived from the optical formula. Diffraction, possible misalignments and manufacturing imperfections are not shown. The scales of all the spot diagrams are the same but their positions in the area detector format are only indicative. Each of the spots is contained within a circle about 9 μm in diameter. The Airy disk size at f/24 and a wavelength of 632.8 nm is 37 μm

Figure 3.1-10 f/24 Area Detection Optical Performance

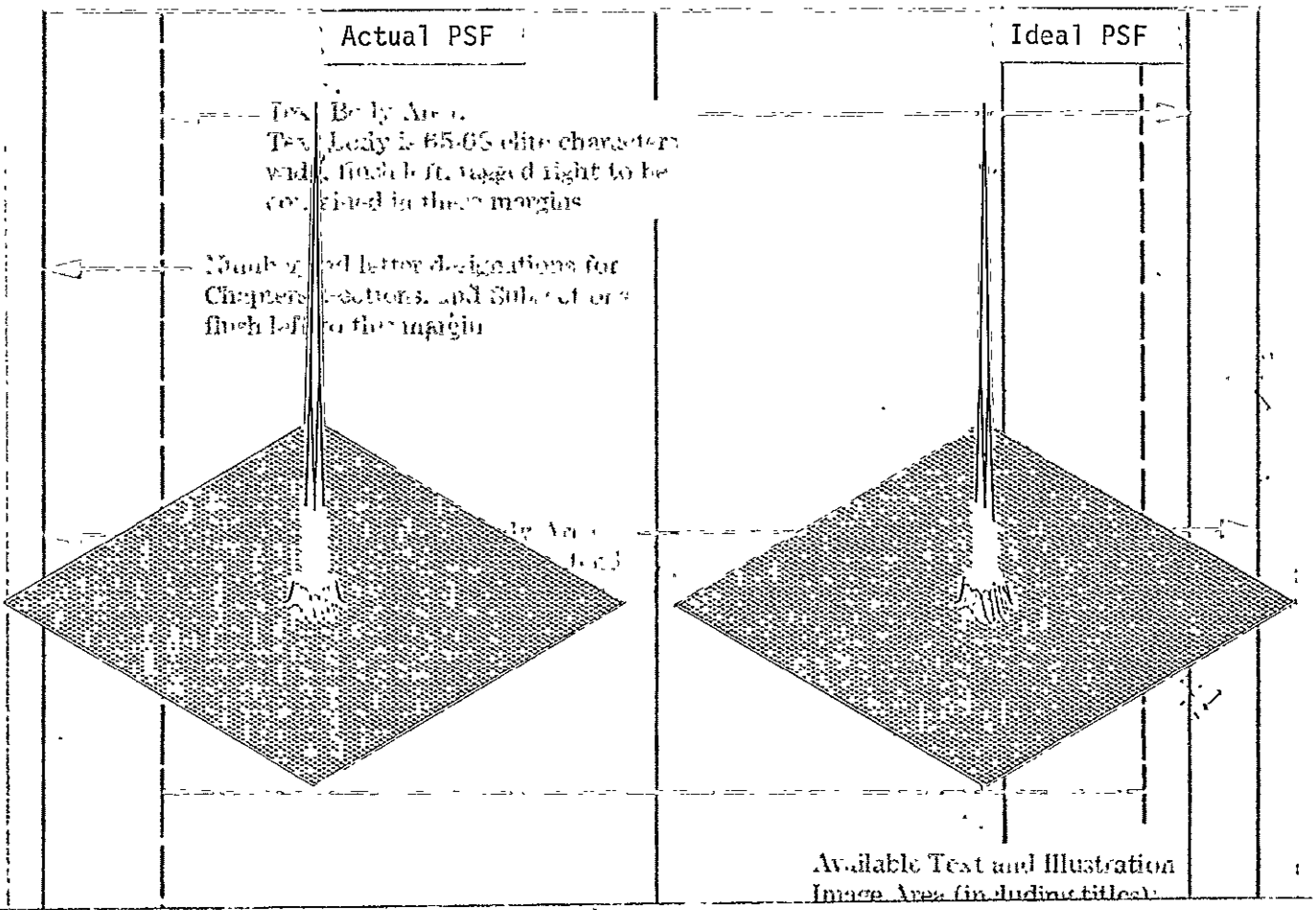

The two point spread functions illustrated were generated by a computer program. The actual psf was computed from the f/24 imaging relay formula at a wavelength of 632.8 nm. The image point was at one corner of the field-of-view where the image was the worst. It is nevertheless essentially diffraction limited as comparison with the perfect psf shows. The small amount of asymmetry in the f/24 psf corresponds to the asymmetry seen in both the wavefront error map and in the geometric ray trace spot diagram. Both psf's exhibit the effect of the OTA central obstruction.

Figure 3.1-11 Point Spread Function for f/24 Relay

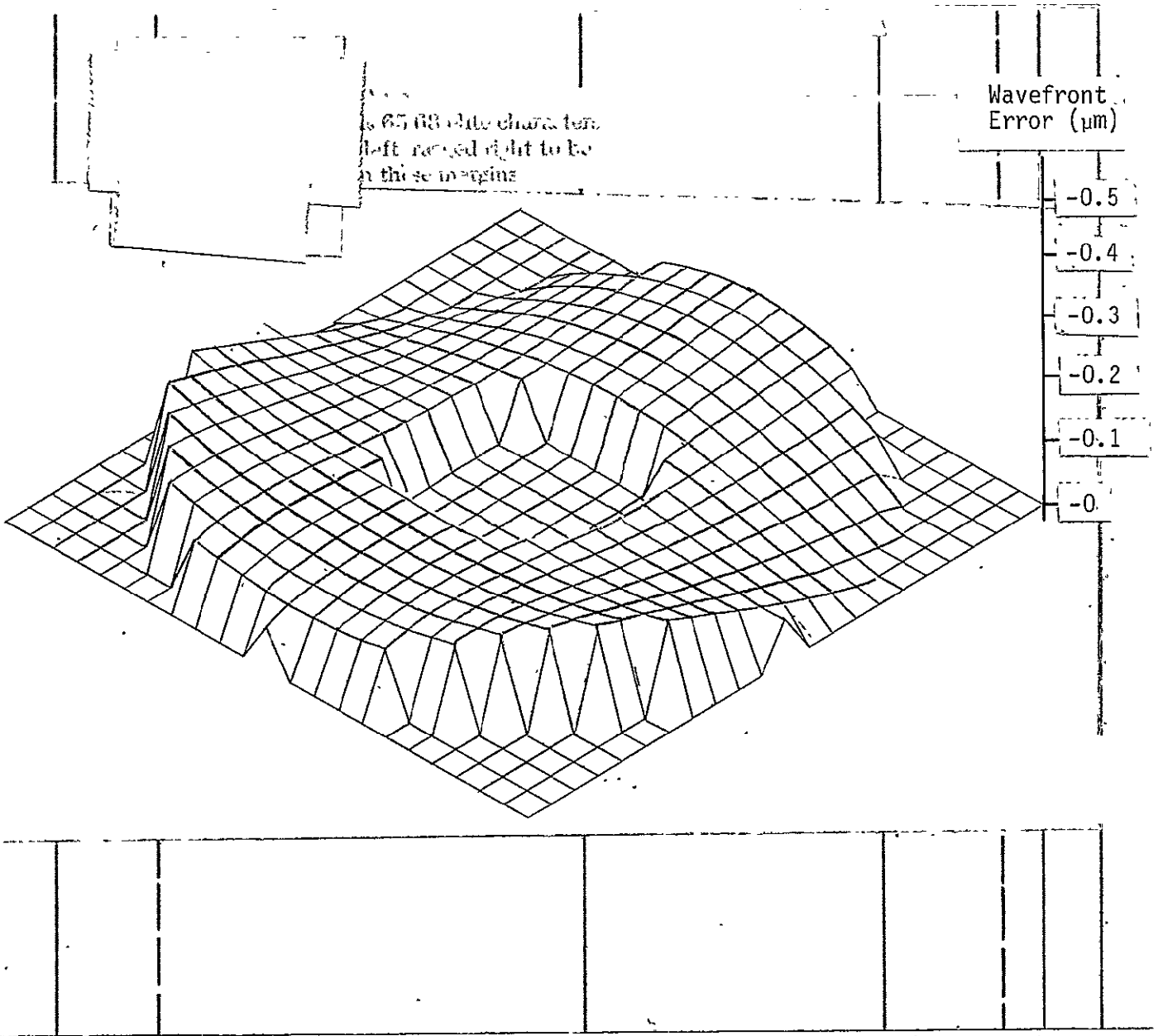

This isometric view of the f/24 relay wfe was generated from the f/24 optical formula by a computer program. The ideal wavefront would be flat and look like an angelfood cake. The hole in the center of the plot is the shadow of the OTA central obstruction. The vertical exageration of the wavefront error is 10^5. By inspection the peak-to-valley wavefront error is about 0.15 μm or about $\lambda/4$ at the wavelength. The horizontal scale is normalized to the exit pupil diameter.

Figure 3.1-12. Wavefront Error at the Exit Pupil of the f/24 Relay

Twyman-Green laser interferometer. The null lens has not been designed as yet. The surfaces can be made with large rotationally symmetric polishing tools which will produce surfaces smooth enough to be satisfactory in the far ultraviolet where non-smooth surfaces cause undesirable light scattering. The formula for the f/24 relay is summarized in Table 3.1-1.

3.1.4.1.2 f/24 Relay Alignment Tolerances

Tolerances to thermal and mechanical strains of the optics mounting structure were studied by varying the separations, tilts, and decenters between optical elements and computing spot diagrams. The effects were modest and could be corrected by refocusing the area detector. The most sensitive parameter is the spacing between photometer primary and secondary mirrors. The accompanying Table 3.1-2 is a brief compilation of raytracing results.

3.1.4.1.3 f/96 Relay System

The f/96 relay optics reimage the OTA Cassegrain focus image onto the area detector with a magnification of four diameters. The f/96 imaging mode may be used with any combination of spectral analysis filters. Imaging can also be accomplished with any entrance aperture although it will be used with an aperture large enough to illuminate the whole area detector format except possibly during target acquisition operations. The relay has been designed to correct the OTA image aberrations which are inherent in the OTA off-axis image. The principal reason for the existence of the f/96 relay is to give sufficient image size ("plate scale") that the resolution would be diffraction limited rather than detector limited. Naturally this implies that the geometric aberrations yield an image which was small relative to the Airy disk diameter.

The geometry of the f/96 system was constrained to match the geometry of f/24 relay. In particular the element spacings were essentially the same in both relays and the optical axis was coincident with that for f/24. The f/96 relay primary mirror is in the same location optically as the f/24 relay primary through the use of a changer mechanism. The f/96 relay secondary was not movable and thus had to be placed where it would neither obstruct the light nor interfere mechanically with the f/24 secondary.

The f/96 design problem was highly constrained but a solution was derived that can, nevertheless, be considered nearly diffraction limited. Raytracing has shown geometric spot diagrams which are somewhat smaller than the size of the Airy disk. The Airy disk diameter at f/96 and at a test wavelength of 632.8 nm is about 148 μm; the geometric spot size is about 72 μm. Similar spot sizes were obtained everywhere on the area detector format although the shapes of the spots were variable. The design process was executed using geometric raytracing with a constraint placed on balancing performance over the field. When the design exhibited geometric spots smaller than the Airy disk size the optical formula was subjected to detailed analyses by additional computer programs. The optical formula is shown in Table 3.1-3; the layout of the elements is shown in Figure 3.1-13.

Table 3.1-1 Optical Formula f/24 Imaging Relay

The f/24 imaging relay is an eccentric pupil finite conjugate Gregorian lens. Both optical elements are concave mirrors which are off axis portions of rotationally symmetric aspheres. The optical axis of the relay connects the center of the entrance aperture to the center of the area detector. The Photometer axis is tilted 4.961° from the telescope optical axis. The entrance aperture is 75 mm from the OTA axis and is located logitudinally at the OTA best compromise astigmatic focus.

Surface	Vertex Radius	Thickness to Next Surface	Medium	Conic Constant	Decenter	Tilt
OTA Image	-625.94 mm	503.80 mm	Air	0	75 mm	5.575°
f/24 Primary	-203.73	-200.36	Refl.	-.1408	0	0
f/24 Secondary	115.46	280.74	Refl.	-.6008	0	0
Final Image	0	-	-	-	0	0

Table 3.1-2 Optical Alignment Tolerances

External Interface	[ℓm]
Entrance Aperture Radial Decenter from OTA Axis	± 1000
Entrance Aperture Longitudinal Despace from OTA Focus	± 500
Internal Interface	
Entrance Aperture to Relay Primary Despace	± 500
Relay Primary Decenter	± 100
Relay Primary to Secondary Despace	± 100
Relay Secondary to Detector Despace	± 150
Detector Decenter	± 100

Table 3.1-3 Optical Formula f/96 Imaging Relay

The f/96 imaging relay is an eccentric pupil finite conjugate Gregorian lens. Both optical elements are concave mirrors which are off axis portions of rationally symmetric aspheres. The optical axis of the relay connects the center of the entrance aperture to the center of the area detector. The Photometer axis is tilted 4.961° from the telescope optical axis. The entrance aperture is 75 mm from the OTA axis and is located longitudinally at the OTA test compromise astigmatic focus.

Surface	Vertex Radius	Thickness to Next Surface	Medium	Conic Constant	Aspheric Coefficients				Decenter	Tilt
					xy^4	xy^6	xy^8	xy^{10}		
OTA Image	-625.94	510.21	Air	0	0	0	0	0	75 mm	5.575°
f/96 Primary	-263.22	200.48	Refl.	-0.331	.189E-8	-.125E-11	.227E-15	-.162E-19	0	0
f/96 Secondary	41.79	275.00	Refl.	-0.6945	- .296E-5	-.112E-10	-.320E-16	.294E-22	0	0
Final Image	-	-	-	-	-	-	-	-	0	0

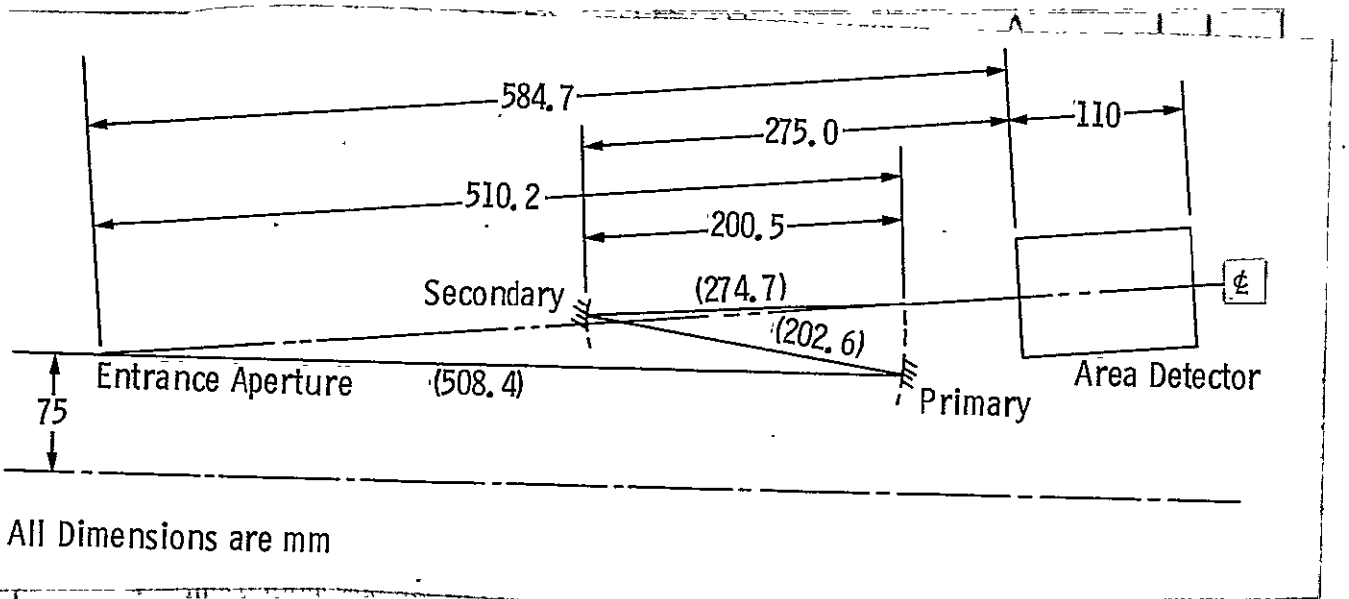

Dashed curves represent cross sections of the optical formula surfaces. The optical elements (Primary and Secondary mirrors) are off-axis parts of those surfaces. Numbers in parentheses are optical path lengths along a ray from the center of the entrance aperture to the center of the area detector. Other numbers are vertex spacings for the formula. The line indicated ℄ is the axis of the optical formula: it goes from the entrance aperture directly to the area detector.

Figure 3.1-13 Optical Layout of f/96 Imaging Relay

The analyses included computation of point spread functions, modulation transfer functions, and wavefront error maps in addition to the usual spot diagrams. Analyses were performed for points all over the field and for various forms positions. Some results of the analyses are shown in the figures. Figure 3.1-14 is a set up spot diagrams for nine points in the area detector field-of-view. The spots show the bilateral symmetry expected from a design which has all element vertices in one plane. The spots vary in shape with field position which is symptomatic of the difficulty encountered in achieving a satisfactory design. One field point was selected for illustration of a point spread function in Figure 3.1-15. The actual psf is contrasted with a truly aberration-free psf. The system's exit pupil wavefront error map is shown in Figure 3.1-16. The wfe is larger than that for the f/24 case and once again shows some coma. The wavefront is smooth and only a small portion very far from being flat. Wavefronts of other field points look basically similar but are different in detail. It is worth noting that it is not apparent that there is any toric power component in the wfe, hence the decision not to use toric surfaces in the design.

To make the f/96 relay geometrically compatible with the f/24 relay, initally an eccentric pupil Cassegrain system was tried. Clearance of the two secondary mirrors was thus assured and the power of the system could be shared well between the relay's primary and secondary mirrors. Several design iterations were made with the design program in an attempt to optimize this configuration, without any real success. Thus the Cassegrain approach was abandoned and a Gregorian design was selected in preference to adding toroidal surface figures to the mirrors.

A design start was made using a Gregorian microscope objective as a first order solution. The radii of curvature of the mirrors was, as expected, more severe than for the Cassegrain attempt. The optical design program was allowed to use conic constants and five orders of higher aspheric coefficients on each surface. Convergence to a solution was achieved slowly and a plateau reached at the design presented here. The design is considered satisfactory but not strongly so. Given the geometric constraints, the f/96 relay design is a good solution, with some improvement still possible through allowing minor geometric manipulation.

The optical surfaces are portions of rotationally symmetric surfaces and thus can be manufactured by ordinary fabrication and testing procedures. The substantial asphericity is, of course, undesirable but can be made using available state-of-the-art methods.

In a further design refinement, we would design the f/96 (or perhaps somewhat faster) relay first and use its geometry to constrain the less critical f/24 design. We would also strive to reduce surface asphericities to facilitate manufacturing and testing and to increase the probability of achieving low-scatter surfaces. The next section also reveals some of the alignment tolerances on the f/96 relay to be stringent. The high magnification of the secondary mirror is the culprit and so is a point for design attention.

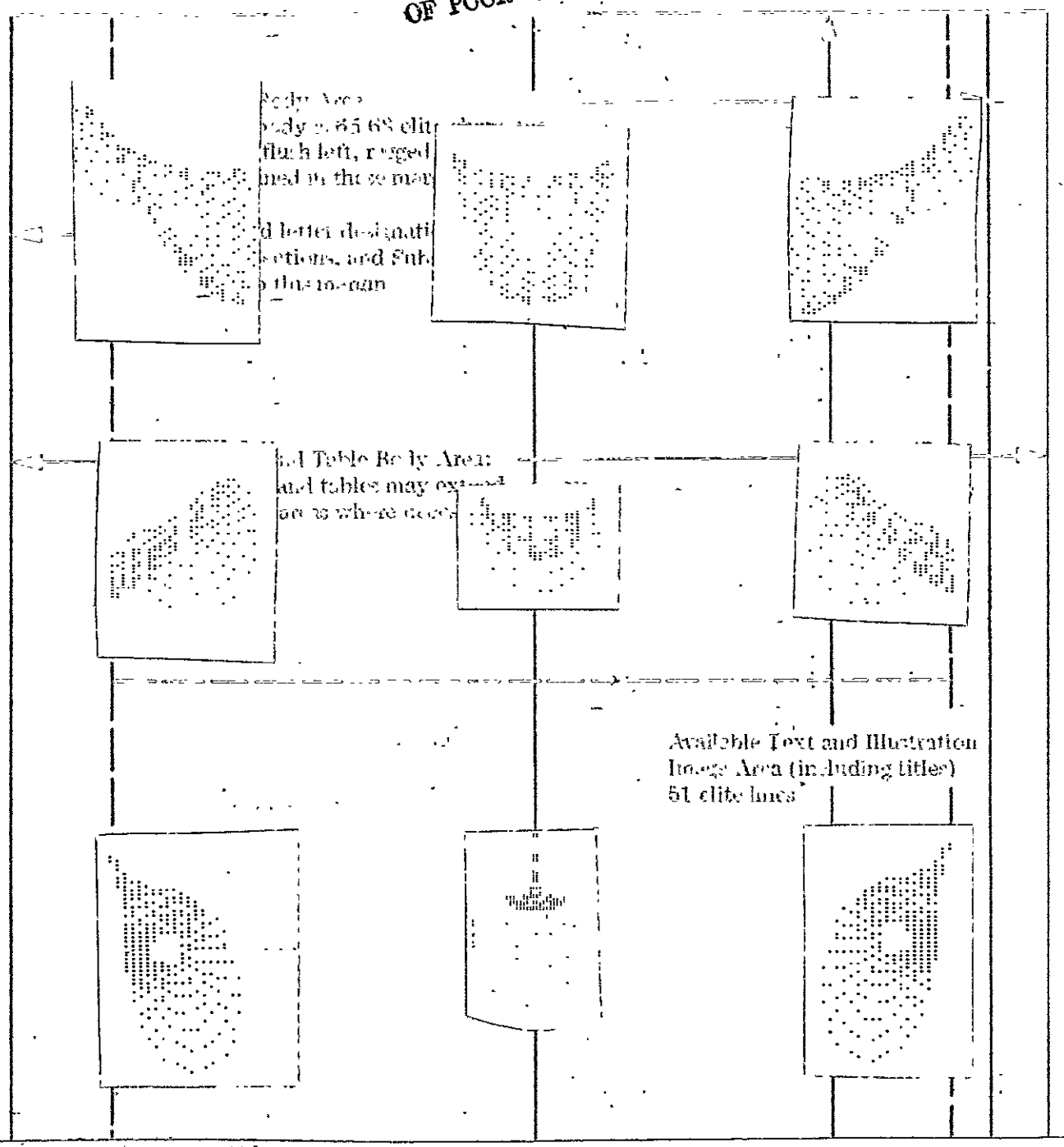

The spots indicated in the figure are geometric predictions derived from the optical formula. Diffraction, possible misalignments and manufacturing imperfections are not shown. The scales of all the spot diagrams are the same but their positions in the area detector format are only indicative. Each of the spots is contained within a circle about 125 μm in diameter. The Airy disk size at f/96 and a wavelength of 632.8 nm is 148 μm.

Figure 3.1-14 f/96 Area Detection Optical Performance

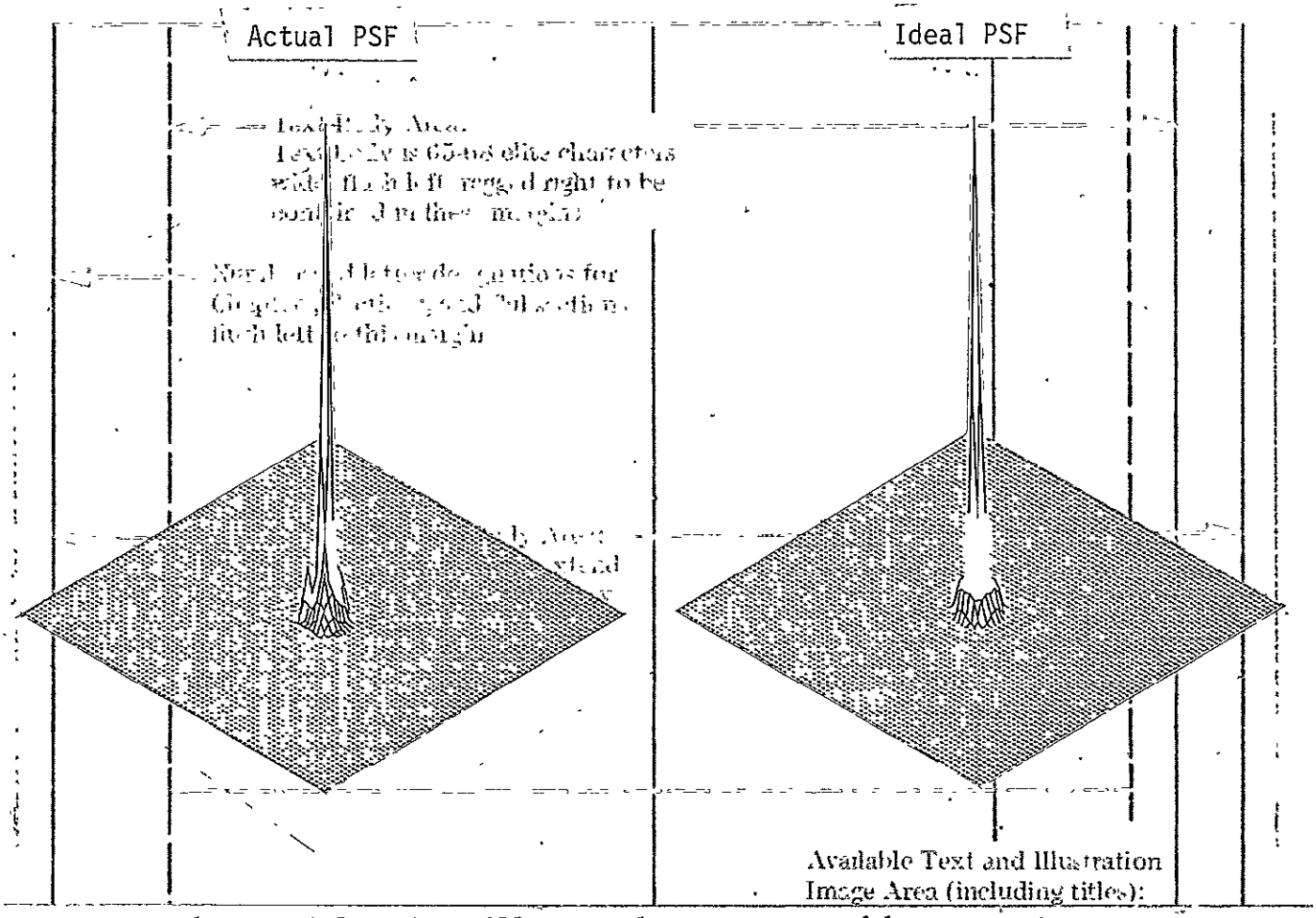

Available Text and Illustration Image Area (including titles):

The two point spread functions illustrated were generated by a computer program. Both were computed at a wavelength of 632.8 nm. The image point for the actual relay was at one edge of the field-of-view. psf's at the other field points were different in detail but basically similar. The asymmetry of the psf corresponds to the asymmetry seen in both the wavefront error map and in the geometric spot diagram.

Figure 3.1-15 Point Spread Function for f/96 Relay

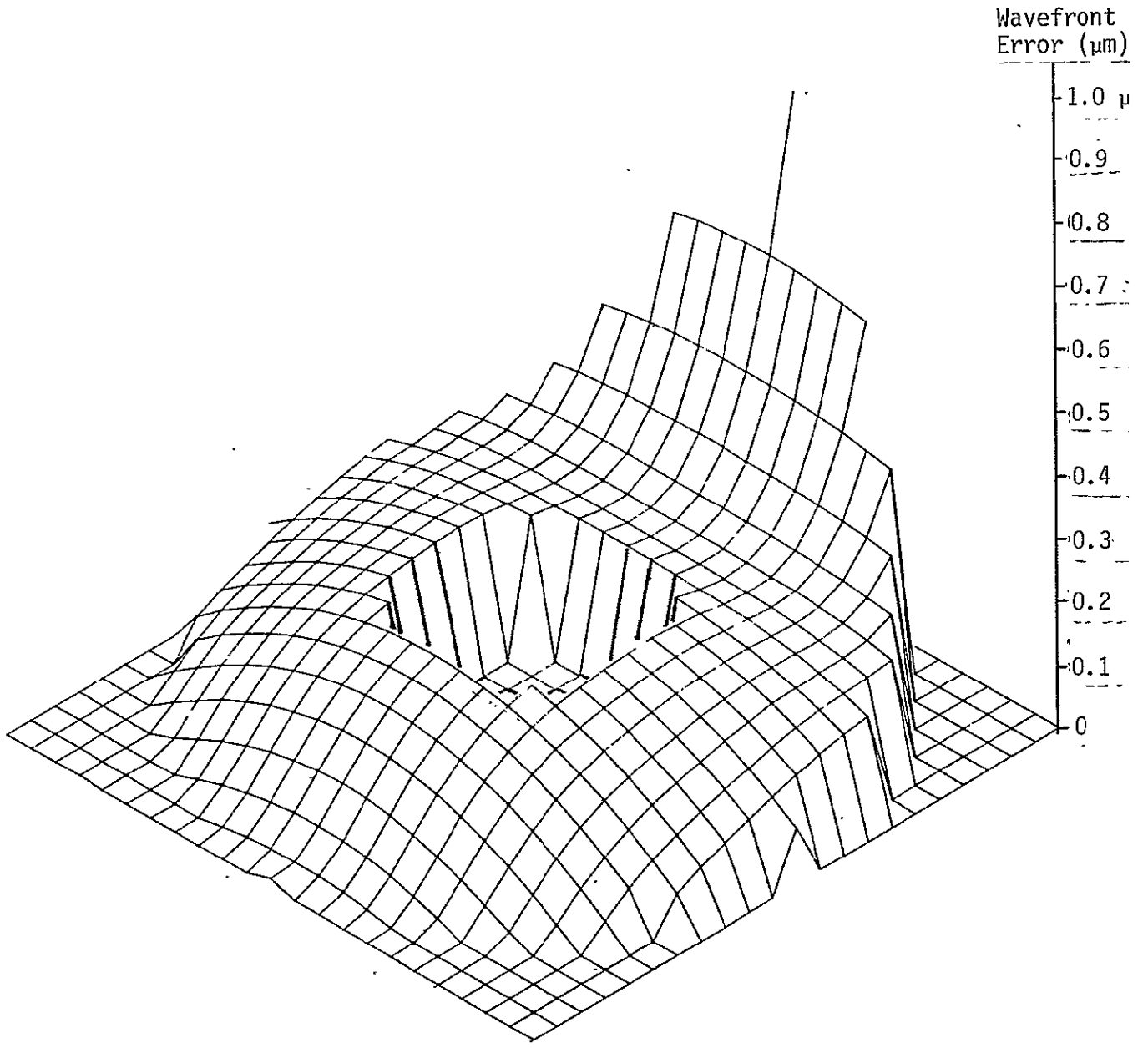

This isometric view of the f/96 relay wfe was generated from the f/96 optical formula by a computer program. The ideal wavefront would be flat. The hole in the center of the map is the shadow of the OTA central abstruction. The vertical exageration of the wavefront error is 10^5. The peak-to-valley wavefront error is about 0.75 μm or slightly more than a full wavelength. Fortunately only a small area of the wavefront is that bad. The horizontal scales have been normalized to the exit pupil diameter.

Figure 3.1-16 Wavefront Error of the Exit Pupil of the f/96 Relay

3.1.4.1.4 f/96 Relay Alignment Tolerances

The optical systems in the Photometer were analyzed for alignment sensitivity by systemmatically varying element tilts and spacings and by varying the position of the whole photometer with respect to the telescope, By far the most sensitivity to misalignment is exhibited by the f/96 relay system for area detection. The principal cause of the sensitivity is the high manification of the f/96 secondary mirror. The requirements for overall 4X magnification and diffraction limited imagery have left relatively little tolerance for alignment and manufacturing error.

Exact tolerance allocation depends on the image quality criteria in use and on existence of a final design. In lieu of better criteria we have allowed a maximum geometric spot diameter of 150 μm (the approximate size of the Airy disk in the visible). The accompanying Table 3.1-4 is a brief compilation of alignment tolerances derived from raytraces.

Table 3.1-4 Optical Alignment Tolerances

	[μm]
External Interface	
Entrance Aperture Radial Decenter from OTA Axis	$\pm$ 1000
Entrance Aperture Longitudinal Despace from OTA Focus	$\pm$ 150
Internal Interface	
Entrance Aperture to Relay Primary Despace	$\pm$ 10
Relay Primary Decenter	$\pm$ 150
Relay Primary to Secondary Despace	$\pm$ 4
Relay Secondary to Detector Despace	$\pm$ 600
Detector Decenter	$\pm$ 100

3.1.4.2 Area Detector

The area detector photocathode is normal to the optical axis of each relay (they have a common axis). Good imagery is obtained across the whole format for both f/24 and f/96 relays. Allowing curvature of the image surface during the design process did not improve the spot diagrams so a nominally flat focal plane is used. The ray bundles are inclined somewhat to the detector's surface normal but the angles are so small (less than 0.1 radian) that there is negligible light loss due to cosine foreshortening.

Resolution of the area detector cuts off at one line pair per picture element spacing or at 40 line pairs per mm. Roughly speaking the modulation transfer function of the detector is the product of two sine functions of the form.

$$M_D = \text{sinc } 2\pi k\nu \cdot \text{sinc } 2\pi k\xi$$

where K = .025mm and ν and ξ are both expressed in mm^{-1}. Notice that the sinc function is non zero for values of ν and ξ larger than the cutoff which is the phenomenon of spurious resoltuion. The mtf of the f/24 optical relays is shown in Figure 3.1-18. Figure 3.1-17 is the mtf for an aberration-free lens. The f/96 mtf shown in Figure 3.1-19 is similar to the f/24 case except that it is assymmetric and generally of lower magnitude.

The mtf of the entire system is the product of the optics and of the detector. The detector requires a minimum input modulation to produce any detectable output modulation. That so-called threshold modulation can be determined by experiment, derived theoretically, or arbitarily set at some value like 10%. The intersection of the system mtf and the threshold modulation can be defined as the system resolution. Resolution is only one of many quality measures that have been derived from the mtf for various purposes.

The cutoff spatial frequency transmitted by the optics depends only on the wavelength and the f-number at the final image. The cutoff spatial frequency is of course higher than the highest resolved spatial frequency. At the test wavelength of 632.8nm the cutoff spatial frequencies for f/24 and f/96 are 27 and 6.75 line pairs (or cycles) per millimeter. Comparison with the detector cutoff of 40 cycles per millimeter shows more clearly our earlier statement that the resolution at f/24 is about equally limited by the detector and the optics and the resolution of f/96 is definitely limited by the optics.

3.1.5 System Performance

The performance of the Photometer is defined by the quality of its measurements in the areas of radiometry, spectral resolution, temporal resolution, and imagery. The spectral resolution is determined by the set of filters used; radiometric, temporal and imaging qualities are determined by the design and operational environment of the instrument.

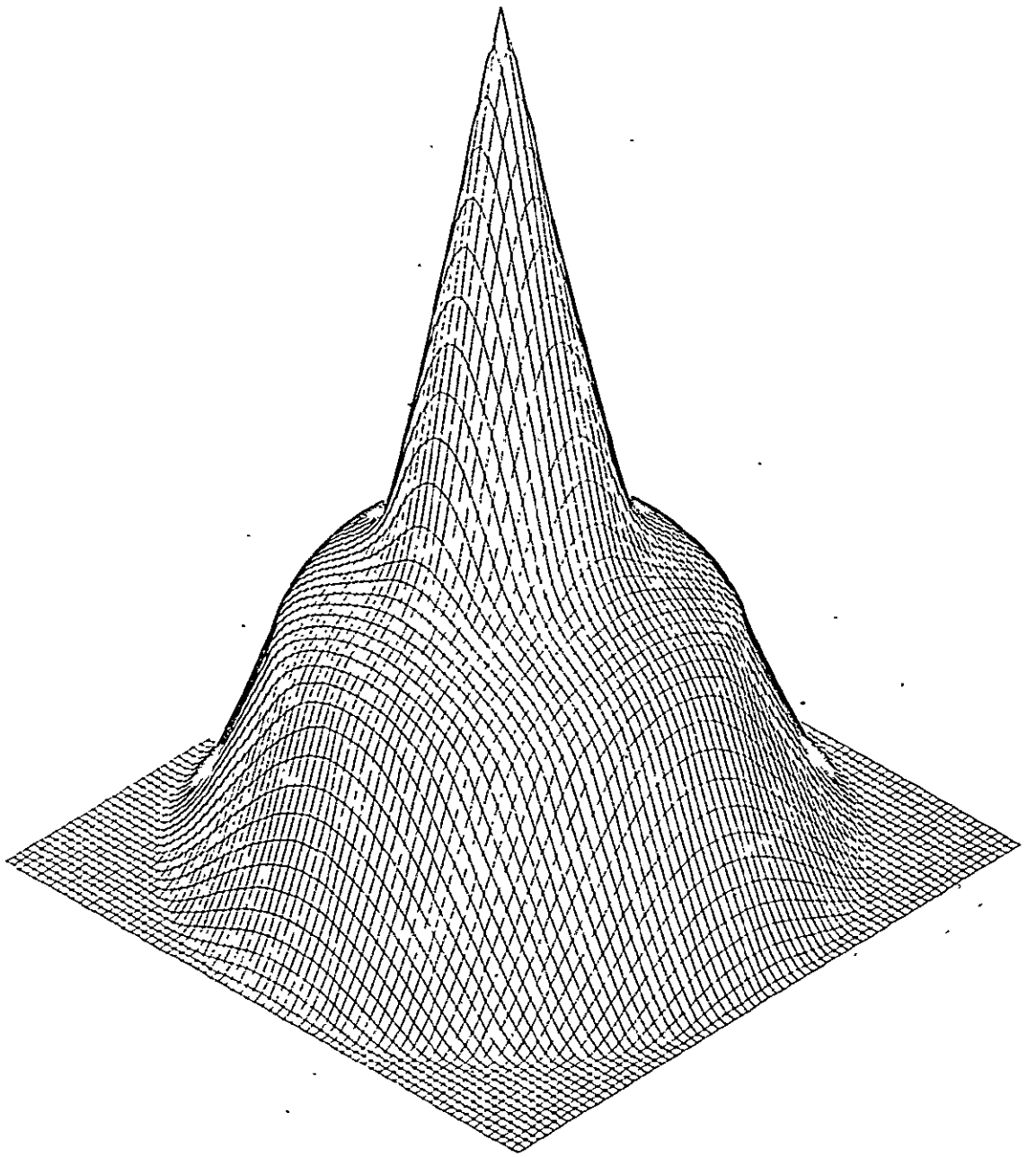

The mtf is two dimensional and rotationally symmetric because the slope of the exit pupil transmittance is a rotationally symmetric annulus. The "shoulder" is due to the central obstruction of the light. As is customary the mtf is normalized to unity at zero spatial frequency (the peak of the solid in the figure). The mtf drops to zero for a spatial frequency of about 27 mm^{-1}. The total width of the solid in the figure is 54 mm^{-1}.

Figure 3.1-17 Aberration-free f/24 Modulation Transfer Function

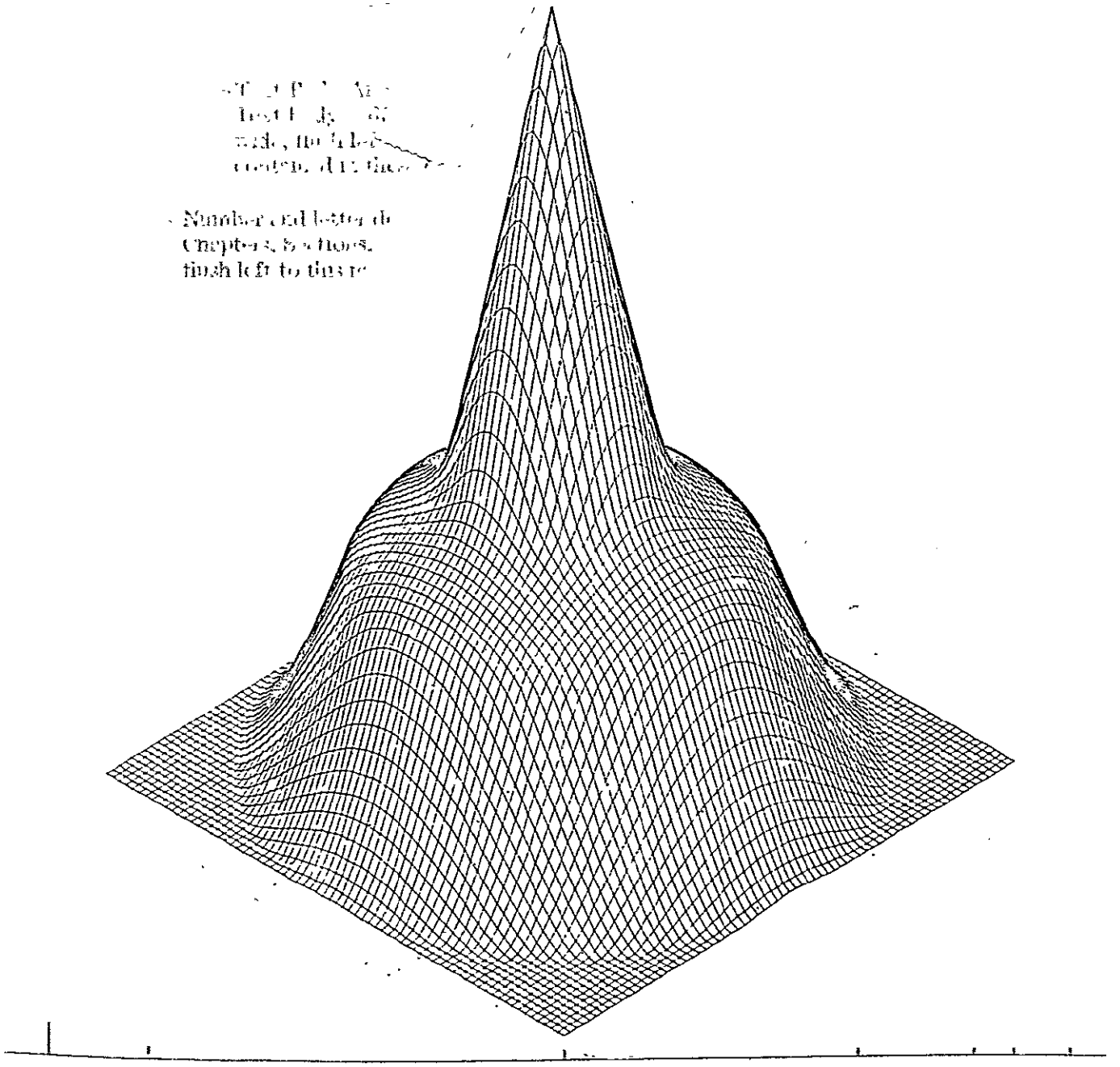

The mtf is just slightly rotationally assymetric because the wavefront error is not identically zero. The mtf is, however, very nearly identical to the perfect case shown in Figure 3.1-17 which is tantamount to saying that the f/24 design is diffraction limited. The peak height is unity (100% modulation transfer) and the horizontal width is again 54 mm^{-1}.

Figure 3.1-18 Actual f/24 Modulation Transfer Function

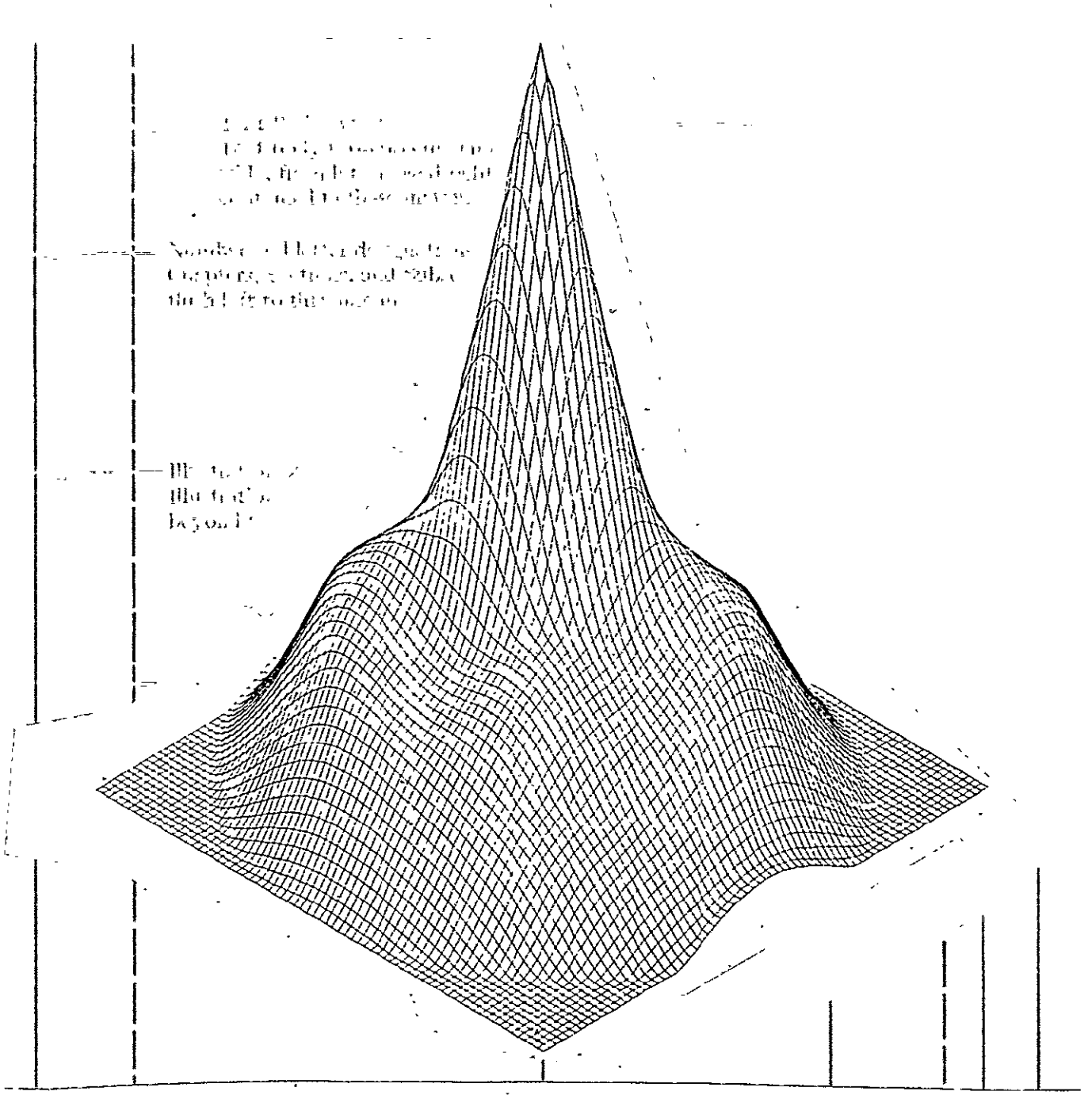

The mtf is not rotationally symmetric because the wavefront errors and corresponding point spread functions and spot diagrams are not symmetric. The general shape is similar to the perfect case and the "shoulder" due to the central obstruction is still apparent. The peak height is unity (100% modulation transfer) and the horizontal width is 14 mm^{-1} in one direction (front left to rear right) and 12 mm^{-1} in the perpendicular direction. The scaling is chosen by the computer plotting routine and is of no great significance.

Figure 3.1-19 Actual f/96 Modulation Transfer Function

3.1.5.1 Radiometry

The radiometric precision is equivalent to the signal-to-noise ratio of observation of a particular object when the observation is corrupted by noise from various sources. Let us consider point photometry mode.

The signal-to-noise ratio at the output of the point detection system is given by

$$SNR = \bar{n}_s / \left(\sum_{n} \bar{n}_n^2 \right)^{\frac{1}{2}}$$

where $\bar{n}_s$ is the average number of photon counts from the signal source (assumed to be stars against a background) and

$$\left(\sum \bar{n}_n \right)^{\frac{1}{2}} = \left(\bar{n}_s + \bar{n}_b + \bar{n}_d + \bar{n}_e \right)^{\frac{1}{2}}$$

where $\bar{n}_s$ is the mean signal count

$\bar{n}_b$ is the mean sky background count

$\bar{n}_d$ is the mean detector noise count from radiation noise and thermionic emission

$\bar{n}_e$ is the mean electronics noise count.

In terms of rates of counts and exposure durations we can write the signal-to-noise ratio as

$$SNR = r_s t / (r_s t + r_b t + r_d t + r_e t)^{\frac{1}{2}}$$

where r's are effective electron count rates.

The rate of arrival of signal counts depends on the irradiance at the entrance aperture of the telescope from the source, the collecting area of the telescope, the detector photocathode sensitivity (quantum efficiency) over the wavelength range of interest and the transmittance of the whole system. The transmittance depends on the reflectivities of all the surfaces in the light path, any bulk absorptivity or other losses of transmitting elements and the size and alignment of the Photometer entrance aperture with respect to the telescope's image.

The photoelectron count rate from a star of magnitude m is

$$r_s = AT\eta H$$

where A = collecting area of the telescope

T = transmittance of the whole optical system preceding the detector

η = the quantum efficiency of the detector

H = the star brightness

for the 2.4m LST

$$A = \frac{\pi D^2}{4}(1-\epsilon^2)$$

where D = the aperture diameter = 2.4m

ϵ = the diametral obstruction ratio = 0.3

so that

$$A = 4.117 m^2$$

The transmittance of the three optical surfaces used for point photometry is about $(0.95)^3 = 0.857$. Some of the image light is not transmitted into the Photometer because it falls outside the aperture. If we ignore the effects of inherent OTA aberrations (which reduce the transmittance of the aperture) and assume that the image is properly centered and focussed, then about 80% of the image light actually enters the Photometer. This gives the equivalent of a transmittance of 0.8. The transmittance of the whole system is thus 0.686 or less. Addition of spectral filters, polarizers, or misalignment, image motion or OTA deforms further reduces the transmittance. To be conservative we can take the transmittance to be 0.5 rather than attempt a more rigorous analysis.

The photoelectron rate is now

$$r_s = (4.117)(0.5)(0.2)(.2x10^{0.4(28-m)})$$

where the quantum efficiency has been set to 0.2 and where m is the visual magnitude of the star.

$$r_s = 8.234 \times 10^{9.2-0.4m}$$

The background radiance of the sky we take to be equivalent to one magnitude 23 star per square arc second. This gives a flux at the entrance of the telescope of about 17 photons per square meter per second per square arc second.

The projected area on the sky of the smallest entrance aperture is

$$\left[\left(\frac{72x10^{-6}m}{57.6\ m}\right)\left(\frac{\pi}{4}\right)\ \frac{180 \times 3600}{\pi}\ \text{arc second}\right]^2 = 0.041\ \text{arc second}^2$$

The telescope's collecting area times the LST transmittance is $2.06m^2$. The image irradiance is then (17)(0.041)(2.06) = 1.44 photons per second. The resultant photo electron count rate is $r_b = 0.29$ counts per second.

The detector noise from thermionic emission is about ten counts per second. The noise from radiation effects is far less certain. Extrapolating from OAO data for a larger photocathode we estimate ten counts per second. The electronics per second is about one. Thus the rms total noise is

$$\left(\sum \bar{n}\right)^{\frac{1}{2}} = (8.234\times10^{9.2-0.4m} + 1.44 + 10 + 10)^{\frac{1}{2}}$$

$$= (8.234\times10^{9.2-0.4m} + 21.44)^{\frac{1}{2}}$$

The signal-to-noise ratio is then

$$SNR = \frac{8.234\times10^{9.2-0.4m}\ t^{\frac{1}{2}}}{(8.234\times10^{9.2-0.4m} + 21.44)^{\frac{1}{2}}}$$

for bright stars (say m = 15)

$$SNR_B = \frac{8.234\times10^{3.2}\ t^{\frac{1}{2}}}{(8.234\times10^{3.2} + 21.44)^{\frac{1}{2}}} \doteq 119.2\ t^{\frac{1}{2}}$$

or in general $SNR_B = 2.87\times10^{4.6-0.2m}\ t^{\frac{1}{2}}$

for dim stars (say m = 30)

$$SNR_D = \frac{8.234\times10^{-2.8}\ t^{\frac{1}{2}}}{(8.234\times10^{-2.8} + 21.44)^{\frac{1}{2}}} = 8.46 \times 10^{-2}\ t^{\frac{1}{2}}$$

or in general $SNR_D = 1.78 \times 10^{9.2-0.4m}\ t^{\frac{1}{2}}$.

Figure 3.1-20 shows the signal-to-noise ratio as a function of target magnitude with exposure time as a parameter.

3.1.5.2 Coincidence Losses

Photo-electron arrival time statistics for ordinary (non-laser) light are Poisson. That is, if the average photon arrival rate is $\bar{n}$ photons per second than is an interval of length t seconds the probability of m photon arrivals is

$$P(m) = \frac{(\bar{n}t)^m \exp\ [-\bar{n}t]}{m!}$$

We wish to be able to observe bright stars which give a large number of counts per second without missing very many counts. Let us assume that the Photometer has limited time resolution. In other words if two photo-electrons occur within some short time interval to each other the counter will only count one rather than two photo-electrons. Such an error is called a coincidence loss.

For illustration let us take the minimum resolvable time interval to be 1 μs (1×10^{-6}s) and say that there can be two or more photon arrivals in 1μs only ten percent of the time.

$$\sum P(m) \leq 0.1 \left(P(0) + P(1) \right)$$

We wish to know what the maximum average photo-electron rate $\bar{n}$ is allowed to be.

$$P(0) = \frac{(\bar{n}t)^0 \exp\left[-\bar{n}t\right]}{0!} = \exp\left[-\bar{n}t\right]$$

$$P(1) = \frac{(\bar{n}t)^1 \exp\left[-\bar{n}t\right]}{1!} = (\bar{n}t) \exp\left[-\bar{n}t\right]$$

It is easy to see that $\sum_{m=0}^{\infty} P(m) = 1$ so that $\sum_{m=2}^{\infty} P(m) = 1 - (P(0) + P(1))$.

Thus $1-(P(0) + P(1) \leq 0.1 (P(0) + P(1))$

and $\frac{1}{1.1} \leq P(0) + P(1)$

or $P(0) + P(1) \geq 0.909090.....$

Substituting

$$F(\bar{n}) = \exp\left[-\bar{n}t\right](1+\bar{n}t) \geq 0.909090....$$

For $\bar{n}t = 0$ $F(\bar{n}) = 1$

and $\bar{n}t = 1$ $F(\bar{n}) = 0$

Successive approximations show that to avoid excessive coincidence loss $\bar{n}t \leq 0.04708$. And this implies that $\bar{n} \leq 4.7083 \times 10^4$ counts per second. Following the assumptions used in the signal-to-noise ratio computation $r_s + r_n \leq 4.7083 \times 10^4$ counts per second. Or $r_s \leq 4.7061 \times 10^4$ counts per second. That number of counts corresponds to a star of magnitude m_c where

$$4.7061 \times 10^4 = 8.234 \times 10^{9.2-0.4\, m_c}$$

$$5.715 \times 10^3 = 9.2-0.4\, m_c$$

$$m_c = 13.6$$

To observe stars of magnitude 7.5 as required the light must be attenuated by 6.1 magnitudes or a factor of about 275. Alternatively the time resolution would have to be increased by a factor of 275 which is possible but more difficult than attenuating the light.

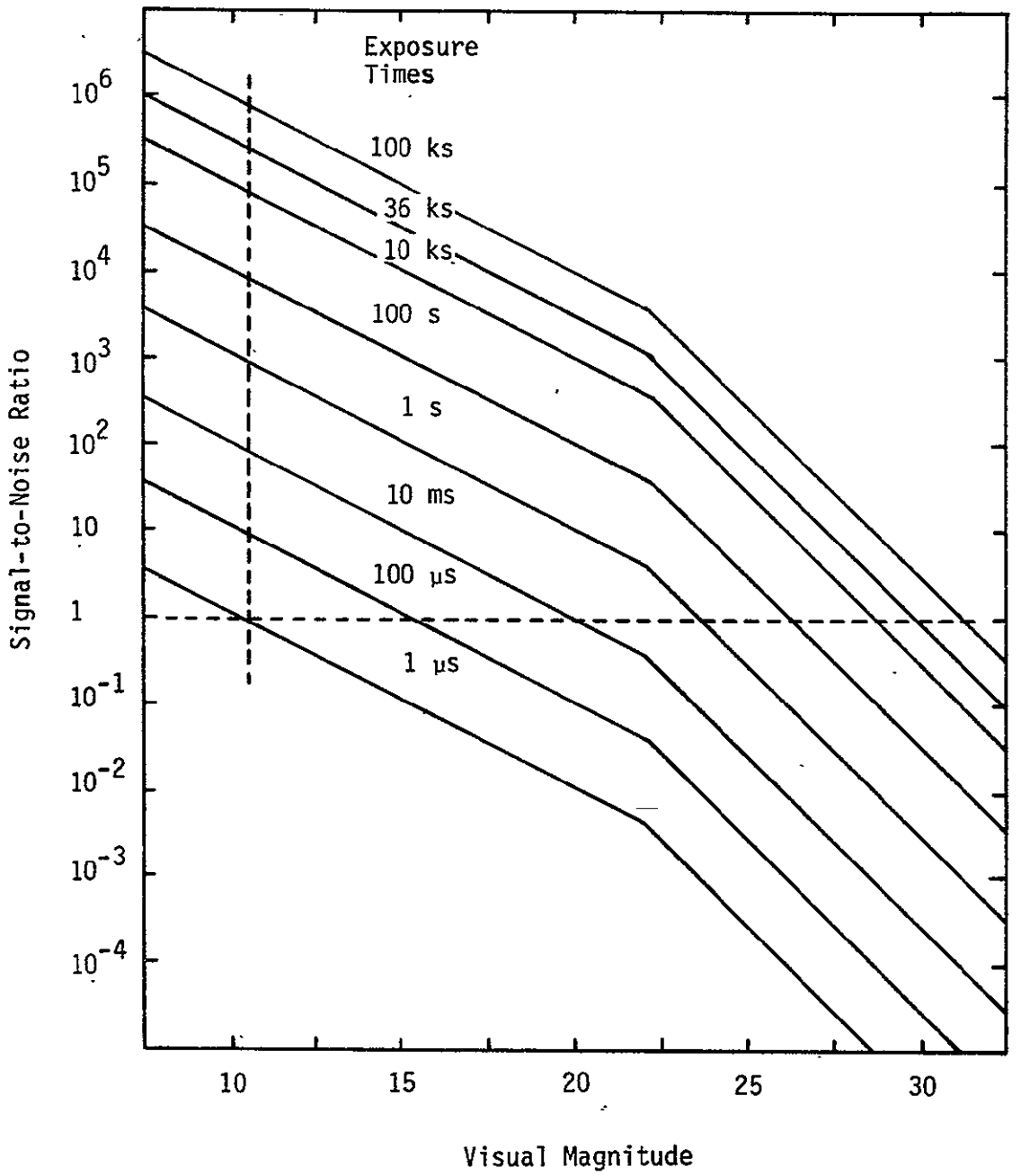

The family of curves of SNR versus magnitude have integration time as a parameter. The vertical dashed line at magnitude 11 is the coincidence loss limit above which stars are too bright for photon counting observation with a point detector. The horizontal dashed line is an SNR of unity. Notice that a curve is shown for an exposure time of 36 ks or 10 hours. That curve indicates that the limiting magnitude for a 36 ks exposure is about 27.5 with a signal-to-noise ratio of ten. The assumptions used to derive the curves are discussed in the text.

Figure 3.1-20 Signal-to-Noise Ratio Obtainable with Stars of Different Magnitudes

3.2 Structures

The Photometer and its primary and supporting structure, opto-mechanical and sensor systems, and associated electronics are contained within the boundaries of an Itek axial bay instrument. Figure 3.2-1 depicts the geometrical configuration, critical mechanical and electrical interfaces and our modular approach. The photometer axial bay module can be dissassembled into three separate subassemblies consisting of the following: (1) the structural housing, (2) the opto-mechanical submodule and (3) the electronics submodule.

3.2.1 Structural Housing - The structural housing is the box-like structure shown in Figure 3.2-1. The box fits within the allowed axial bay module envelope.

The structural housing is designed to: (1) enclose and protect the optics and associated electronics subsystems, (2) facilitate handling, installation, attachment and alignment to the OTA/Focal Plane Assembly, (3) provide primary hard points and load paths to accommodate preload forces induced by the locking mechanisms when attaching the Photometer to OTA/Focal Plane Housing, (4) provide a measure of contamination control by environmentally sealing the electronics and optics subsystems from exterior sources of contamination, and (5) provide mounting structure for brackets, clamps and other support hardware for electronics packaging and cable routing.

The Photometer (and other axial bay instruments) is supported near the OTA center-line at a point near the aft end and at two points on the forward plate near the plane of the Focal Plane Assembly. Each support point provides only two degrees of restraint assuring a statically determinate system. An alignment pin attached to the "christmas tree structure" engages the aft point, providing lateral restraint (y, z directions). Registration blocks attached to forward bulkhead stiffeners provide (a) axial restraint (x direction) and lateral restraint (z direction only) on one side and (b) lateral restraint (y, z directions) but no axial restraint in the x direction on the other side (Refer to Figure 3.2-2). Mechanical attachment is accomplished by seating the registration blocks with an over-center draw-down latch located near the forward end of module. The action of the draw down latch applies a controlled preload force to a centering lug pushing the structural housing toward the telescope centerline. Direct load paths are provided by an internal structural subsystem shown in Figure 3.2-3 referred to as the strongback assembly.

The primary functions of the strongback assembly are: (1) to stiffen and rigidize the housing on the discontinuous or open side which accepts the opto-mechanical and electronics modules, and (2) to provide a direct load path (axial loads, no bending) for clamp-up loads which are not radial. Inertia loads in the x and z directions are carried primarily by skin panels attached to spaced ring frames and to the lower mounting plate of the strongback assembly. For inertia loads in the y direction the skin panels support the opto-mechanical and electronics submodule by membrane action. Torsion loads introduced by eccentricity between C.G. and the aft reactive point is resisted by the two forward registration fittings and the damping lug interface. The bulkhead frame at the aft support (at alignment fitting)

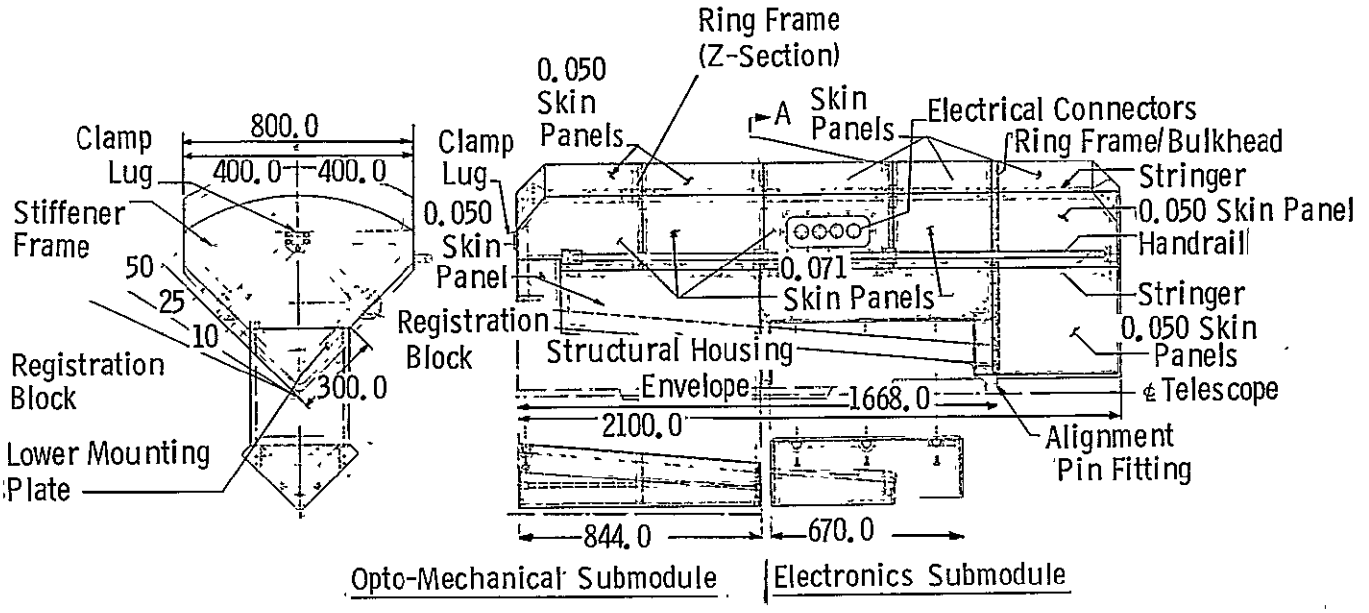

Opto-mechanical and Electronics submodules can be easily detached from the structural housing to facilitate optical alignment and bench checkout. The submodule attachments are statically determinant to prevent optical alignment changes whether attached or not.

Figure 3.2-1 Separation of Submodules from the Structural Housing

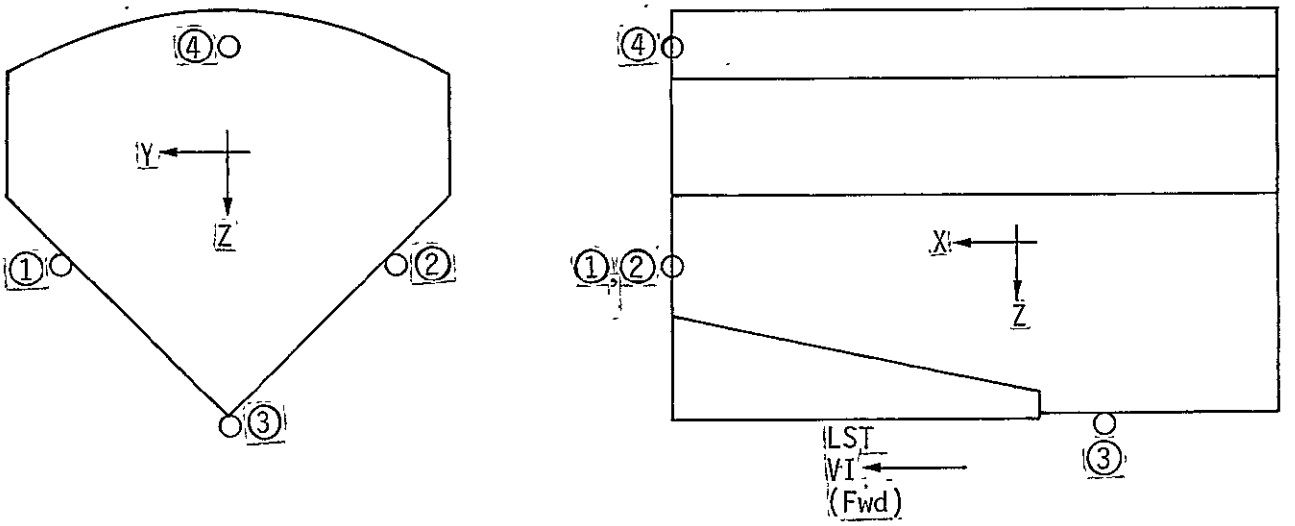

The positions of the Photometer locating devices are shown. Load estimates are presented in Table 3.2-1.

Figure 3.2-2 Structural/Mechanical Interface of Photometer to Focal Plane Assembly

Available Text and Illustration Image Area (including titles): 51 elite lines

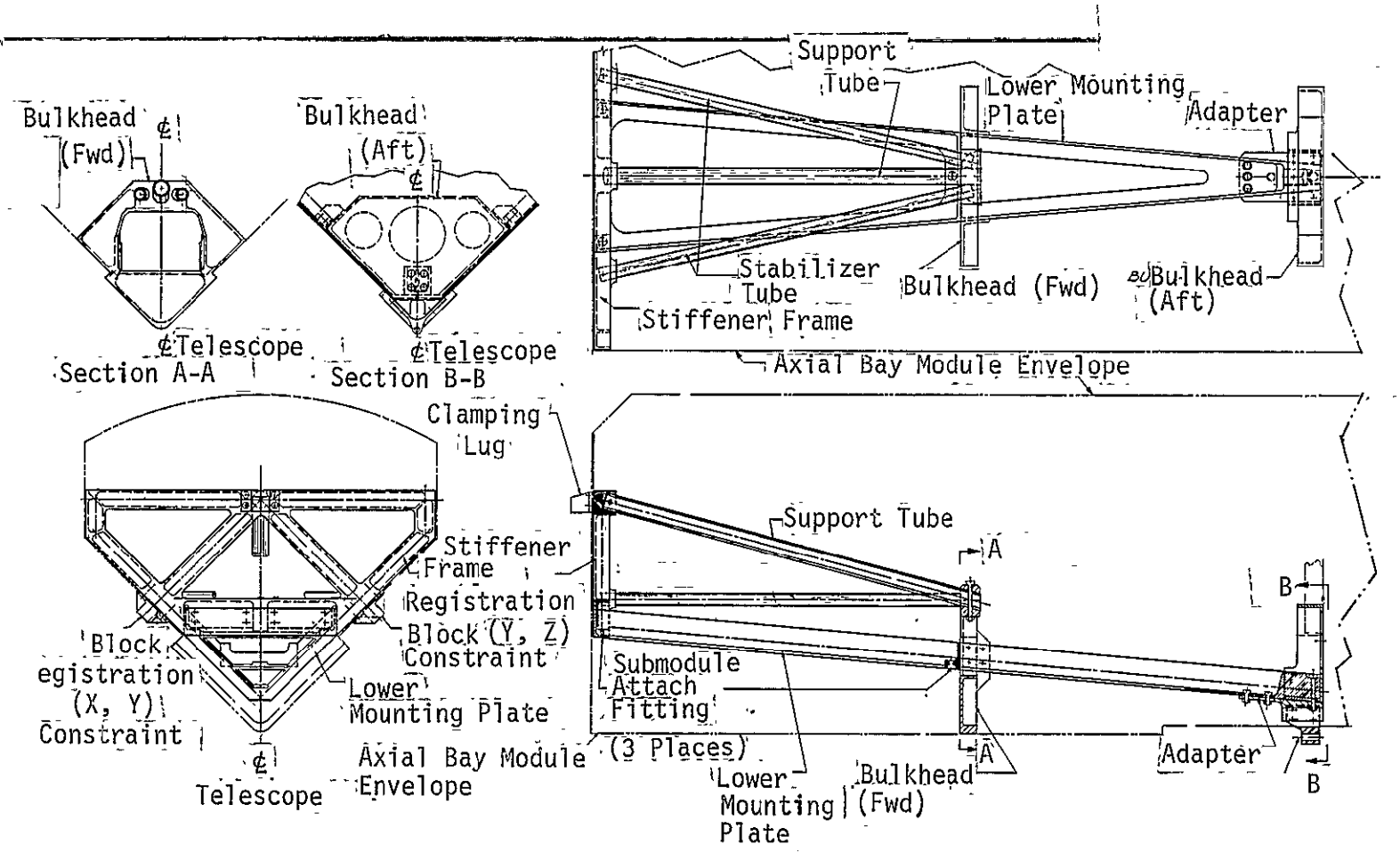

The strongback internal structure of the structural housing stiffens and makes rigid the open side of the housing which accepts the opto-mechanical and electronics submodules and provides direct load paths for the clamp-up preloads used to resist launch loads.

Figure 3.2-3 Strongback Assembly

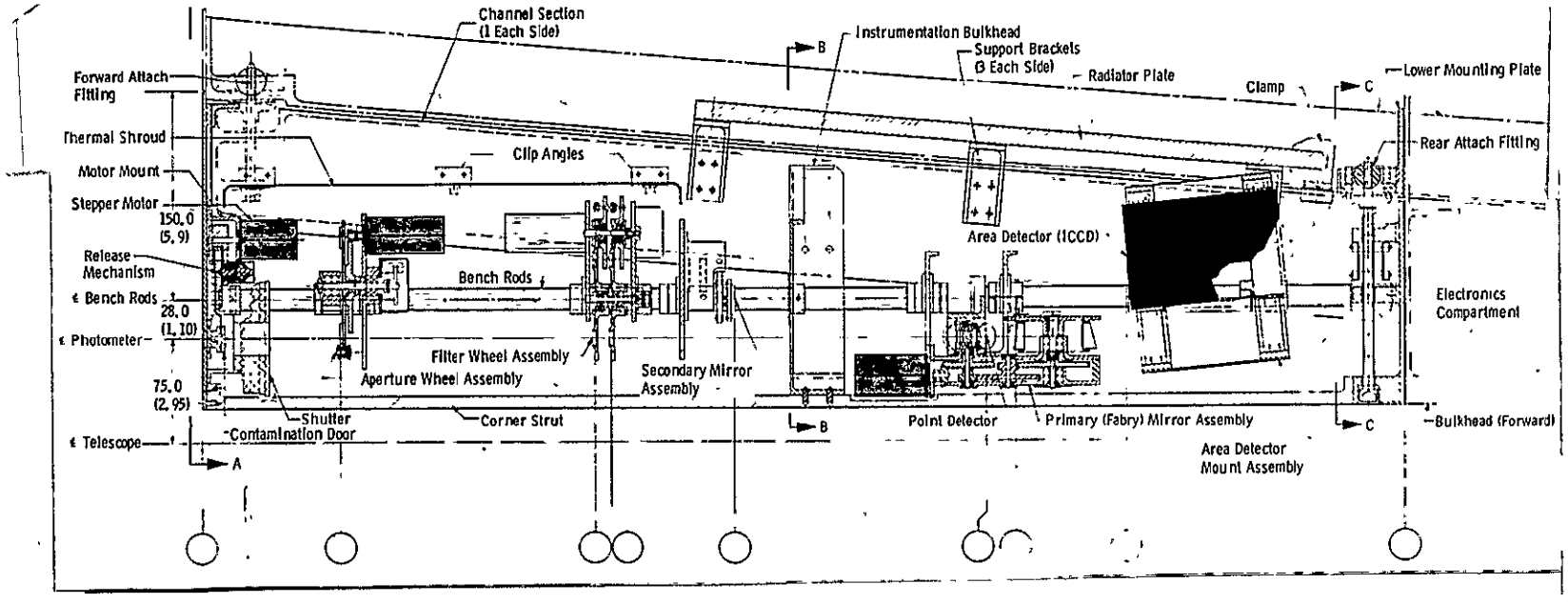

The opto-mechanical submodule has ample structural stiffness to maintain optical alignment during ground operations including alignment, bench checkout, testing, and transportation. The submodule is a tapered triangular prism defined by two lengthwise panel sections, an apex beam, and two rigid invar end plates. The optical bench rods run the length of the submodule and are held in position by the end plates and an intermediate bulkhead.

Figure 3.2-4 Opto-mechanical Submodule

TABLE 3.2-1 Design Limit Interface Loads

LOAD CONDITION	LOAD APPLIED TO OTA INTERFACE (kN)[1]						
	$\bar{P}_{①x}$	$P_{①z}$	$\bar{P}_{②y}$	$\bar{P}_{②z}$	$\bar{P}_{③y}$	$\bar{P}_{③z}$	$P_{④z}$
PRELOAD	0	1516	0	15.6	0	0	-31.3
PRELOAD + 10 G's X	8.04	1516	1606	1516	-1606	0	-31.3
PRELOAD - 10 G's X	-8804	1516	-1606	1516	1.06	0	-31.3
PRELOAD + 10 G's Y	0	1855	3893	1278	411	0	-3038
PRELOAD - 10 G's Y	0	1278	-3893	1855	-411	0	-3038
PRELOAD + 10 G's Z	0	16.6	0	1636	0	411	-2933
PRELOAD - 10 G's Z	0	1497	0	1497	0	-411	-3332

NOTE: Refer to Figure 3.2-2 for load locations and sign convention.

3.2 (Continued)

rigidizes the box cross-section and distributes the aft reactions into the box skin panels.

The stiffener frame provides for the attachment of two stabilizer tubes (25 mm dia x 2.5 mm wall thickness), one support tube 38 mm dia x 3 mm wall thickness), and the lower mounting plate. The lower mounting plate is essentially a beam spanning from the stiffener frame to the aft alignment pin fitting. It is machined from a single plate of 2024-T4 aluminum. The primary function of the lower mounting plate is to provide in-plane lateral and longitudinal stability for the attachment of the opto-mechanical submodule.

Mechanical attachment of the opto-mechanical submodule to the structural housing is accomplished by installing threaded fasteners into special fittings designed to provide only two degrees of freedom at each of three attachment locations. This approach gives a statically determinant structure. These fittings, incorporated in "beefed-up" sections of the lower mounting plate, are designed to allow rotation in any direction, precluding the introduction of bending moments into the opto-mechanical submodule. In addition all attachments provide reactive points and restraint in the z direction. One of the forward attach fittings and the aft attach fitting provides lateral (y direction) restraint while the other forward attach fitting provides longitudinal (x direction) restraint. The degree of freedom at each attach point is provided by a high-precision ball slide assembly which serves as a carrier for an internally threaded spherical ball. The threaded ball receives the whole threaded portion of a high torque bolt assembly on the opto-mechanical submodule. Worth noting is an alternate approach to providing only two degrees of restraint at the attach point which features a standard rod end bearing which allows approximately 10^{o} misalignment. Although this approach takes somewhat more space it is more conventional and friction free.

A bulkhead machined from 7075-T6 aluminum alloy separates the opto-mechanical submodule from the electronics module. This bulkhead is attached directly to the lower mounting plate, support tube and stabilizer tubes. A second bulkhead is placed aft of the electronics submodule at the transition in the axial bay module. This bulkhead facilitates assembly of the structural housing and encloses the electronics.

The aft end of the strongback assembly terminates at the intersection of the support tube and the lower mounting plate. An adapter fitting allows the installation of the alignment pin fitting. The overall strongback configuration comprises a stiff truss structure capable of accommodating clamp-up preloads and launch loads without excessive deflections.

Using the strongback assembly as the primary structure, the remainder of the structural housing is conventionally framed with ring stiffeners and longitudinal stringers which allow installation of .050 in thick 6061-T6 aluminum panels. Stringers and frames are also fabricated from 6061-T6 aluminum.

3.2.2 Opto-mechanical Submodule - Maintaining the alignment of the Photometer optical system is extremely important to the overall performance of the instrument. To assure satisfactory performance thermal and structural interaction between the optics systems and the primary structural enclosure must be held to acceptably small levels. Our approach employs a detachable submodule which is a totally self-contained, operational unit and can be easily checked out, tested, calibrated and aligned. Figure 3.2-4 shows in a sectional view, the opto-mechanical submodule including the opto-mechanical subassemblies. The submodule has ample structural stiffness by itself to withstand ground operations including bench checkout, alignment, testing, and transportation.

The basic submodule consists of a compartment approximately 853 mm long, which is triangular in cross-section to fit into the axial bay module envelope. Invar end-plates are connected and held torsionally rigid by channel shaped sections at each side and by a corner angle near the apex of enclosure. Removable side panels (two on each side) complete the closure.

All of the mechanisms, sensors and optical elements are mounted directly to two parallel "optical bench rods" which provide continuous longitudinal support. The rods are fabricated from graphite-epoxy composite, a material of extremely low coefficient of thermal expansion ($\alpha = 0.18 \times 10^{-6}$ mm/mm°C) to assure adequate longitudinal stability in a variable thermal environment.

Special "bosses", machined on the interior surface of forward closure plate have reamed holes which accept one end of each bench rod. The bench rods are inserted into these holes with a light drive fit and pinned to provide a rigid attachment. Separation distance between holes is held constant by the thermally stable Invar closure plate. The pair of bench rods are further supported by flexure attachments at the aft closure plate and by an intermediate bulkhead stiffener. (Refer to Section 3.2.4 and Figure 3.2-5). The flexural attachments are bolted to sleeve sections which guide and separate the bench rods. Flexures are "soft" parallel to the length of the rods (x direction) but provide restraint in the perpendicular plane (y, z). This approach allows the longitudinal channel sections to change length due to temperature differences without affecting the length, parallelism, or separation of the optical bench rods.

The removable side panels are fabricated from 6061-T6 aluminum sheet with thickened sections at edges for accepting countersunk screwheads. The average thickness of these panels is 0.100 cm (0.040 in.). The longitudinal channel sections and corner angles will be machined from 7075-T73 aluminum bar stock. Anchor nuts are installed to stiffeners where required to accept panel fasteners.

The interior walls of the opto-mechanical submodule are insulated with multilayer aluminized mylar insulation attached directly to the removable panels.

The two channel sections and corner angle are fabricated from 7075-T73 aluminum alloy.

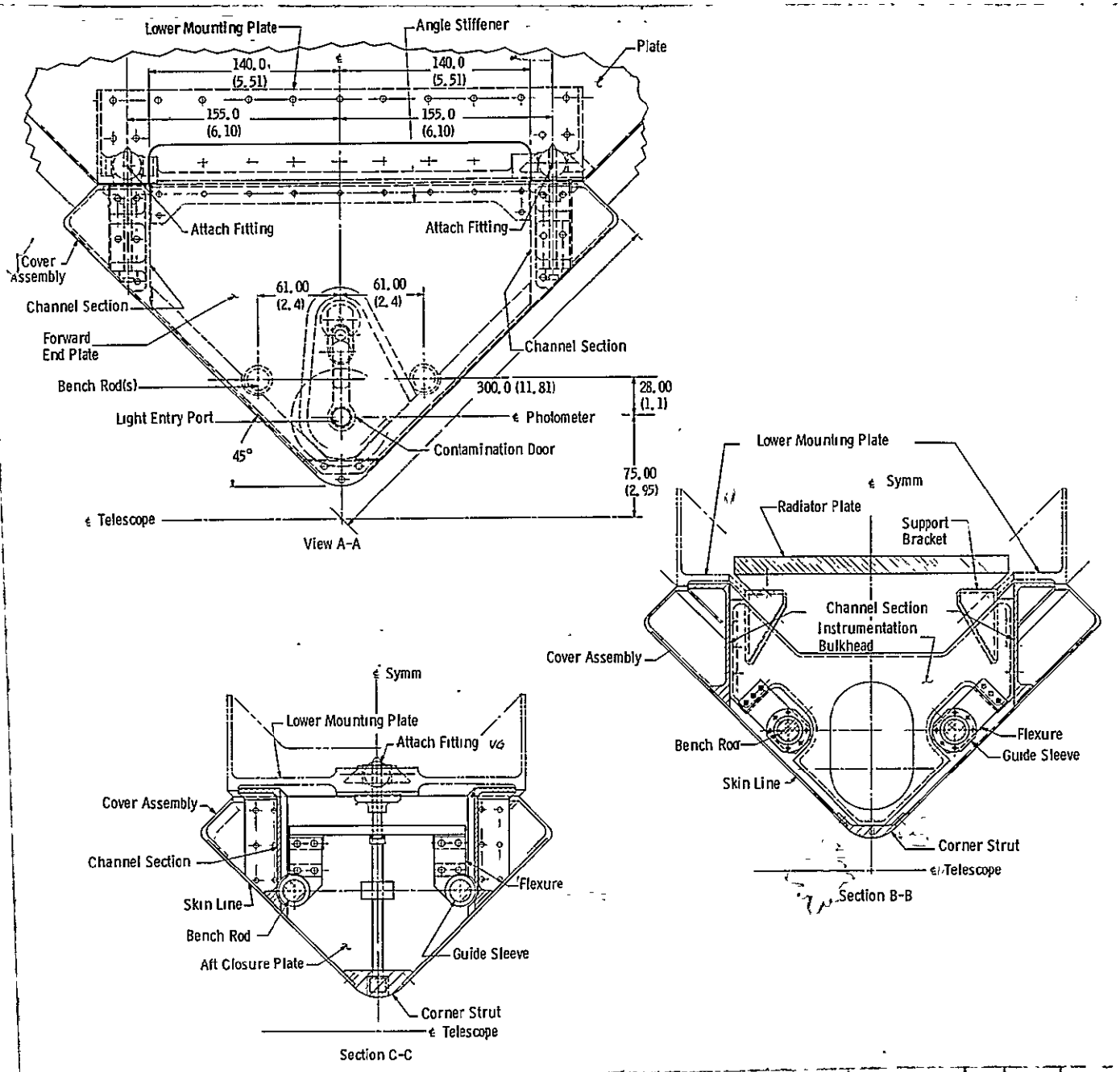

The graphite-epoxy composite bench rods are pinned to the forward plate (View A-A), and attached by longitudinally soft flexures at the intermediate and aft bulkheads (Views B-B and C-C). The opto-mechanical submodule can deform thermally without applying longitudinal strains to the optical bench rods which would adversely affect image quality.

Figure 3.2-5 Bench Rod Attachments to Forward Plate, Intermediate and Aft Bulkheads

3.2.2 (Continued)

Attachment of the opto-mechanical submodule to the structural housing is accomplished by engaging three 0.250 in. diameter threaded bolts through special fittings integrally machined on the undersurface of the strongback mounting plate. These three mechanical attachments constitute a statically determinate system which provides freedom for the structural housing to flex or twist along its longitudinal axis without inducing distortion into the opto-mechanical module itself.

3.2.3 Electronics Submodule - Packaging the electronics within a separate, detachable module facilitates the assembly and checkout of the electronics and internal power supplies. The electronics submodule conforms to the presecribed envelope in its outboard configuration, blending with the contours established by the structural housing. Structurally, the self-contained unit consists of forward and aft machined plates which slip between the two lower bulkhead fittings of the structural housing with an overlapping fit. Longitudinal stiffeners on each side and at apex of triangular box along with fixed skin panels complete the enclosure. Attachment of electronics submodule to the structural housing is accomplished by engaging six bolts (3 each side) into threaded bosses integrally machined into edge stiffeners spanning the two lower bulkhead fittings. Required electrical connections are made prior to mechanically attaching the submodule to the structural housing. It is necessary to arrange the electronics subsystem packages such that they will clear the lower mounting plate of the strongback assembly when in operational position. Under this constraint all electrical components must be mounted directly to the enclosing skin panels. This approach opens up the center portion for cable routing and connections.

3.2.4 Stress Analysis - Deformations - The structural stability requirements of the opto-mechanical submodule have exerted the primary influence on our structural preliminary design. Yield and/or ultimate allowable values were utilized where strength, stability or resistance to buckling was the critical factor as opposed to Precision Elastic Limit design where precise mechanical or optical alignment was the driving consideration. All allowable stress levels are based on material properties outlined in MIL-HDBK-5B.

Safety factors adopted for the photometer stress analysis were 2.0 using allowable yield stress values and 3.0 on ultimate stress allowables. These somewhat conservative values are justified since no weight constraints have as yet been imposed and the structural integrity of the photometer will be verified by analysis rather than structural load tests for a significant program costs saving.

In structural subsystems closely associated with primary optical systems, dynamic stress levels induced during launch must be maintained at levels below the micro-yield strength of the material to preclude permanent plastic deformation which could adversely affect precise alignment of optical components. Micro-yield strength of a material is defined as the sustained

3.2.4 (Continued)

stress level necessary to cause a permanent strain of 1 μ m/m in the material under load. In order to assure that micro-yielding will not occur at anticipated load conditions, an additional safety factor of 2 was applied to the yield factor of safety for a total F.S. = 4 on yield value where microyield is critical. Although arbitrary, this approach was considered satisfactory for preliminary design stress evaluation. Structure distortions occurring during launch and reentry do not degrade instrument performance provided no permanent set or microyielding is experienced, since instrument is non-operational during this period.

Critical loading conditions which provided basis for stress analysis were: (1) 1.0 g condition during ground checkout, alignment and calibration, (2) preloading operation during installation and lock-up of axial bay module to Focal Plane Support Structure, (3) thermal cycling during operational phase, (4) transient loads caused by random vibration during launch and reentry and (5) pressure differential loads occurring during venting and/or purging operations.

The optical bench rods located in the opto-mechanical submodule provide the primary support and alignment for the optics and sensors. Stiffness, strength and low-coefficient of thermal expansion are vital considerations in the design of these rods. Three materials; graphite-epoxy, 7075-T73 aluminum and Invar were considered for fabrication of the optic bench rods. Graphite-epoxy, because of its ideal thermal expansion stability and high strength-to-weight ratio has been used. Random vibration loads produce working stresses in the rods of 4725 $N\text{-}cm^{-2}$ (bending) which is less than the allowable limit stress of 17,250 $N\text{-}cm^{-2}$. The maximum deflection in the rod due to a 1.0 g load (valid during ground checkout and alignment) is 65 microns which is less than 100 μm permissible according to alignment criteria specified in section 3.1.4.3. The bench rods are rigidly pinned at the forward end of opto-mechanical submodule. Additional rod support is provided by guide sleeves and flexures at the approximate midspan and opposite end of each rod. The "flexures" are soft in the longitudinal direction while providing a positive, rigid restraint in the lateral directions. Longitudinal expansion of the structural enclosure for the opto-mechanical submodule due to temperature excursions causes the flexures supporting the bench rods to translate longitudinally. Due to the extremely low stiffness of flexures in this direction, only a very small axial load is imparted through the flexures to the bench rods. A temperature difference of 10°C changes rod length by a total of 0.6 μm which is well within the allowable 4 μm deduced in Section 3.1.4.3.

The loading condition which governed the design of the structural housing are the 10 g random vibration loads and the clamping loads associated with the attachment of axial bay module to focal plane support structure. The structural housing supports the opto-mechanical submodule, the electronics submodule and its own weight by membrane and shear stresses in the external skin panels. Buckling of the skin panels is the governing factor with typical working stresses of 260 $N\text{-}cm^{-2}$ (compression) and 740 $N\text{-}cm^{-2}$ (shear). These working stresses are applied against allowable working stresses of 610 $N\text{-}cm^{-2}$ in compression and 1000 $N\text{-}cm^{-2}$ in shear.

3.2.4 (Continued)

The stiffener frame located at the forward end of the structural housing (adjacent to focal plane assembly) reacts the applied "clamp-up" force of 4800 N with a working stress of 2520 N-cm^{-2} in the strut against an allowable of 11,470 N-cm^{2}. Movement of the opto-mechanical submodule occurs as the preload force is applied to the clamp lug. This preload produces a lateral translation of 36.3 m in the y direction and a rotation of the photometer centerline of 22 μ radians. Both values are within acceptable limits.

The structural housing was investigated for effects of pressure differential. Results indicate that the baseline configuration can withstand 0.031 N-cm^{-2} differential pressure or greater than 4 times the required 0.070 N-cm^{-2} differential.

The use of the strongback structural subsystem in our configuration provides a means of controlling load paths from external forces applied through the clamping lug, the registration blocks and the alignment pin fitting. By restricting all loading to direct tension or compression and minimizing internal bending loads, deflections and thus distortions causing misalignment are reduced greatly. In addition the strongback provides a control surface for attachment of the opto-mechanical submodule.

3.2.5 Dynamics - We studied the relative internal motions of the Photometer caused by motion inputs from the environment. The particular disturbances considered were reaction wheel unbalance in the LST pointing control system and motion of the Photometer aperture wheel.

The results indicate maximum angular motions of the parts of the instrument to be 7.6 nrad for reaction wheel unbalance and 0.48 μ rad for aperture wheel torques.

Approach

To determine the motions of the parts, we developed a structural dynamic mathematical model. This model treats only the optical bench and makes the implicit assumption that the housing to which the bench is mounted is rigid.

A sketch of the model, its geometry and mass distribution is shown in Figure 3.2-6. The model is a simplified version of the real structure of the photometer. In the actual hardware the pieces are redundantly connected to the graphite epoxy rods. This additional stiffness was ignored in the analysis that follows, hence adding a degree of conservatism.

The additional assumption that the Photometer structural housing is rigid seems reasonable at this point in the design phase. The housing is triangular in cross-section package. Figure 3.2-4 is a sketch of the housing cross-section showing the optical bench rods.

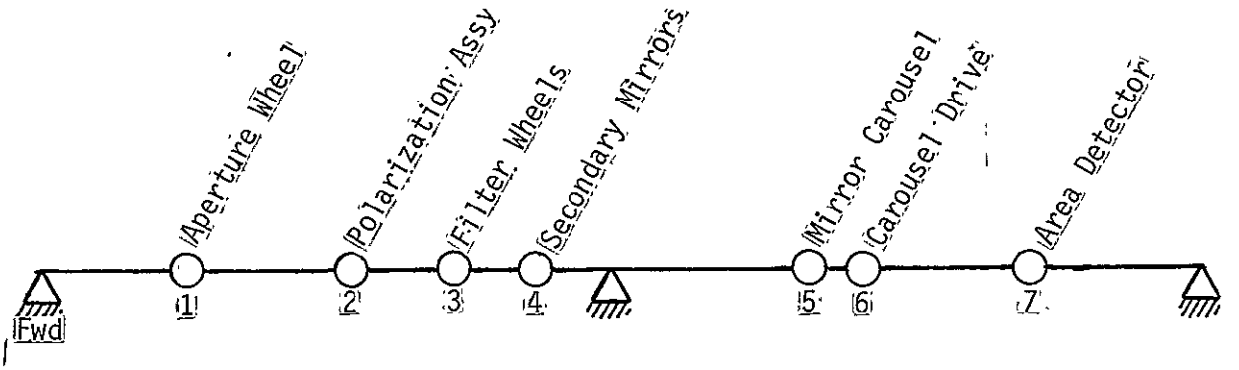

Item	Mass, kg	Inertia, kg-cm^2
Aperture Wheel	0.68	8.8
Polarization Assy (Optional)	1.13	14.6
Filter Wheels	0.91	11.7
Secondary Mirrors	0.23	0.7
Mirror Carousel	0.45	2.9
Carousel Drive	0.57	7.3
Area Detector	2.83	36.6

The masses and relative locations of components on the bench rods are shown as they were applied to a mathematical model. The rods were taken to be 1.6 cm in diameter and have a modulus of 7×10^6 kg-cm^{-2}.

Figure 3.2-6 Optical Bench Rod Mass Distributions

3.2.5 (Continued)

Mass and stiffness data from the mathematical model were used to calculate the undamped natural frequencies and mode shapes. The three lowest frequencies and their associated mode shapes are illustrated in Figure 3.2-7. The fundamental frequency is 172 Hz. This frequency is higher than those appearing in the environment.

The most significant motion inputs to the Photometer are due to momentum wheel unbalance forces which drive the whole LST continuously. Other inputs to the system (tape recorder, aperture doors moving, etc.) are short time phenomena, hence, will not affect the long time integration of the photometer. The momentum wheel unbalance forces are limited in frequency to 50 Hz. When wheels reach 50 Hz, they are despun to 0 Hz. It is good that the fundamental frequency of the photometer is 172 Hz. Disturbing motions are of lower frequencies. The Photometer does not exhibit large resonant amplification.

The Photometer responds essentially statically in the frequency range of its motion inputs. The equations of statics for a mode driven by an acceleration input is

$$\omega_i^2 \xi_i = - \phi_i^T M T \ddot{q}_b$$

where ω_i^2 = circular frequency squared of the ith mode

ξ_i = modal displacement of ith mode

ϕ_i^T = ith mode shape transposed

M = model mass matrix

T = rigid body transformation

$\ddot{q}_b$ = acceleration of supports of bench

The largest coupling coefficient ($\phi^T MT$) exists for the first mode due to angular motion inputs and has a value of 2.587. Maximum expected motion inputs calculated from a previous 3.0 meter LST model were 9.25×10^{-8} radians. Assuming the first mode to occur at 25 Hz results in maximum rotations of the model pieces listed in Table 3.2-2.

The maximum relative rotational motion was between elements 4 and 7 (area detector secondary mirror mounts and the area detector) and was 7.6 nrad.

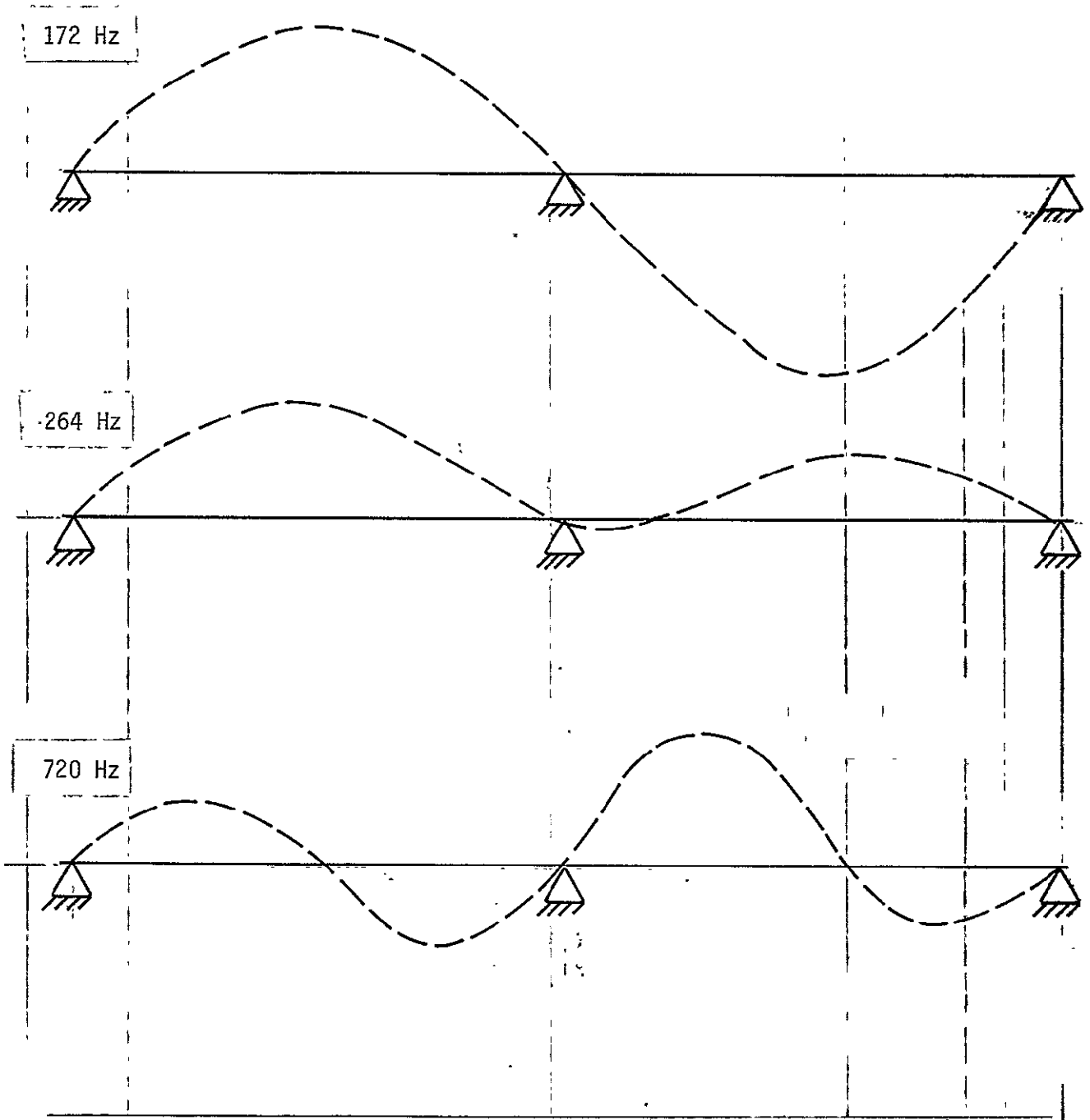

Shapes of the optical bench rod bending modes were computed and are shown greatly exaggerated. The rods were restrained forward, aft and near their midpoint.

Figure 3.2-7 First Three Bench Rod Bending Modes

TABLE 3.2-2 Optical Bench Rod Dynamic Motions

Model Piece	Rotation nrad	Displacement m
1	-3.37	4.21×10^{-4}
2	-6.20	6.07×10^{-4}
3	2.47	5.21×10^{-4}
4	4.23	3.05×10^{-4}
5	3.85	-6.33×10^{-4}
6	2.96	-7.20×10^{-4}
7	-3.34	-7.17×10^{-4}

We also calculated the response of the optical bench to the torque applied to the aperture wheel. The torque of 0.072 kg-cm was assumed to be 0.07N of force so that it may be applied to the beam model available. This gives an order of magnitude estimate of the problem. A typical torque time history is shown below,

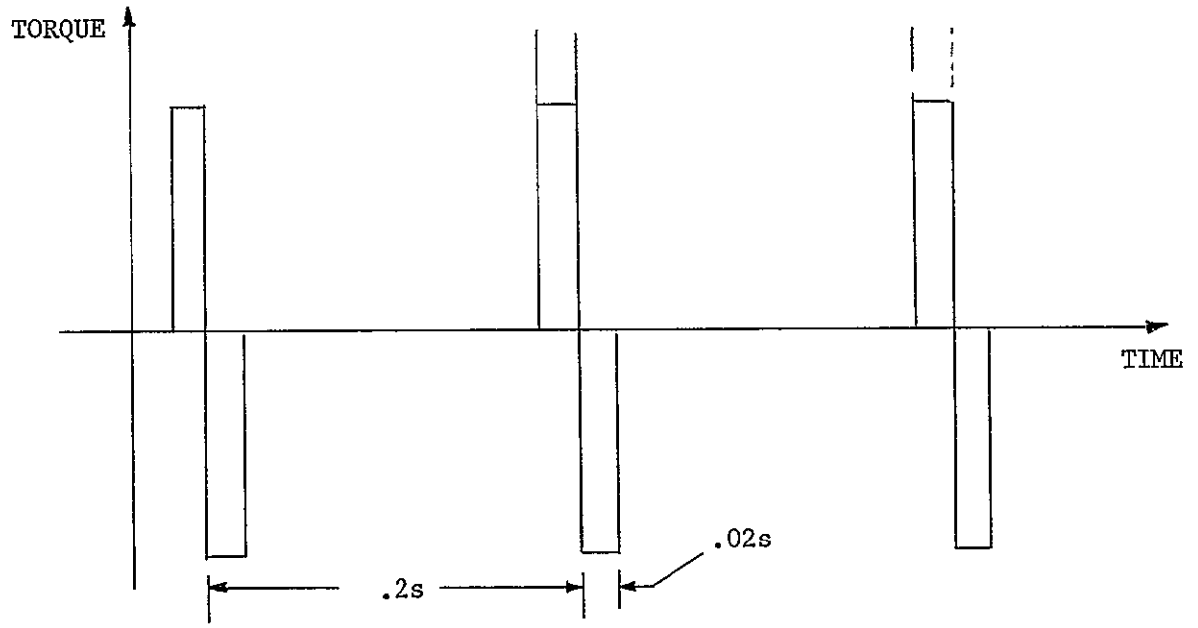

The response of the 172 Hz mode to this type of forcing function is given by a series of responses of the type

$$\xi(t) = \frac{1}{\omega^2}\left(1-\cos\omega t\, e^{-\rho\omega t}\right)$$

Where ρ = damping ratio (assume .0001)

ω = circular frequency

For the forcing function shown, this yielded a peak value of rotation of 0.5 μ rad. This will decay at a rate of 64% every 10 seconds. Hence, at 10 seconds would be 0.17 μ rad, at 20 seconds would be 0.06 μ rad, etc.

Damping is not yet known but we feel the above estimate is realistic. The damping will not have a significant effect on the response - only on the time to decay.

The results are qualified by the assumptions made in arriving at them. The design is still preliminary and should be reviewed if the results presented above are critical in the instruments operation.

3.2.6 Materials - Material selection, evaluation and testing as well as development of materials processes is an essential function of the Photometer instrument design/development program.

We selected only structural materials which are well within the "State-of-the-Art". High resistance to stress corrosion cracking, low coefficient of thermal expansion, ease of machinability and fabrication, economy and availability are some of the specific factors considered in the selection of materials for specific applications. Table 3.2-3 summarizes the materials to be used for structural application in the Photometer.

Nonstructural metallic applications include bronze for bushings and plain bearings and copper for thermal conduction.

Table 3.2-4 summarizes selected nonmetallic materials for possible use in the Photometer.

3.2.7 Mass Properties - The total estimated weight of the Photometer instrument assembly, including the structural housing, opto-mechanical submodule, the electronics module and associated cabling, bracketry, fasteners and interface hardware is 91 kg (201#). A +5% contingency allowance is included in this weight estimate for growth potential. A summary of weights by subassembly is shown in Table 3.2-5. C.G. locations are shown in Figure 3.2-8.

TABLE 3.2-3 Structural Materials

Material	Modulus of Elasticity $kg/cm^2 \times 10^6$ ($psi \times 10^{-6}$)	Density gm/cm^3 (lb/in^3)	Yield Stress $kg/cm^2 \times 10^3$ ($psi \times 10^{-3}$)	Thermal Expansion Coefficient $1^oC \times 10^6$ ($1^oF \times 10^6$)	Application
Aluminum					
2024-T4	.74 (10.5)	2.77 (.100)	2.82 (40.0)	23.2 (12.9)	Spur gears
2024-T851	.74 (10.5)	2.77 (.100)	4.08 (58.0)	23.2 (12.9)	Machined frames
6061-T6	.71 (10.1)	2.71 (.098)	2.46 (35.0)	25.2 (14.0)	Skin panels
7075-T73	.74 (10.5)	2.80 (.101)	3.94 (56.0)	23.4 (13.0)	Machined frames
Graphite Epoxy					
	1.06 (15.0)	1.58 (.057)	4.93 (70.0)	0-.18 (0-.10)	Optical bench rods
Steel					
303 CRES	2.05 (29.1)	7.92 (.286)	*	14.9 (8.3)	Shear pins, shafts
440 CRES	1.97 (28.0)	7.76 (.28)	*	11.7 (6.5)	Bearing races
17-4 PH	2.01 (28.5)	7.81 (.282)	*	10.8 (6.0)	Springs, flexures
A-286	2.05 (29.1)	7.94 (.287)	6.68 (95.0)	16.6 (9.2)	High strength mechanical fasteners
Invar	1.41 (20.0)	8.03 (.290)	2.81 (40.0)	1.26 (0.7)	Optical hardware supports
Unispan LR-35	1.41 (20.0)	8.03 (.290)	2.81 (40.0)	.63 (0.35)	Optical hardware supports
Titanium					
6 Al-4V	1.13 (16.0)	4.43 (.160)	8.46 (120)	9.5 (5.3)	Support bracketry

*Will vary on specific application and hardness required

TABLE 3.2-4 Non-metallic Materials

Material	Specification	General Applications
Nonmetallics		
Epoxy Adhesive EC 2216 B/A	MMC M358	General Flexible Structural Bonding
Epoxy Adhesive EA 934	MMS M434	General Structural Bonding
Epoxy/Glass Laminate	MMS A268	Structural Isolators
Flouroelastomer Viton 747-70	Commercial	Seals
Flouroplastic Teflon TFE	MMS B636	General Use Plastic (nonstructural)
Glass (low α)	Commercial	Mirrors, Filters
Perfluoronated Grease Braycote 813	Commercial	Peroutgassed Lubricant, Used "Silver" Filled
Polyterapthalate Mylar	Commercial	Super Insulation Component
Polyamide Plastic Vespel Sp-1	EMC A505	Structural Isolators - General Structural Plastic
Polyester Adhesive	MMS M173	Securing Enclosed Fasteners
Magnesium Flouride	Commercial	UV Transmitting Optics
Electrical Materials		
*Epoxy/Glass Boards FR-4	MIL-13949 MIL-18177 MIL-55619	Printed Circuit Boards, Terminal Boards, Multilayer Boards
*Polyeurethane Coating Solithane 113	MMS K775	Conformal Coating
Polyeurethane Potting	MMS L650	Encapsulation
*Stycast 10905L		
Polyeurethane Potting	MMS L650	Encapsulation
*Stycast 2850GT		
*Silicone Potting DC 93-500	EMCM 710A	Encapsulation
Teflon TFE/Polyamide Wire & Cable	STM E921 STM E922 STM E843	General Use Wiring
Viton/Glass Lacing Cord STUR - 40	MMS F415	Lacing Cord for Wire Bundles
*PVF Tubing	MMS F237	Shrinkable Tubing
*Teflon FEP Tubing	MMS F235	Shrinkable Tubing

*Used in Closed Electrical Assembly

TABLE 3.2-5 Photometer Weight Summary

MAJOR SUBASSEMBLY	ITEM	WEIGHT - KG	(LBS)
STRUCTURAL HOUSING	Skin Panels	22.14	(48.8)
	Int. Bulkheads	1.50	(3.3)
	Lower Mount. Plate	2.18	(4.8)
	Fwd Stiffener Frame	3.22	(7.1)
	Fittings	4.54	(10.0)
	Tubing	2.27	(5.0)
	Stringers	3.99	(8.8)
	Frames "z" Sect & Angle	1.86	(4.1)
	BKHD & Cover Frame	3.49	(7.7)
	Fasteners, Clips, Rails	3.85	(8.5)
		49.04	(108.1)
OPTO-MECHANICAL SUBMODULE	Fwd Closure Plate	.87	(1.92)
	Contamination Door	.08	(.18)
	Mounting Bracket	.10	(.22)
	Shutter	.26	(.57)
	Contamination Door Motor	.22	(.49)
	Aperture Wheel Assembly	1.00	(2.20)
	Filter Wheel Assembly	.74	(1.63)
	Secondary Mirror Mount	.21	(.46)
	Intermed. Bulkhead	.29	(.64)
	Primary/Fabry Mirror	1.05	(2.31)
	Point Detector Mount	.34	(.75)
	ICCD Support Assembly	7.26	(16.01)
	Radiator Plate	2.94	(6.48)
	Thermal Shroud	.34	(.75)
	Aft End Plate	1.22	(2.69)
	Attach Fitting (AFT)	.06	(.13)
	Attach Fittings (FWD)	.11	(.24)
	Bench Rods	1.16	(2.56)
	Channels	1.73	(3.81)
	Wiring	.11	(.24)
		20.09	(44.28)
ELECTRONICS SUBMODULE	Structural Case	4.67	(10.3)
	Electronics	9.16	(20.2)
		13.83	(30.5)
TOTAL INSTRUMENT WEIGHT =		82.96	(182.88)
+ CONTINGENCY (x 1.05)		87.11	(192.02)

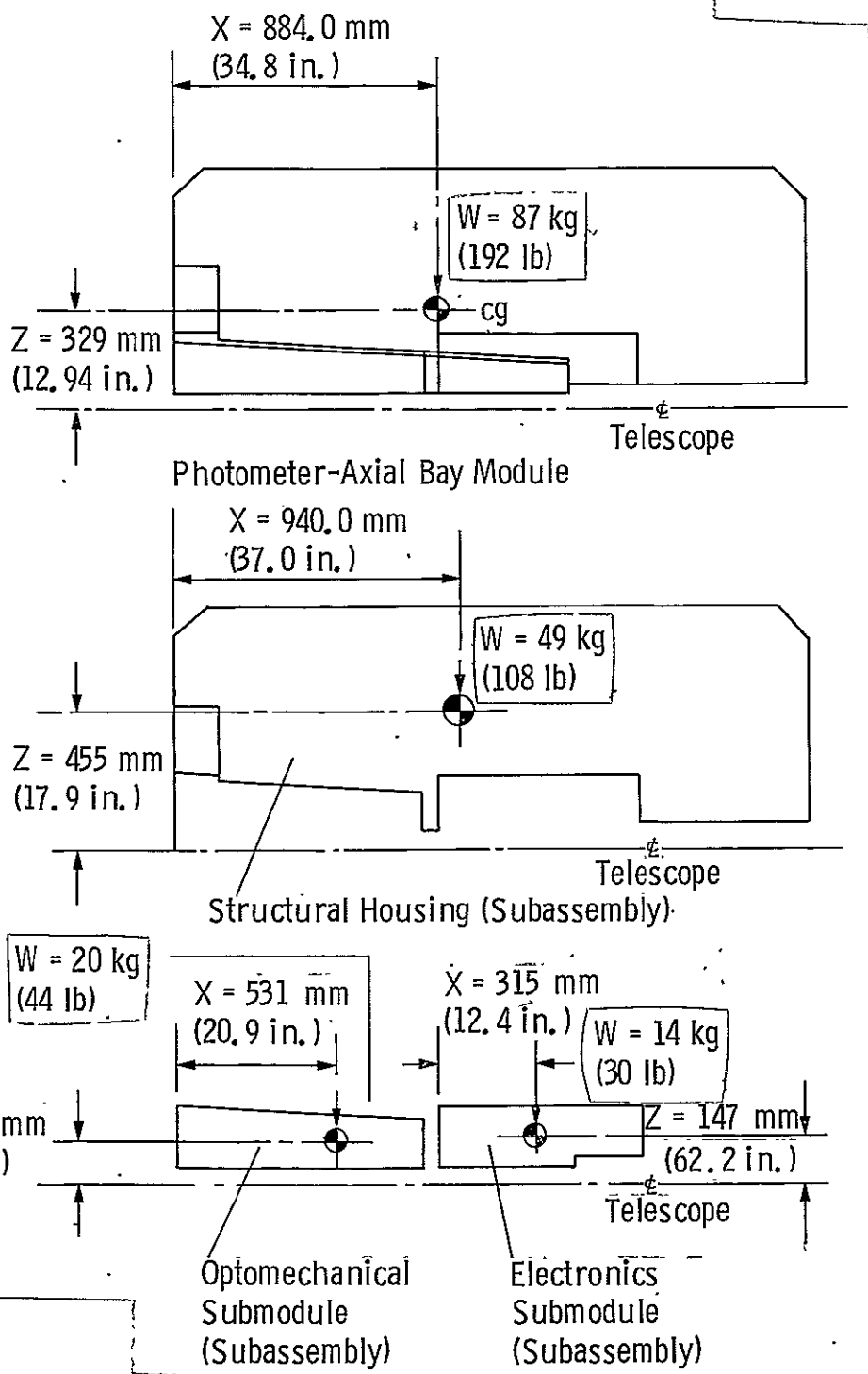

Computed masses of the submodules are summarized and their centers-of-mass shown.

Figure 3.2-8 Masses of Submodules

3.3 THERMAL CONTROL

The preliminary thermal control concept uses a cold-biased design with thermostatic heaters for control. Temperatures can be maintained with multi-layer insulation and appropriate coatings during both area detector and point detector operating modes under hot and cold conditions. A dormant case was also considered. Required optics compartment heater power is less than 8 watts, while required electronics compartment heater power is less than 1 watt.

3.3.1 Requirement Derivation

Photometer thermal control requirements are derived from the need to maintain the area detector no warmer than -40°C in some operational modes and the need to maintain opto-mechanical alignment in all operational modes. The thermal control concept has considered the requirements, knowledge of the thermal environment and the impact of other features of the Photometer design.

3.3.1.1 Interfaces

The Photometer interfaces are with the telescope (OTA), the other axial bay modules, and the Scientific Instrument (SI) compartment. The OTA is assumed to have a worst case variation of 15.6°C (60°F) to 26.7°C (80°F), with a nominal temperature of 21.1°C (70°F). The other axial bay modules are assumed to be adiabatic. The aft SI compartment wall is expected to be insulated. The outboard SI compartment wall thus forms the sink for Photometer heat rejection, and its temperature variation (from Itek) is -45.6°C (-50°F) to 8.9°C (16°F) depending on SI module location and orbital environment.

3.3.1.2 Temperature Requirements

3.3.1.2.1 Opto-Mechanical Submodule - Although the instrument can be built to maintain proper alignment to any one temperature within the range required by its components, the ambient temperature (21°C) was selected as the nominal operating temperature for ease of assembly and calibration.

To maintain the alignment established during assembly, temperature tolerance requirements are necessary for the most critical optical components. These tolerances are dictated by the thermal expansion characteristics of the component materials, and by the geometry of the components. Axial error refers to errors in spacing of optical components along the long axis of the instrument. Radial error refers to errors in component spacing in the transverse direction, either horizontally or vertically. Tilt refers to an angular displacement of components with respect to the transverse axis.

Allowable optical alignment errors were derived from geometric raytracing of the optical designs. The f/96 relay in general imposed the most restrictive tolerances. For the thermal design the allowable errors were as follows:

Component	Tolerance (μm)
Entrance aperture radial decenter from OTA axis	$\pm$ 1000
Entrance aperture longitudinal despace from OTA focus	$\pm$ 150
Entrance aperture to f/96 primary mirror despace	$\pm$ 10
f/96 primary mirror decenter	$\pm$ 110
f/96 secondary mirror decenter	$\pm$ 110
f/96 primary to secondary mirror despace	$\pm$ 4
Area detector decenter	$\pm$ 100
Vertex Tilts	$\pm$ 0.125 μrad

3.3.1.2.1 (Continued)

These values represent total errors, due to structural and other influences, as well as thermal expansion. One-third of the total alignment error is assumed to be due to thermal influences. The materials chosen for various HSAP components are:

Material	Component	Expansion Coefficient
Fiberglass	Area Detector Mount	30.6×10^{-6} mm/mm°C
Invar	Structure, Wheels	1.26×10^{-6} mm/mm°C
Titanium	Aperture Wheel Support	9.0×10^{-6} mm/mm°C
Graphite Epoxy	Bench Rods	0.18×10^{-6} mm/mm°C

Based on the expansion coefficient, geometry, and allowable excursion, maximum temperature tolerances have been computed for various critical components. These tolerances are:

Component	Temperature Tolerance	Direction of Expansion
Bench Rods	$\pm$ 284.7°C	Axial
Bulkheads	$\pm$ 161.7°C	Horizontal
Aperture Wheel	$\pm$ 32.5°C $\pm$ 28.3°C	Horizontal Vertical
Filter Wheels	$\pm$ 214.7°C $\pm$ 131.9°C	Horizontal Vertical
Mirrors	$\pm$ 11.0°C	Temperature Difference Between Bench Rods

If one bench rod were to expand relative to the other (due to a temperature difference) an angular displacement in each mirror would result. The mirror tolerance is thus based on the total accumulated tilt error along a typical light path from forward end plate to mirror carousel to secondary mirror to area detector, accounting for the magnification in alignment error due to the mirror curvature.

3.3.1.2.2 Area Detector - The area detector CCD must be cooled to 230°K (-45°C) for proper operation in target acquisition mode (the worst case).

3.3.1.2.3 Electronics Submodule - The temperature limits identified for the instrument electronics are as follows:

	Minimum Temp.	Maximum Temp.
Operating	-10°C (14°F)	60°C (140°F)
Dormant	-50°C (-58°F)	120°C (248°F)

3.3.1.3 Power Dissipation

The preliminary estimate of the power dissipated by the instrument components in the point detector mode follows. The time averaged values are determined from the preliminary timelines in Figure 3.1-1.

Point Detector Mode:

Component	Power (Watts) Min.	Power (Watts) Max.	Time Averaged Power (Watts) Min.	Time Averaged Power (Watts) Max.
~~Point Detector (2)~~	0.035 ea	1.0 ea	0.03 total	0.76 total
Stepper Motor (8)	0	12.5 ea	0	0.36 total
Electronics	15	20	15	20

The estimated power dissipation for the area detector mode follows. The time line in Figure 3.1 was used to time-average the stepper motor power, but constant CCD cooling was assumed for the detector.

Power Detector Mode:

Component	Power (Watts) Min.	Power (Watts) Max.	Time-Averaged Power (Watts) Min.	Time-Averaged Power (Watts) Max.
Area Detector CCD	0.05	0.15	0.05	0.15
Area Detector Cooler	7.3	10.7	7.3	10.7
Stepper Motor (8)	0	12.5 ea	0	0.36 ea
Electronics	15	20	15	20
Area Detector Memory	25	25	25	25

3.3.2 Thermal Design

The design philosophy used in this analysis is to cold-bias the design while providing thermostatic heater control in both the optomechanical submodule and the electronics. Area detector cooling is accomplished with a thermoelectric device and radiator. The overall thermal design concept is shown in Figure 3.3-2.

3.3.2.1 Structural Housing

The structural housing will have an external coating of white paint to prevent high temperature in case of solar exposure during on-orbit maintenance. The interior surface of the curved radiator wall will be black, while the remaining interior walls will be covered with multilayer insulation to isolate the module from the influences of adjacent modules and the focal plane housing.

3.3.2.2 Opto-Mechanical Submodule

All surfaces within the opto-mechanical submodel will be black for optical purposes. Multilayer insulation will be used to line the interior of the instrument housing side walls and forward end plate to isolate the compartment from the

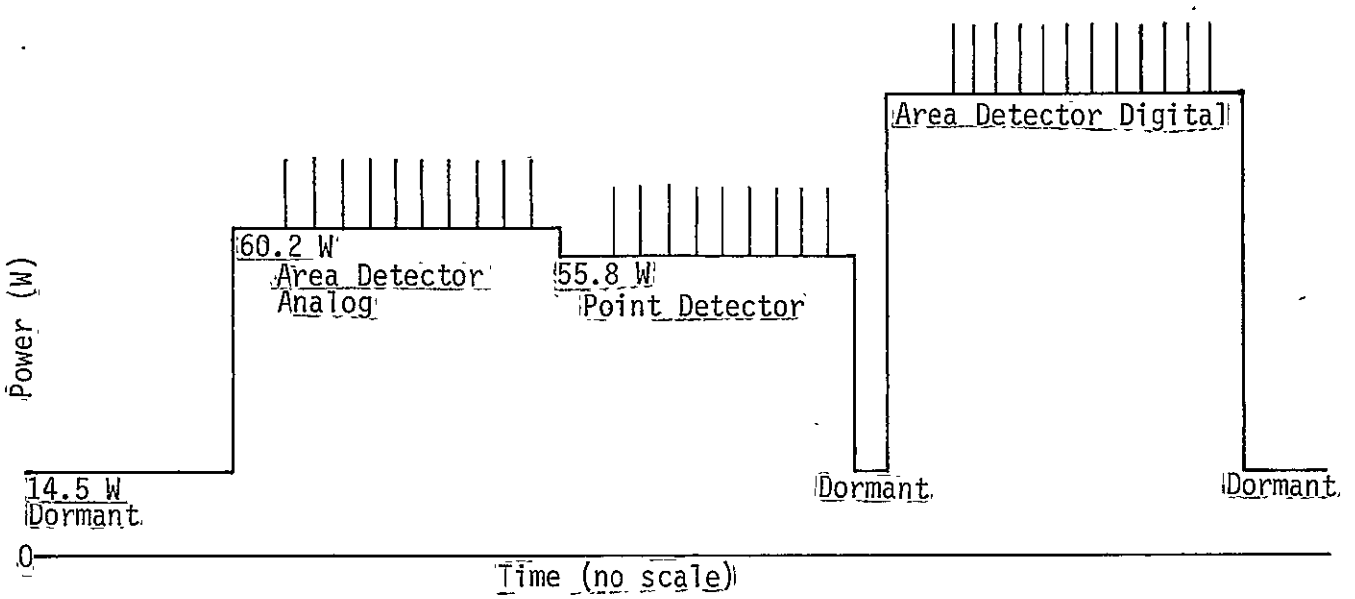

A simplified version of the electrical power consumption timeline (Figure 3.5-7) was used to deduce temperatures in the Photometer under various operational and environmental conditions. Spikes are from motor operations which contribute nearly nothing to the average heat load.

Figure 3.3-1 Thermal Dissipation Timeline

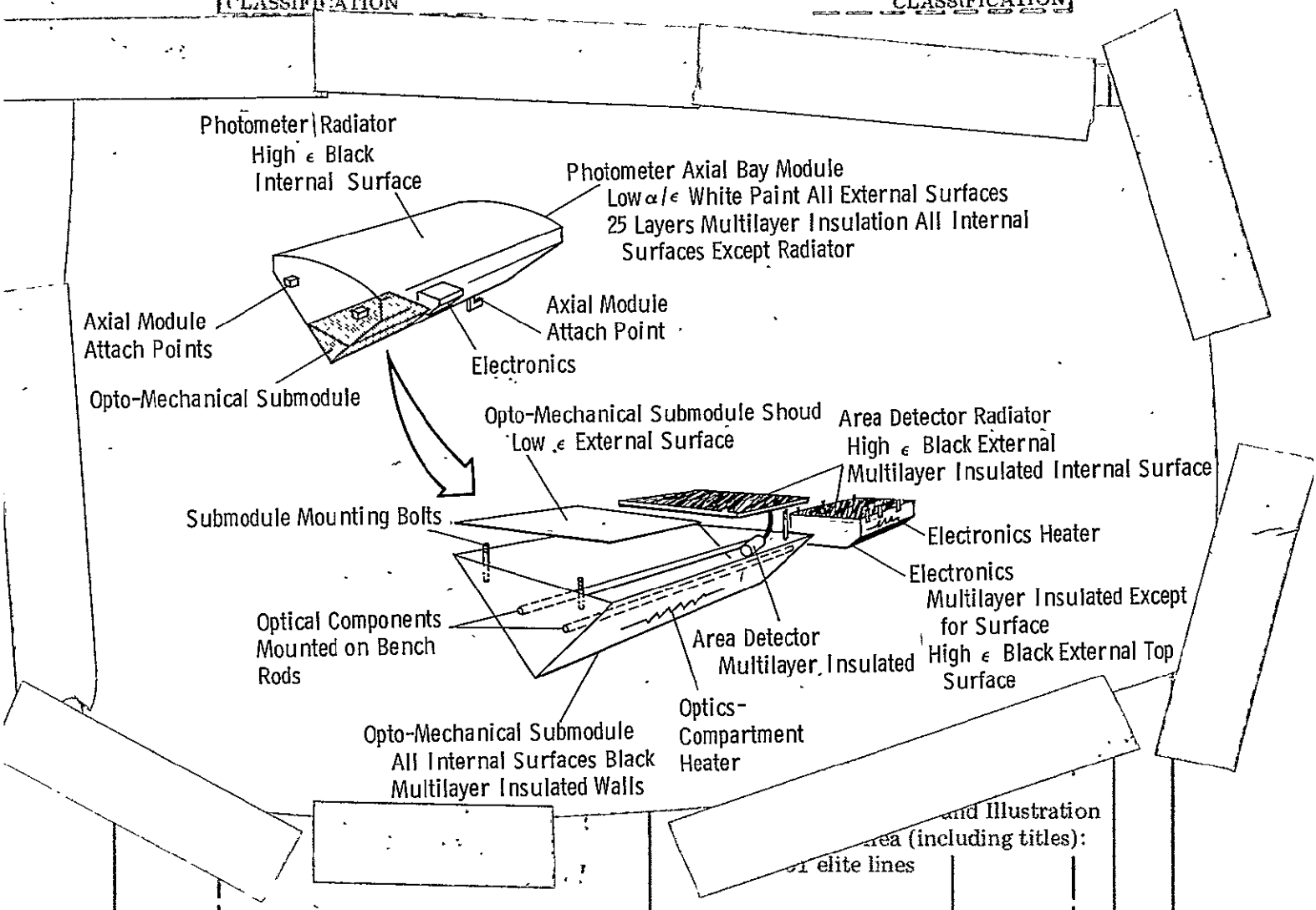

nd Illustration
ea (including titles):
elite lines

The design philosophy used was to cold-bias the design while providing thermostatic heater control in both the optomechanical submodule and the electronics. Area detector cooling is accomplished with a thermoelectric device and radiator.

Figure 3.3-2 Overall Thermal Design Concept

3.3.2.2 (continued)

the adjacent modules and focal plane housing. The exterior surfaces of the side walls and forward end plate will be white. Heaters will be attached to the instrument side walls to maintain $21^{o}C \pm 5^{o}$ during low load and environment periods.

A shroud will cover the forward 38.0 cm (15 inches) of the instrument to minimize heat leaks and resultant heater power in the low-power dissipation forward portion of the compartment. The shroud will have a low emissivity coating on its external (axial bay module) side. The remaining 46.0 cm (18 inches) of instrument length will be covered by a radiator, detailed in Section 3.3.2.3. The aft end plate of the instrument will be insulated with multilayer to isolate the compartment from the influence of the electronics mounted aft of the instrument.

3.3.2.3 Area Detector

The area detector (ICCD) must be cooled to $230^{o}K$ ($-45^{o}F$) for proper operation. This cooling will be accomplished with a thermoelectric cooling device, which is attractive from a size, reliability, and cost standpoint. A thermostat will be necessary to control the ICCD temperature. Its principal disadvantage is low efficiency; consequently, heat leaks into the detector must be minimized, and a means must be provided for removal of the relatively high power dissipated by the cooler.

Heat leaks will be minimized by wrapping the detector in multilayer insulation and providing a low conductance mount. Fiberglass standoffs appear to be the most attractive means, from thermal and strength standpoints, of attaching the detector to its support structure. The support structure can then be clamped to the bench rods with a standard mount. A preliminary design consists of six standoffs supporting the detector case within two equilateral triangular mounts. The standoffs would be 1.0 mm (.039 in) thick, 10 mm (.39 in) wide (axial) and 38 mm (1.5 in) long (radial), producing a heat leak of less than 100 mw. The radiation through the multilayer is also computed at less than 100 mw. For a detector power dissipation of 50 to 150 mW and a cooler efficiency of 3%, approximately 7.3 to 10.7 W of power is required.

This power dissipation must be transferred to a radiator for rejection due to the small available detector area and the relatively high available sink temperature. Two methods of achieving this transfer are available. The least costly and most reliable, but heaviest, method is a flexible copper strap. In order to keep the cooler temperature difference below $90^{o}C$, the temperature drop through the strap must be kept below about $5^{o}C$. For a 150 mm (6 inch) long strap, the cross-sectional area must be approximately 9.7 cm^2 (1.5 in^2). Such a strap would weight about 2 kg (4.4 lb). Interfaces with the strap should be brazed or welded to reduce temperature drops. The second method of transferring the heat is through a flexible heat pipe, a much more costly, less reliable method, although feasible. If the detector power dissipation becomes larger than current estimates, the heat pipe may be necessary to avoid excessively large strap cross-sectional areas or temperature drops.

3.3.2.3 (Continued)

The area detector radiator will form a cover for the aft 460 mm of the optics compartment. It will be insulated with multilayer on the compartment side, and painted black on the axial bay module side. Its fin effectiveness should be greater than 0.9, which for the copper strap concept requires a 6.5 mm (0.25 in) thick copper plate or a 15.5 mm (0.61 in) thick aluminum plate. Such a copper plate would weight about 4.5 kg (9.91b) while aluminum would weigh about 3.31 kg (7.3 1b). The heat pipe concept would require only a 1 mm (0.039 in) thick aluminum sheet due to the high effective conductance of the heat pipe.

3.3.2.4 Electronics Submodule

The electronics submodule will be insulated with multilayer except on its top surface to isolate it from the adjacent axial bay modules. The electronics are thermally mounted close to the inside of the top surface, with the power dissipating equipment as uniformly distributed as possible. The top surface may require thickening to distribute the heat if a reasonably uniform distribution is not possible. The outside of the top surface will be painted black with low emissivity tape overlaid to tailor the heat rejection capability to the electronics heat load. An emissivity of 0.6 (approximately 60% black, 40% tape) is required to reject the current estimated maximum load of 45 watts, requiring a minimum of heater power for the current estimated minimum load of 15 watts. If the predicted electronics load increases, the effective emissivity of the top plate can be increased by removing tape. A maximum heat rejection capability of approximately 75 watts is available for the 0.26 m^2 (400 in^2) surface if all the tape were removed. Electronics load growth beyond 75 watts will require an increased electronics compartment size. Additional electronics compartment size can be provided easily.

3.3.3 Analysis Approach

The approach used in this analysis was to divide the instrument into nodes representing the forward end plate, aperture assembly, filter assembly, mirror carousel plus both point detectors, area detector case, area detector back, aft end plate, electronics, instrument housing (8 nodes), shroud (2 nodes), area detector radiator, bench rods (four nodes each). There are nodes on the structural housing side walls, curved (outboard) radiator surface, forward surface, aft surface, as well as the SI compartment aft surface and adjacent SI's. The Focal Plane Assembly (FPA) and SI compartment side wall were used as boundary conditions.

The radiation interchange between components within the opto-mechanical submodule was computed manually, as was the radiation interchange within the whole structural housing. The axial module external surfaces were assumed to view only those surfaces directly facing them. Conduction was considered at all instrument housing joints except to the shroud, radiator and end plates, which were assumed to have poor joint conductance. Conduction along the bench rods as well as between the bench rods and each optical component was considered. Conduction through the bolts mounting the opto-mechanical and electronics submodules to the structural housing was also included, as was the conduction from the structural housing to its surroundings through its mounting brackets.

3.3.3 (Continued)

The network resulting from these computations was then input to the MITAS thermal analyzer computer program where several steady-state cases were investigated. The hot case assumed maximum boundary temperatures and internal power dissipations, while the cold case used corresponding minimums. Each of these cases was subdivided into a point detector mode and an area detector mode, since both could not be used simultaneously. A dormant case (no internal power, minimum boundaries) was also investigated, with and without heater power.

3.3.4 Analysis Results

3.3.4.1 Hot Case

The hot case area detector mode results are presented in Figure 3.3-3. As can be seen, gradients are less than 3.3°C (5.8°F), and no heater power is required. The area detector back temperature is 37.8°C (100.1°F), within the 47°C upper limit dictated by the 90°C temperature rise available from the cooler. A CCD maximum power dissipation growth to 93 milliwatts (29% increase) can be tolerated without increasing the length or thickness of the area detector radiator. Reduction of the size of the detector case would allow further load growth.

The hot case point detector mode results are presented in Figure 3.3-4. Gradients in this case are about 4.4°C (8.0°F), and 1.5 watts of optics compartment heater power are required.

3.3.4.2 Cold Case

The cold case area detector mode results are shown in Figure 3.3-5. Gradients are about 8.3°C (15.0°F) and 5.1 watts of optics compartment heater power are needed. The area detector back is 7.0°C (44.6°F).

The cold case point detector mode results are presented in Figure 3.3-6. Gradients are about 12.8°C (23.0°F) and 7.0 watts of optics compartment heaters are necessary. Additionally, 0.6 watts of heat are needed in the electronics compartment to maintain -6.7°C (20°F), for a total of 7.5 watts of heaters in this case.

The gradients indicated in the cold cases are a result of the white paint coating the external surface of the forward end plate, combined with the bolt conduction through the opto-mechanical submodule to structural housing interface The gradients, although well within tolerances, can be reduced to approximately 4.6°C (8.2°F) by eliminating these influences. A constraint on Photometer position relative to the sun during on-orbit changeout or covering the forward end plate would allow a low emissivity coating, reducing the gradient resulting from the white paint. Low conductivity bolts attaching the opto-mechanical submodule to the structural housing would reduce the gradient due to that influence, as would end plate heaters.

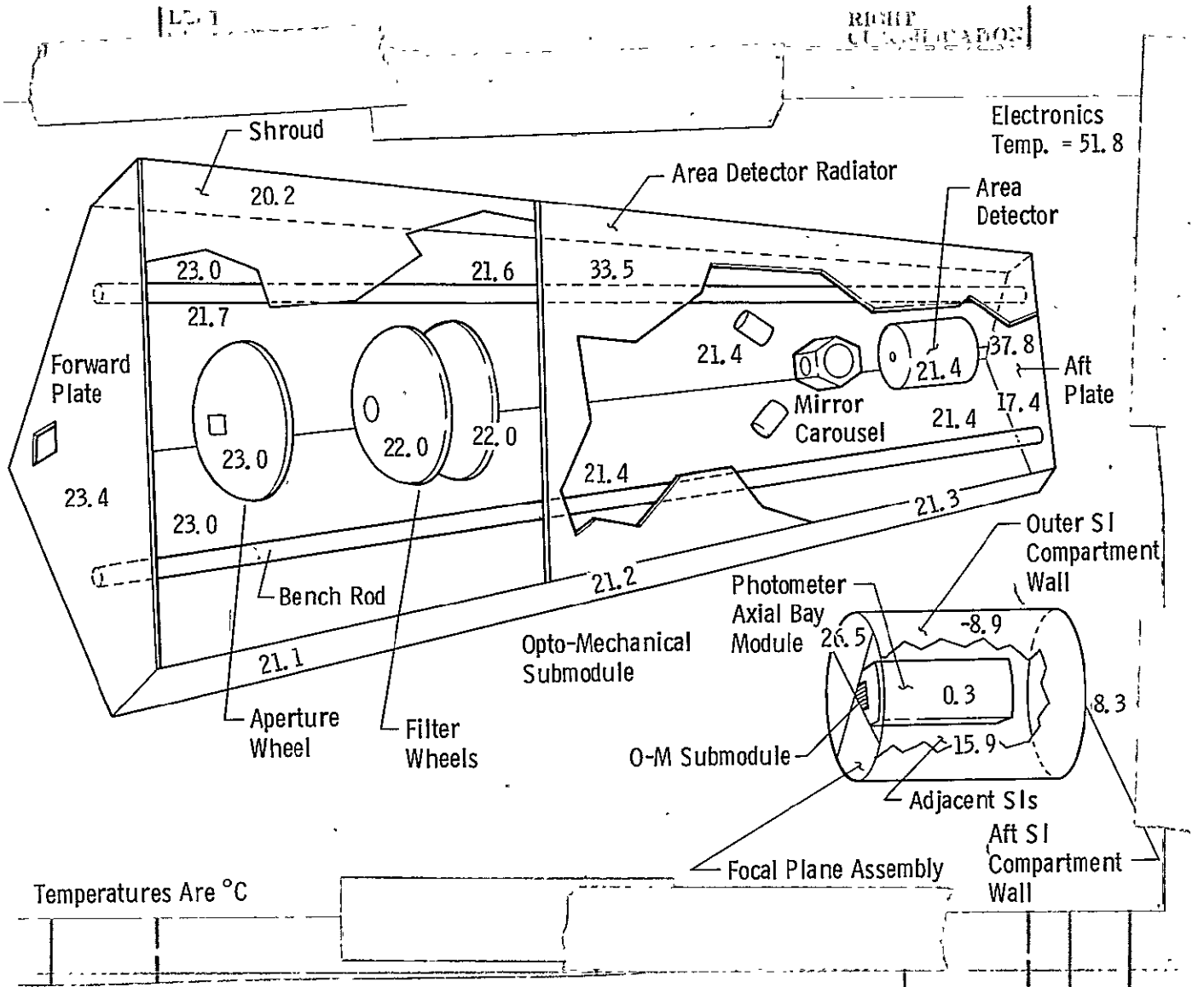

Figure 3.3-3 Hot Case, Area Detector On

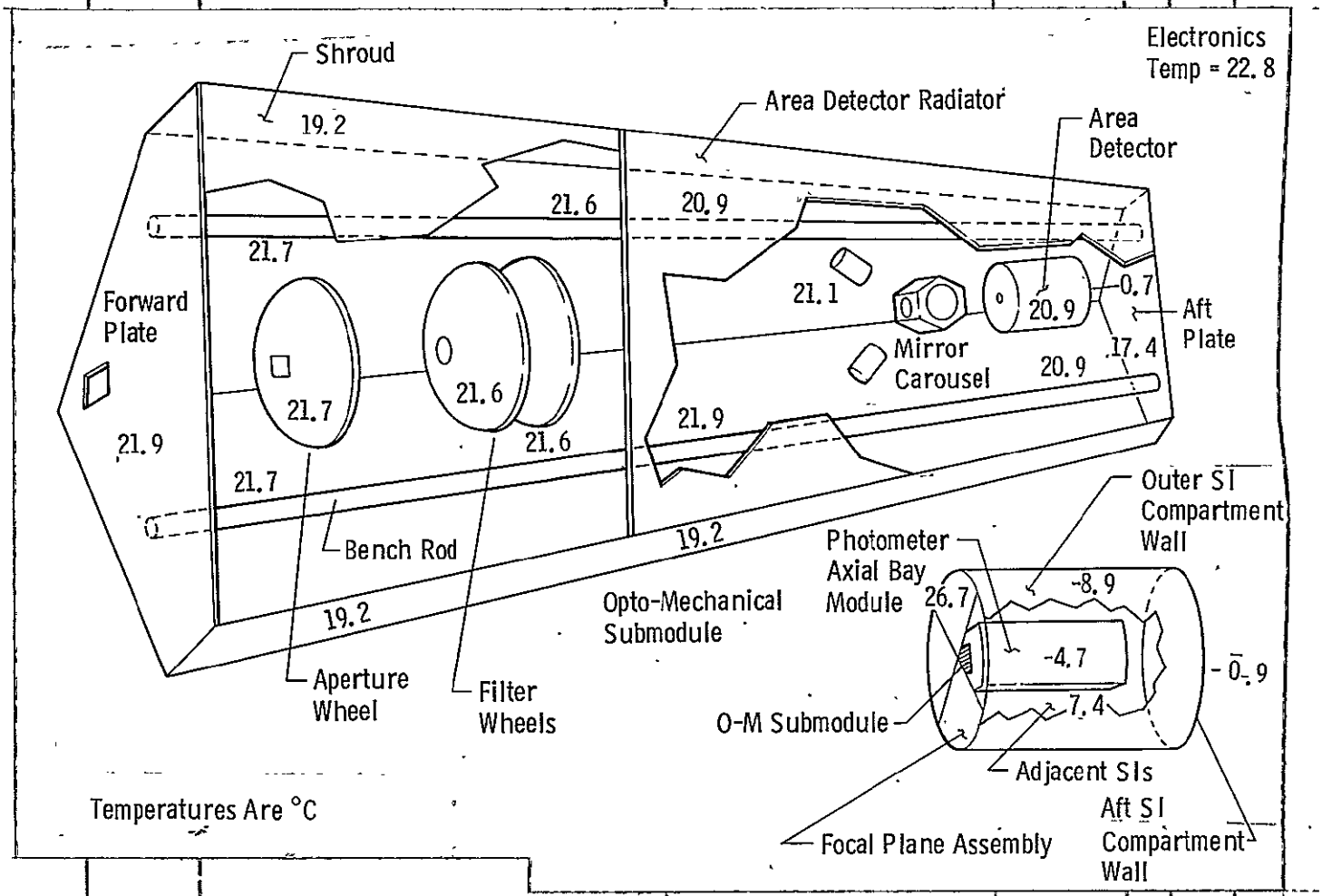

Figure 3.3-4 Hot Case, Point Detector On

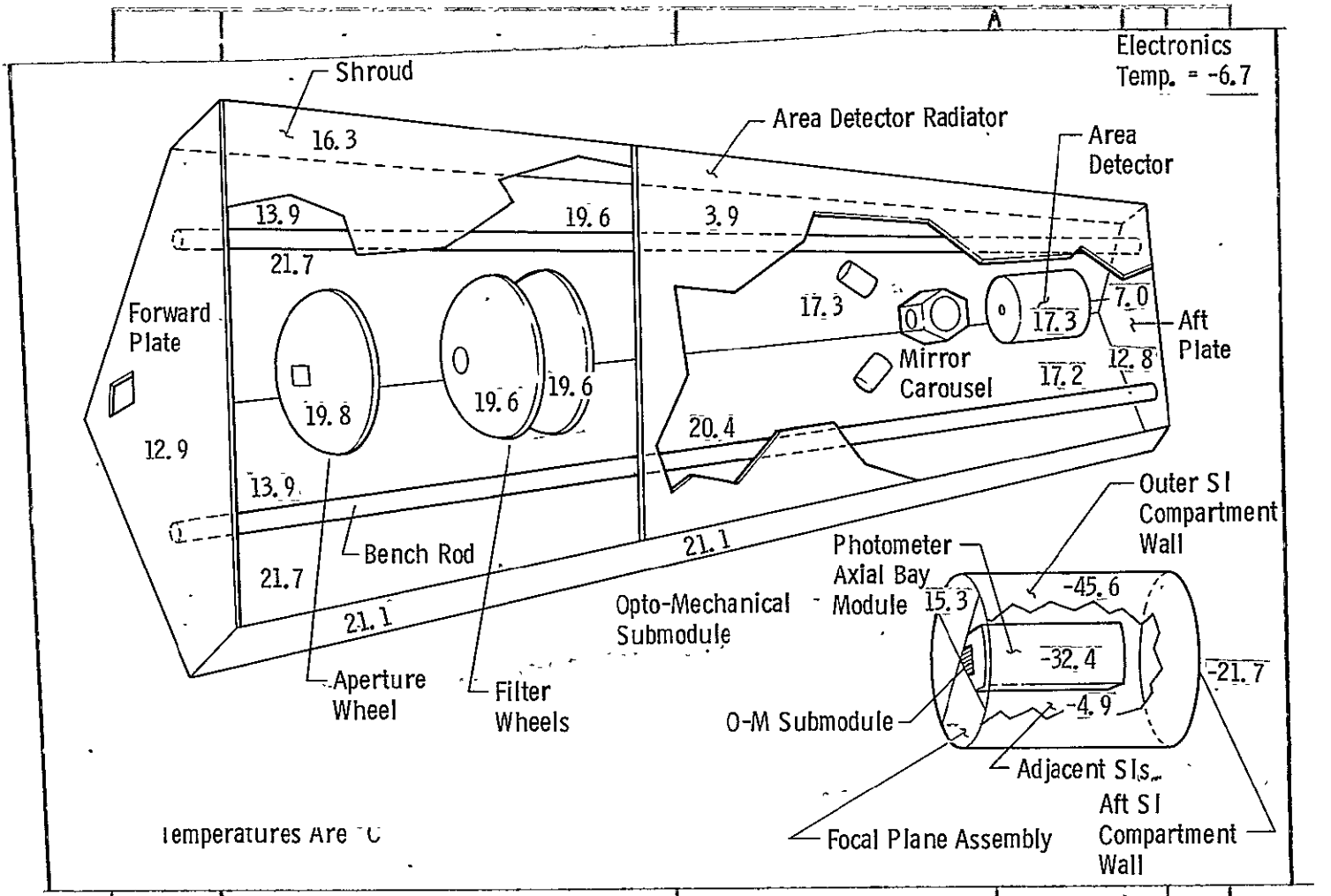

Figure 3.3-5 Cold Case, Area Detector On

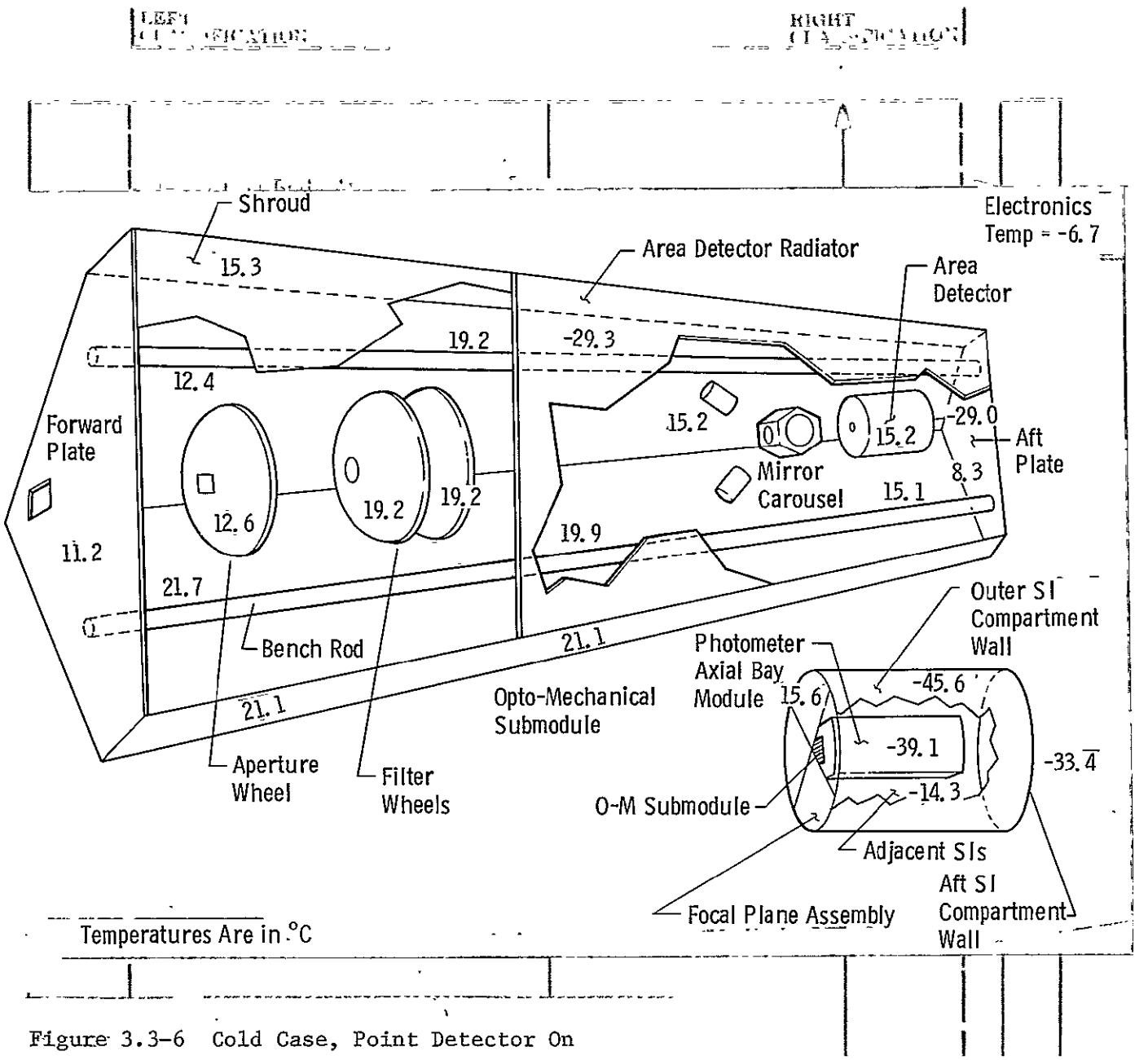

Figure 3.3-6 Cold Case, Point Detector On

3.3.4.3 Dormant Case

Analysis has shown that the average instrument temperature could be as low as -40°C (-40°F) without heater power in the dormant (no internal power) case with minimum environments. A case was then run with optics heaters activated, and the results are shown in Figure 3.3-7 (gradients in the opto-mechanical submodule were approximately 14.8°C (26.6°F) and 7.8 watts of heater power was required. The electronics temperature was about -38.5°C (-37.3°F), within the minimum dormant temperature of -50°C. Further analysis has shown that about 15.5 watts of heat would be necessary to keep the electronics at -6.7°C (20°F) during dormancy.

3.3.4.4 Maximum Bench Rod Temperature Difference

Due to the symmetry between the two axial halves of the instrument, and its relative isolation from the influences of adjacent scientific instruments, a significant temperature difference across the bench rods is virtually impossible. A case setting a 220°C (400°F) temperature difference between the two adjacent SI's revealed a bench rod temperature difference of less than 1°C.

3.3.5 Conclusions and Recommendations

3.3.5.1 Conclusions

- A preliminary thermal design has been completed.
- No thermal problems have been identified in this anlayisis. All gradients are within tolerances dictated by allowable optical alignment errors.
- Required optics compartment heater power is approximately 7.0 watts during operation, and 7.8 watts during dormancy.
- Electronics heating is required for operational electronics loads of less than about 15.6 watts. No heater power is necessary during dormancy unless an independent warming capability is desired. Maintaining electronics temperature at -6.7°C (20°F) during dormancy would require 15.6 watts. Consequently, maintenance of -6.7°C in the electronics compartment requires heater makeup to 15.6 watts for any electronics load less than 15.6 watts.
- Gradients can be reduced, if desired, by constraining on-orbit change-out to eliminate solar impingement and by using low-conductance bolts to attach the opto-mechanical submodule to the structural housing.
- A radiator is required to remove the heat dissipated in cooling the area detector ICCD.

3.3.5.2 Recommendations

- A transient analysis should be undertaken when weights and duty cycles are further defined.

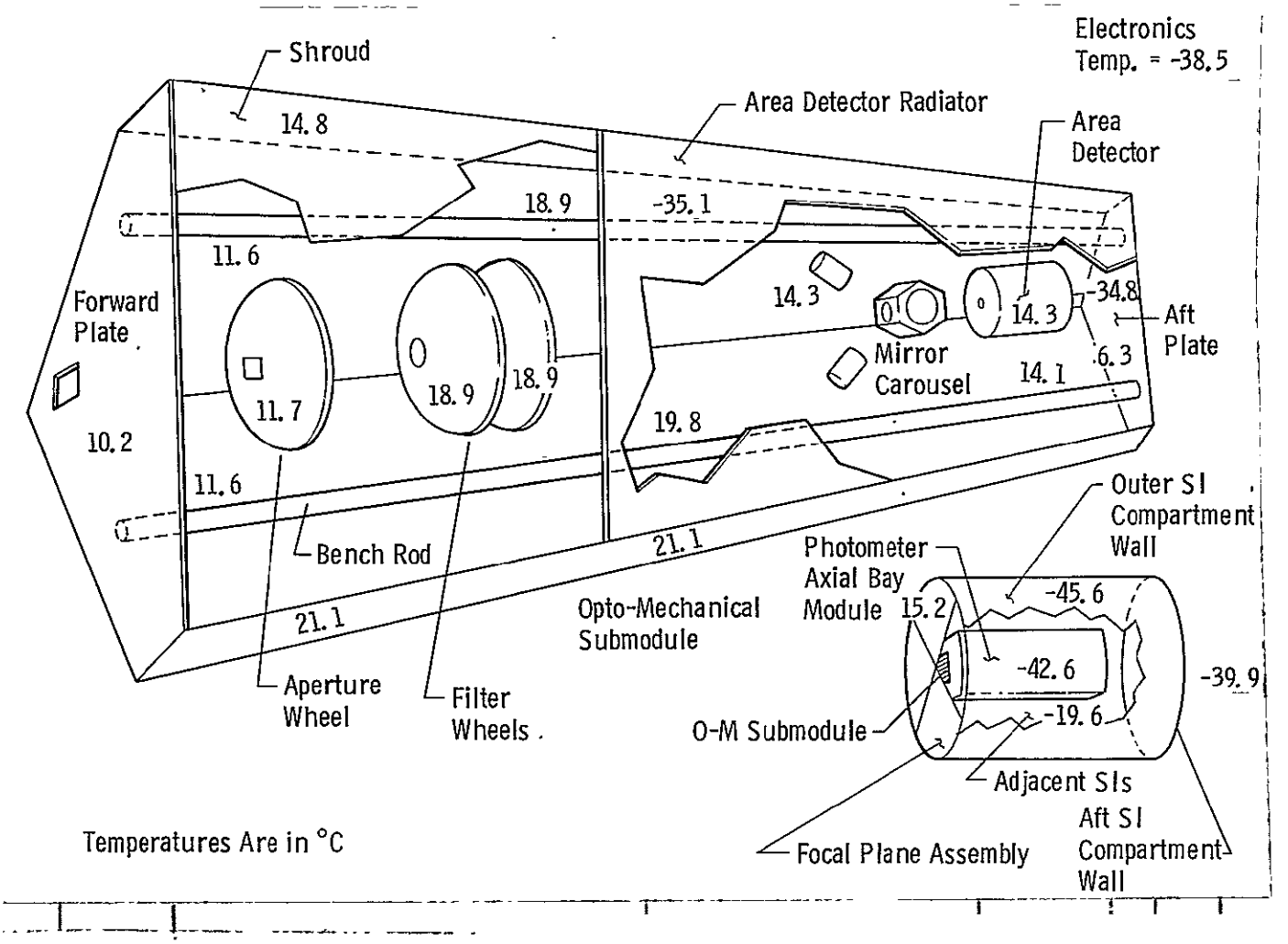

Figure 3.3-7 Dormant Case

3.3.5.2 (Continued)

- A determination of desired maximum temperature gradients based on other than thermal considerations should be accomplished. Reduction of gradients through the methods described in Section 3.3.4.2 can be implemented if desired.

- A more detailed analysis using the TRASYS program for view factor determination should be done when the configuration is finalized.

3.4 MECHANISMS

3.4.1 General Approach

Satisfactory performance of the Photometer depends in part on the precision and reliability of mechanical positioning devices. We have sought simplicity of design wherever possible to facilitate analysis, manufacturability, and good performance. The following considerations were employed to guide the design:

1) Build reliability and life into the mechanical components.

2) Use space proven motorized mechanisms

3) Select the optimum motor for the given application assumpt that the components being driven are properly designed in accordance with the motor limitations.

4) Evaluate bearings and lubrication, considering the specific applications and operating environment.

5) Provide positional readout for multiposition mechanisms.

6) Identify potential failure modes and eliminate them where possible by design emphasis on critical singlepoint failures. Avoid failure modes that can occur without warning.

7) Monitor motor temperatures to detect incipient failure and drive mechanism to desired failure-mode position.

8) Provide positional readout for multiposition mechanisms.

3.4.1.1 Bearings

The precise positioning demanded by the optical components has been addressed by careful attention to selection of bearing types and to their installation.

Normally bearings are selected on the basis of applied loads and speed of operation. Bearings on mechanisms, however, are used primarily as locating devices selected for bore diameters and radial ploy characteristics. As a result all bearings are used well within their ratings. In most cases angular contact bearings are used since they can be preloaded. All backlash, radial and end ploy is eliminated thereby. Duplex bearing pairs have been used where high moment rigidity is required. ABEC 9 precision grade bearings are used in the aperture wheel and the Fabry/Relay mirror assembly. ABEC 7 precision grade bearings are used in all other applications.

3.4.1.2 Lubrication

The lubricant and lubrication system for bearings have been chosen mainly to prevent contamination of optical surfaces by either condensation of

3.4.1.2 (Continued)

lubricant vapor or by particulate contamination from untrapped wear products. The use of lower vapor pressure lubricants and minimizing of line of sight paths from bearings to optics effectively preventes contamination of optics by condensation. Creeping of lubricant on surface is prevented by barrier films where needed.

Choice of lubricant is also influenced by the need to survive extensive ground testing. The tests subject lubricants to more extreme environments than several years of on-orbit operation.

It has been demonstrated that rolling element bearings under similar load and environmental conditions have exhibited outstanding reliability in space experiments, using a combination of solid film raceway lubrication type ball separators; we propose the same type of lubrication as follows:

1) The spluttered or impingement type of MoS_2 dry film on raceways and balls. Film thickness approximately 1 μm (40 micro inches)

2) Duroid ball riding retainers; this material is 60% PTFE (Teflon) reinforced with glass fibers and impregnated with 3% of MoS_2. There is test evidence to the effect that such bearings can be expected to reach 10^9 revolution without failure. Special run in and care is necessary as defined in NASA Spec 764-001.

A preconditioning run-in procedure will remove wear debris resulting from the initial, high rate, wear-in period. The ensuing "normal" wear rate will produce minimal debris which will be contained within the bearing by using shielded type bearings.

3.4.1.3 Motors

Inertias of the various mechanisms are small enough to permit stepper motors with small gear ratios for all applications.

The advantage of stepper motors is inherent simplicity. The motors consist of a simple solid rotor mounted on bearings within a would stator. They avoid the complexity of other types of motors, i.e., the wound rotor, brushes and commutator in the case of DC motors and the need for an inverter and shielded cabling in the case of AC motors. The high operating speeds of AC and DC motors would require high ratio gear boxes. Of course, the stepper will neeed a pulse generator, but pulse rate can be slow enough that no gear reduction is needed to control speed.

The philosophy given above for the lubrication of bearings also pertains to the motor bearings. In the case of the gear meshes it may be necessary to apply a bonded dry film MoS_2 lubricant by burnishing and subsequent run-in.

Table 3.4-1 summarizes the motor selections for the various mechanical functions. It will be observed that in the case of the contamination door closure, that an Abram's type stepper motor is proposed. This motor has positive mechanical latching incorporated and has been used successfully in many orbital payloads for similar functions.

Table 3.4-1 Motor Summary

Motor Type	Size	Internal Gear Ratio	External Gear Ratio	Usage
Latching Stepper Motor (A)	11	NA	NA	Contamination Door Closure (2 Position)
Linear Solenoid	-	NA	NA	Dark Shutter Actuator
Permanent Magnet Stepper/ Gearhead 90° Step Angle	11	22.5:1	4:1	Aperture Wheel Drive (12 Position) (See Note (1))
Permanent Magnet Stepper/ Gearhead 90° Step Angle (Two required)	15	45:1	NA	Filter Wheel Positioning Mechanism-Geneva Driver (8 Position)
Permanent Magnet Stepper/ Gearhead 90° Step Angle	11	22.5:1	4:1	Mirror Positioning Mechanism (5 position) (See Note (1))

Note (1) - These functions could be accommodated by using a variable reluctance stepper motor to take advantage of the smaller step angle characteristic. They do not , however, offer the detent torque feature of the PM stepper.

3.4.1.3 (Continued)

All the other stepper motors are conventional permanent magnet or variable reluctance types which have an excellent record of success in space programs (see MMC Survey of Motors used in space Report T-71-48890-003).

3.4.1.4 Position Indication

The optical encoder has been selected as the optimum form of position indicator. It involves no sliding contact element and the particular type adopted installs on existing shafts without need for additional bearings or lubricantion. Encoders embody a diode light source of exceptional reliability. Furthermore, dual readout channels are suggested for added reliability since additional channels are available on the existing product.

3.4.1.5 Modularity

The optical elements, mechanisms and detectors are all held by carriers which are mounted on a pair of parallel rods which we call the optical bench. Individual carriers are independently installed, adjusted, maintenance and removed from the optical bend rods.

The carriers are removable from the bench rods on the ground without difficulty but no provision has been made for their removal on-orbits. It has been suggested that single point failures of mechanism could be worked around by removal of entire failed mechanisms. We feel that removal provisions are not necessary because we will use designs and where possible components known to have high reliability. An analysis of reliability using a failure model of the Photometer is underway. The analysis will allow us to quantify reliability of a design without provisions for removal of whole mechanisms and will, we hope, show that sufficient reliability can be realized through careful design and component selection.

The choice to be made is between a design which has built in single point point failures but which is unlikely to fail (and thus expensive) and a design which can work around failures with additional mechanisms and can thus have a higher failure rate (and be less expensive). We can further reduce the problem to the relative expense and confidence we can have in achieving a low likelihood of failure versus a design that can overcome failures.

A design of any bench mounted assembly can be analyzed to estimate failure rates for various types of failures. Some criterion is also chosen for tolerance failure rates. Components which are identified as causing numerous or obvious failures can receive special design attention. Choice of parts of proven high reliability, testing, special fabrication procedures and so on are then applied as appropriate.

The use of additional removal mechanisms requires that the primary mechanism such as a filter wheel drive be designed to accommodate the additional mechanism. The accommodation is virtually certain to compromise the original wheel design and have an adverse effect on its reliability. Simply the addition of an extra removal mechanism increases the number of components which must be designed, fabricated, assembled and tested. Of course the backup removal mechanism can fail even though it is intended to be used only once or preferably not at all.

3.4.2 Contamination Door

The Photometer has a mechanical shutter at its entrance port which can be command to close when necessary to exclude contaminants or excessive light. The contamination door will be closed whenever the instrument is not in use. On-orbit the allowable failure mode for the door is open. During launch, return, maintenance visits and on the ground the door should be closed. The shutter is optically opaque so it can be used to exclude light as well as contaminants. The light exclusion function is redundant with the dark count shutter discussed in 3.4.3 and with the LST excess light closure mechanisms.

The door is a motor driver lever device, which through a spring arm and self-aligning cover plate closes and opens the entrance port on command. The motor is a size 11, 36° permanent magnet stepper with positive mechanical lock. The slight pressure exerted by the copper-beryllium leaf spring against the mounting plate assures a metal-to-metal contact. Positive stops at each extreme of the 36° rotational travel of the cover plate in conjunction with type micro-switches provide open or closed position readout.

A back-up device for assuring a "fail-open" condition is shown in Figure 3.4-1. This device consists of a spring loaded plunger (shear pin) which rigidizes the two piece swing arm under normal conditions. In the event of motor failure to plunger spring can be released allowing the link of swing arm to pivot under the action of a flexural pivot. The plunger is held cocked in the energized position by a finger spring collasped around the plunger neck and held in position by hoop tension in several turns of fusible wire. Passing current through the wire melts the wire allowing finger spring tangs to expand releasing the plunger.

3.4.3 Dark Shutter

There is a fast-acting mechanical shutter behind the contamination door. The primary function of the shutter is to allow dark current or dark count rate measurements to be made without disturbing the alignment of the Photometer. The shutter is a camera leaf-type driven open by a linear solenoid and closed by its own internal spring. The clear aperture need be only 8 mm. A secondary use of the shutter is for protection of sensitive Photometer defectors from excess light inputs. When the shutter is closed no light can enter the instrument.

The functions of the shutter can be performed by use of the dark position of the aperture wheel. The response time of the aperture wheel is slower and alignment would be disturbed by driving the aperture wheel. It is, however, usable if the mechanical shutter should fail. The allowable failure mode for the shutter is open.

3.4.4 Aperture Wheel Assembly

The aperture wheel assembly is clamped to the optics bench rods with the apertures positioned at the LST focal plane. The wheel assembly is shown in Figure 3.4-2.

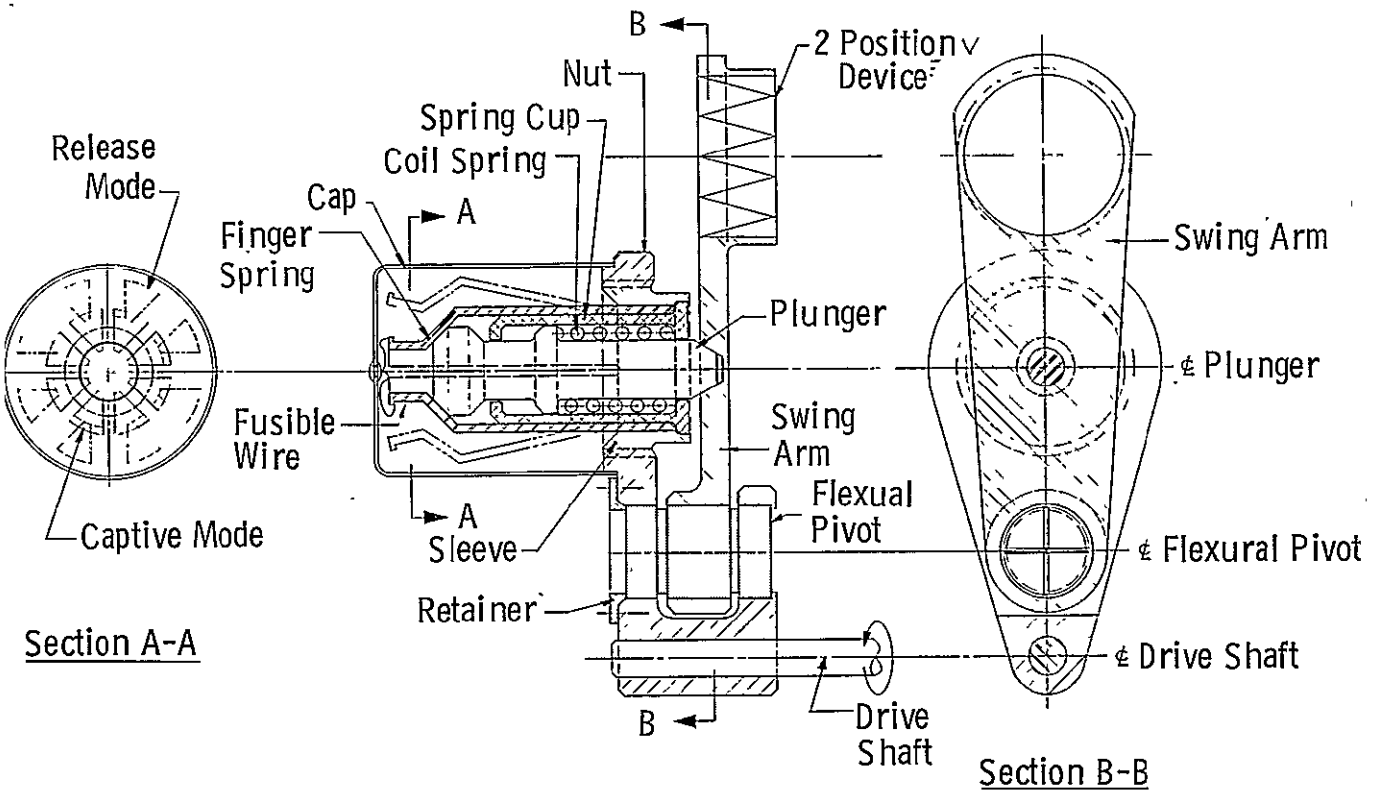

This device is used to prevent the contamination control door from failing in a closed position. The device is actuated by passing an electrical current through the fusible wire causing it to melt and rupture. The particles are retained within the sealed case. Rupture of the wire allows the springloaded plunger to release the swing arm which is rotated by a springloaded flexural pivot to a position which allows light again through the entry port. Once this device is actuated the door cannot be reclosed. However, since the door's main function is to keep the instrument clean during the pre-launch and launch phases, it will have served its main purpose.

Figure 3.4-1 Failure Override Device for Two Position Mechanisms

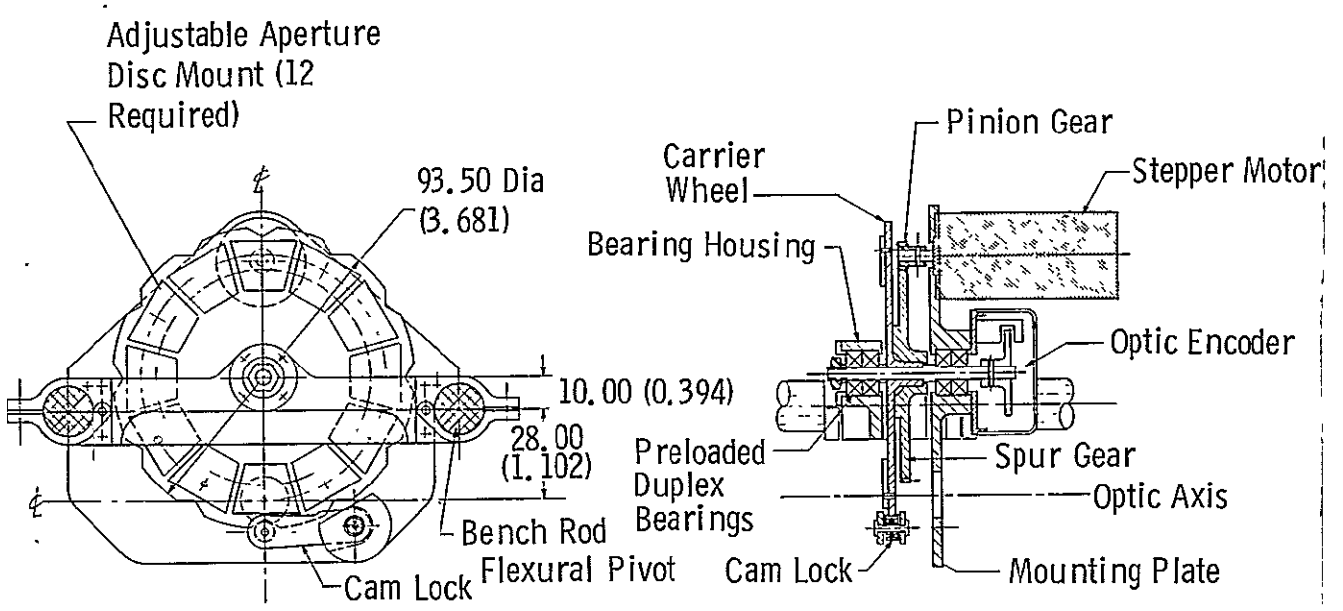

Various sized apertures are used to limit the field of view. The smallest is approximately two Airy disks in diameter or 60 μm. The need to center a point source within this opening is a controlling requirement on alignment tolerances for the apertures. Initial calibration of the aperture positions can be done using the area detector in series with the aperture to locate the aperture with respect to the image on the area detector. After this initial calibration, it is highly desirable to have repeatability in positioning of the apertures so that it is not required to use the area detector to locate the apertures, whenever the aperture wheel is moved.

The wheel is driven by a stepper motor and positioned by a spring loaded cam which seats into detents on the rim of the aperture wheel to assure repeatability of positioning. An optical encoder controls the positioning and closes the loop to indicate position. The entire assembly is mounted to the optical bench rods.

Figure 3.4-2: Aperture Wheel Assembly

3.4.4 (Continued)

The aperture wheel serves as the carrier for the ten selectable apertures. Each circular aperture is a commercially available, precision pinhole, centered on a separate plate of nickel stock approximately 10 μ m thick. This plate is laminated to a disc substrate of nickel, approximately 500 μm thick and 0.3 cm in diameter. The discs are mounted in an aperture plate as shown in Figure 3.4-3.

The aperture plates are attached to the carrier wheel by two screws with the clear aperture opening as close as possible to required position.

Two offset shoulder bolts rotating in elongated holes in the aperture plate provide for fine adjustment of aperture position.

The aperture carrier wheel is 93.50 mm in diameter with aperture plates equally spaced at 36^{o} intervals with centers on a 76.00 mm diameter circle. In order to minimize the radial displacements of aperture centers with respect to center of rotation due to temperature gradients, an athermalized system has been implemented. The wheel mounting geometry allows the use of Invar ($\alpha = 1.26 \times 10^{-6}$ mm/mm^{o}C) for the carrier wheel and titanium ($\alpha = 8.28 \times 10^{-6}$ mm/mm^{o}C) for the mounting plates, which for $\Delta T = 5^{o}$C results in a net change in radial geometry of .000154 mm. In addition to the aperture wheel, the titanium mounting plates are designed to incorporate the bearing housings for wheel shaft bearings, the motor mounting and the bench rod clamps.

Positioning of the apertures is accomplished by a permanent magnet stepper motor driving the carrier wheel through a 9:1 external gear ratio. A size 15 stepper motor provides an adequate operating margin and for a 30^{o} aperture indexing would need 3 pulses to move one increment in .15 seconds.

Due to the radial tolerance requirements imposed on centering the aperture on optic axis a secondary mechanism is used to override any misalignments, resulting from gear backlash, lost stepper pulses, or radial play in bearings. This device consists of a spring loaded lever arm which applies a constant normal and tangential force to the perimeter of the carrier wheel. These loads are transmitted through a 6.35 mm diameter ball bearing cam roller. The carrier wheel.

Preloaded bearings are essential to eliminate radial and axial play; the back-to-back configuration will be used for better moment stability. The use of one flanged bearing is proposed since it provides the simplest form of axial fixation and more importantly, it facilitates through boring of the bracket assembly in which the bearings are installed. The sizing of this bore is extremely important and the lack of internal shoulders enhances machining accuracy and permits honing to final size, if necessary. The bearings should be a zero clearance fit in this bore, yet the floating bearing must drift to accommodate the effect of temperature change on the different materials, 440C stainless steel for the bearings and titanium for the housing.

The preloaded duplex bearing pair(s) illustrated are angular contact bearings.

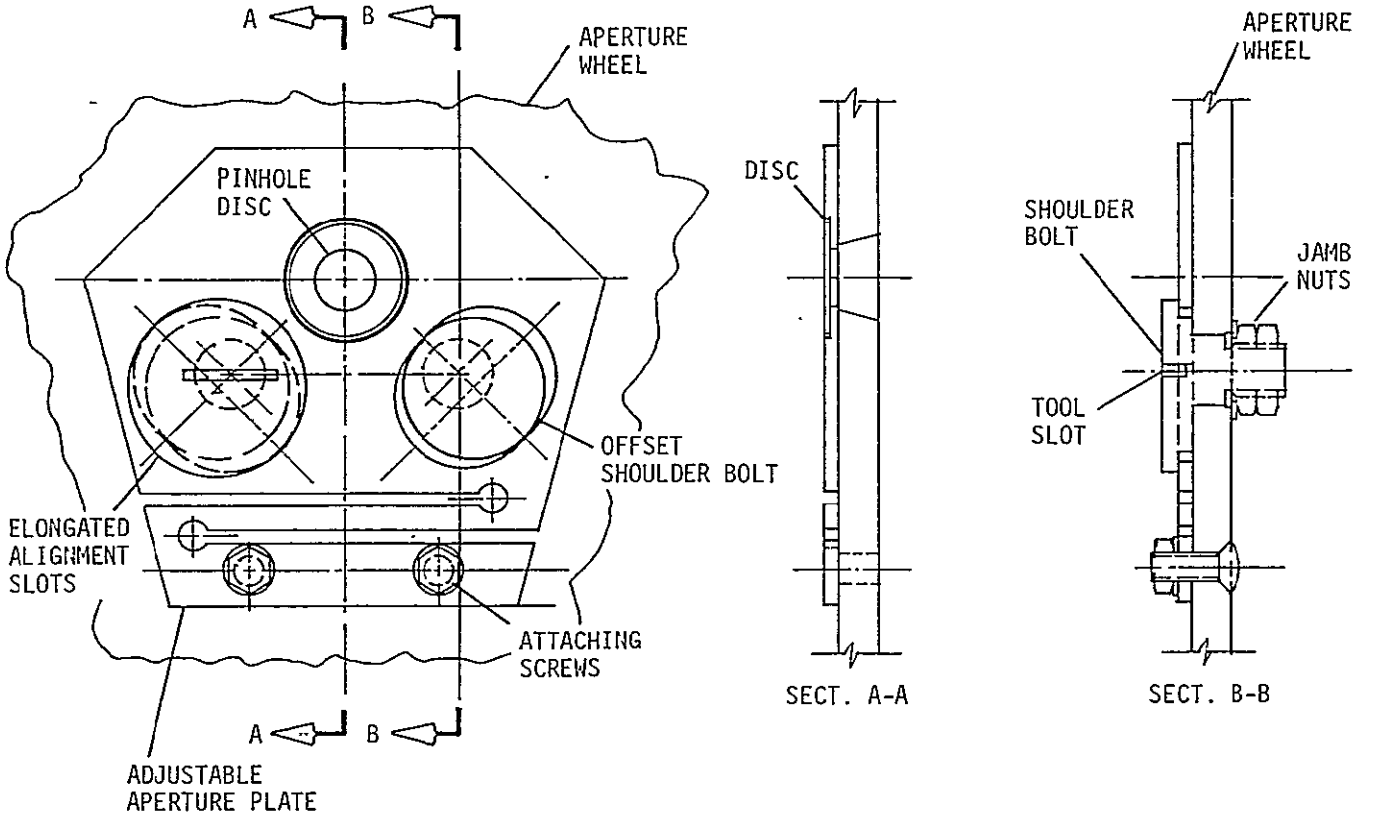

The aperture wheel serves as the carrier for the ten selectable apertures. Each circular aperture is a commercially available, precision pinhole, centered on a separate 26 mm square plate of nickel stock approximately 10 microns thick. This plate is laminated to a disc substrate of nickel, approximately 500 μm thick and 0.3 cm in dia. The discs are mounted in an aperture plate as shown in the figure.

The aperture plates are attached to the carrier wheel by two screws with the clear aperture opening as close as possible to required optic axis centerline. Two offset shoulder bolts rotating in elongated holes in the aperture plate provide for fine adjustment of aperture with respect to optic axis.

Figure 3.4-3 Aperture Plate Mounting Concept Detail

C 12

3.4.5 Filter Wheel Assemblies

The filter wheel assembly is clamped to the optics bench rods with the front surface of "A" wheel filters about 200 mm aft of the aperture wheel, the "B" wheel filters are 25 mm behind the "A" wheel. The axis of rotation is parallel to optic axis (X-axis). Figure 3.4-4 depicts the mechanical arrangement which features two filter wheels in tandem configuration. Each wheel has provisions for 8 equally spaced filter positions. Positioning of any filter element in the flight path is accomplished by a Geneva mechanism consisting of an 8-tooth Geneva wheel, cam driver and stepper motor. Since precise positional location is not critical, the Geneva mechanism was chosen for its basic simplicity and integral locking feature.

The Geneva wheels which serve as carriers for the filters are fabricated from 6061-T6 aluminum since thermal distortion is not of serious consequence. The two mounting plates which provide support for drive motors and the fixed 404 Cres wheel shafts, are also fabricated from 6061-T6 aluminum.

Each motor shaft extends through the mounting plates and is supported near the end where an optical encoder is mounted. Pinion gears are pinned to each motor shaft which mesh with the combination spur gear and cam driver.

A pulse rate of 5 pps has been selected for the permanent magnet stepper motors, since at this operating rate, stepper motors exhibit maximum ability to overcome load inertias. A size 11 permanent magnet stepper motor provides an operating margin of 128% for the system inertias and friction.

The filter wheels are mounted to a common fixed shaft attached to the bench rod mounting plates. Preloaded, duplex bearing pairs are utilized to support each wheel on the fixed shaft. Bearings are deep grove radial bearings with shields. The use of back-to-back bearings in this application is recommended primarily for moment rigidity since reduction of axial and radial play is not a critical factor.

Each of the combination spur gear/cam driver assemblies are also supported on a common shaft with similar bearing application as described above.

Optic encoders of the type discussed in Section 3.4.1.4 are placed on each motor drive shaft to give positional indication.

3.4.5.1 Motor Selection and Sizing

A pulse rate of 5 pps has been selected since at this operating rate, stepper motors exhibit maximum ability to overcome load inertias, thus resulting in the smallest and lowest weigh motor capable of the particular function. The following analysis examines the situation when the cam follower is at the bottom of the Geneva slot, the point of minimum mechanical advantage.

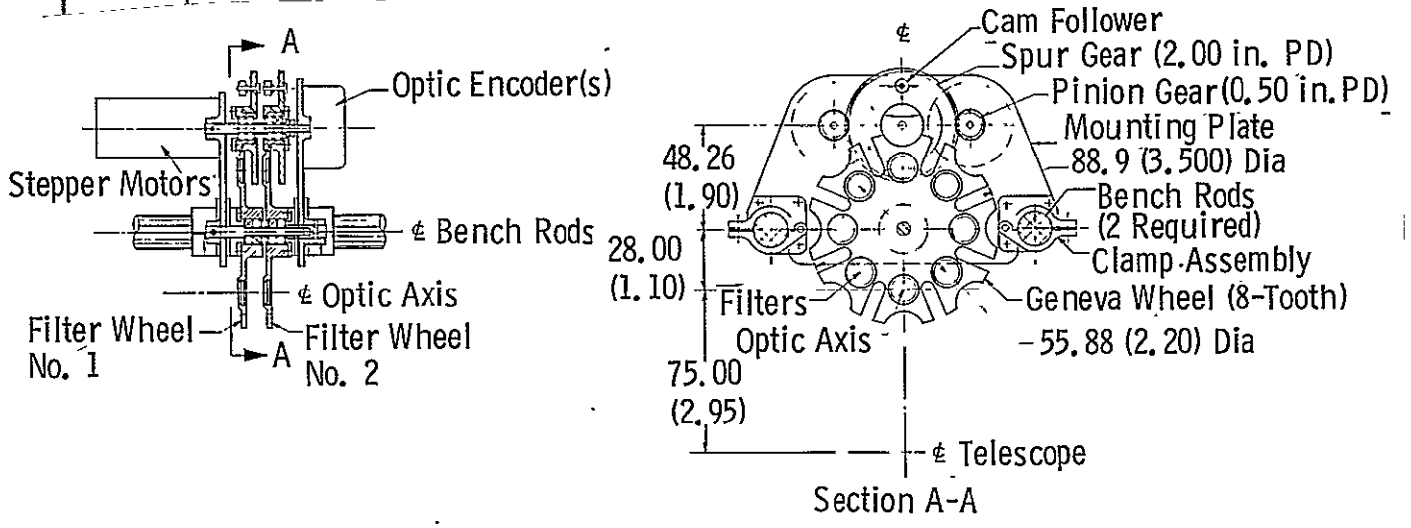

The two filter wheels are each independently controlled and independently driven by stepper motors and Geneva drives. Encoders are furnished to provide positioning information. No provision is made for fine adjustment since alignment tolerances are not critical. Each wheel has an open position so that filters can be used either separately or in combination between the wheels. A closed position is not furnished since the shutter can perform the shut off function.

Figure 3.4-4 Filter Wheel Assemblies

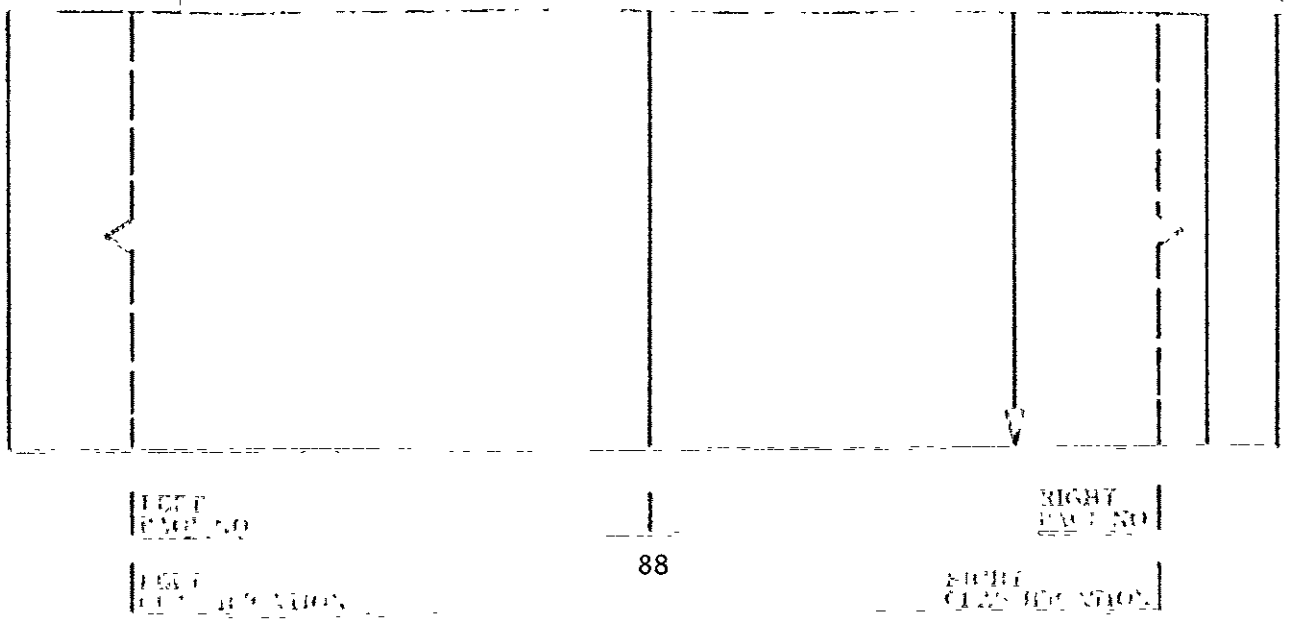

3.4.5.1 (Continued)

			gm cm^2
Moment of inertia of filter wheel			282
Moment of inertia of Geneva wheel			58.6
Moment of inertia of drive pinion			.56
Total inertia reflected on motor: (I_ϕ /gear ratio)			
Pinion		=	.56
Geneva Drive Wheel	$58.6/4^2$	=	3.66
Filter Wheel at 22-1/2° Displacement.	$\frac{282}{4^2 \times \left(\frac{1.1}{.8}\right)^2}$	=	9.3
Encoder Disc		=	2.82
Motor Rotor Inertia		=	1.20
			17.54 gm cm^2

Friction Torques

		Oz. In.	(gm-cm)
Geneva Wheel			
Preloaded angular contact ball bearings = 01			
Torque reflected onto motor = .1/gear ratio		= .025	(1.8)
Cam Follower			
Ball Bearing Torque = .02			
Torque reflected onto Geneva Wheel = $\frac{.02}{.1/0.7}$	= .14		
Torque reflected onto Motor Shaft = .14/4		= .035	(2.5)
Filter Wheel			
Ball Bearing Torque = .1			
Torque reflected onto Motor = $\frac{.1}{1.1/.7 \times 4 \times \text{Mech. Effec.}}$		= .017	(1.2)
Total Frictional Torque Load At Motor Shaft.		= .077	(5.5)

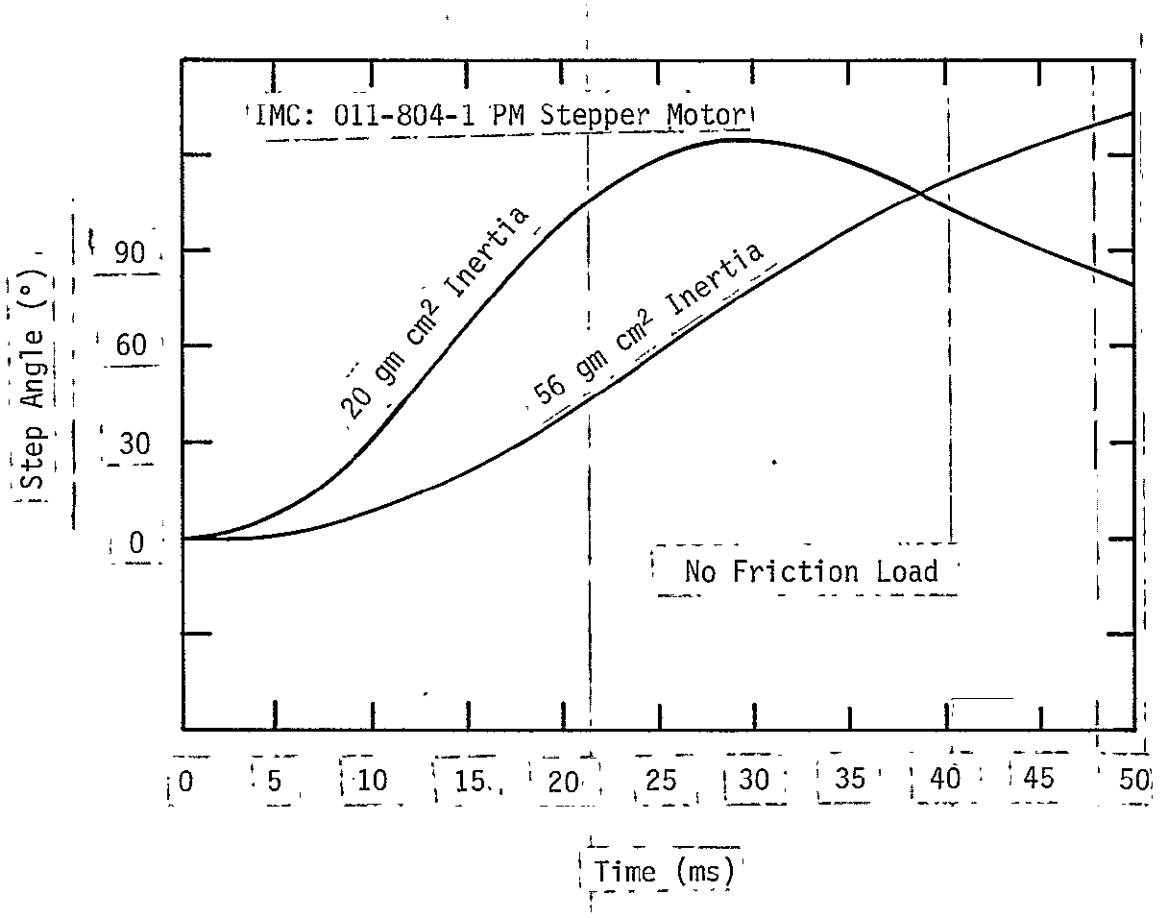

Figure 3.4-5 Motor Inertial Capability

3.4.5.1 (Continued)

Motor Inertial Capability

The following curves provided by IMC Magnetics Corp, of actual test data illustrate the inertial ability of the motor selected. It will be noted that the 56 gm cm^2 load is three times greater than that computed for the Geneva drive (at zero friction torque).

Maximum Driving Torque - Analysis

Formulas for maximum driving torque and other parameter are provided in "Geneva Mechanism" by F. G. Fenton, Machine Design, January 21, 1965: -

$$\text{Maximum Driving Torque, } M_d = I W_d^2 (K + C)B$$

Where I = Moment of inertia, gm-cm-sec with respect to wheel axis

W_d = Geneva drive velocity rad/sec

K = Torque ratio $T/I W_d^2$

T = Working torque with respect to wheel axis

B = Velocity ratio - taken from given figure

C = Acceleration ratio taken from given figure

A driving velocity W_d appropriate to the 17.54 gm cm^2 inertia jolt by the motor may be taken from the foregoing figure of step angle vs. time for a 20 gm cm^2 load. A peak value amounts to 65 radian/sec divided by the gear ratio of 4 giving 16 radian/sec.

M_d = .0003 lb ins sec^2 x 16^2 (1.55).5

= 68.4 gm-cm at the Geneva drive shaft

= 16.6 gm-cm at motor

This value occurs 18^o prior to the mid point of wheel motion.

Frictional + Inertial torque = 5.5 + 16.6

= 22.1

Motor torque margin = $\frac{50.48}{22.1} - 1$

= 128%

This margin is considered satisfactory though not sufficiently large to justify the use of the smaller size 8 motor.

3.4.6 Primary Mirror Carousel

The two area detection primary relay mirrors and the two point photometry Fabry mirrors are mounted on a six sided turret or carousel. There are positions for two additional mirrors which are not used at present. The turret may be rotated upon command to place the desired mirror in position. Each mirror has has the appropriate surface shape and/or tilt to direct light to one of two area detection secondary relay mirrors or to one of two point detectors.

The mirror changer assembly is clamped to the optics bench with the mirror surfaces 510 mm from the entrance aperture. Due to the optical geometry requirements, the size and shape of the area detector, it was necessary to locate the drive motor and gear trains low in the compartment Ideally, the carousel would be direct driven by a permanent magnet stepper motor located inside the turret shell, eliminating the need for off-set reduction gears in complex arrangements. An alternate approach is discussed at the end of this section.)

Figure 3.4-6 depicts the baseline concept for the mirror carousel. A size 11 permanent magnet stepper motor is used to rotate the carousel in 60^{o} increments. At least one of the spur gears in the systems is an antibacklash type. The spindle shaft which rotates the turret shell is rigidly mounted in bearing housings which accommodate duplex pairs of angular contact high-precision instrument bearings. These bearings can be preloaded to eliminate most of the radial and axial play associated with bearing assemblies. The bearing housings for the spindle shaft as well as the two-sets of reduction cluster gears are integrally machined into the motor mount frame assembly. The frame assembly consists of an upper and lower plate which are attached to a motor mount plate at one end and spacer posts at the other. Line drilling and boring would be accomplished at the assembly level. Two invar plates are used to attach the frame assembly to the optic bench rods, using a typical damping device as described in section 3.4.8. In a manner similar to that described for the aperture wheel, a spring loaded detent mechanism is utilized to override any inherent looseness in the spindle mount. This assures repeatability of a selected mirror position. Positional knowledge is achieved by mounting LED unit to look through coded hole patterns in the extended lip of carrousel turret.

Each mirror is individually adjusted and locked-up in its turret mount.

The alternate concept mentioned previously provides a simpler and more compact arrangement as shown in Figure 3.4-7. This concept is predicated on modifying the optical requirements to allow the turret spindle shaft to extend approximately 125 mm above the top of the turret shell without obscuring the light path coming into the area detector. A size 15 permanent magnet stepper motor is required for this concept.

3.4.7 Secondary Mirror Mount

The secondary mirrors and their mounts are shown in Figure 3.4-8. A common mounting plate is attached to bench rods with a typical clamp assembly. The mirror mount is based on a cardo hinge concept which provides a two-axis mount and

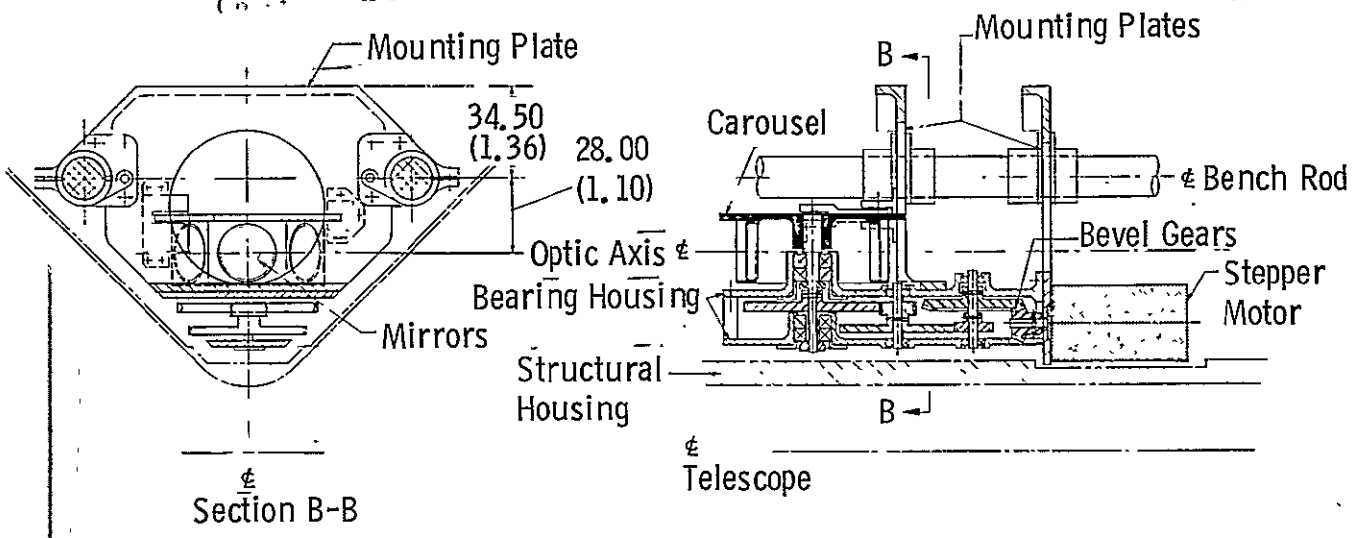

The carousel is hexagonal, providing for the mounting of six different relay mirrors. Four positions are used, two Fabry mirrors for the point detectors and two primary mirrors for the f/24 and f/96 imaging systems. Each mirror design is optimized for its function in its optical system and each is so positioned on a face of the carousel to direct the beam to the proper next element for each system.

The stepper motor rotates the carousel in sixty degree increments. A spring loaded detent mechanism overcomes bearing play and assures repeatability in positioning. Each face of the turret is identical.

A gear train has been used because of space constraints near the edge of the axial module.

Figure 3.4-6 Mirror Changer Carousel

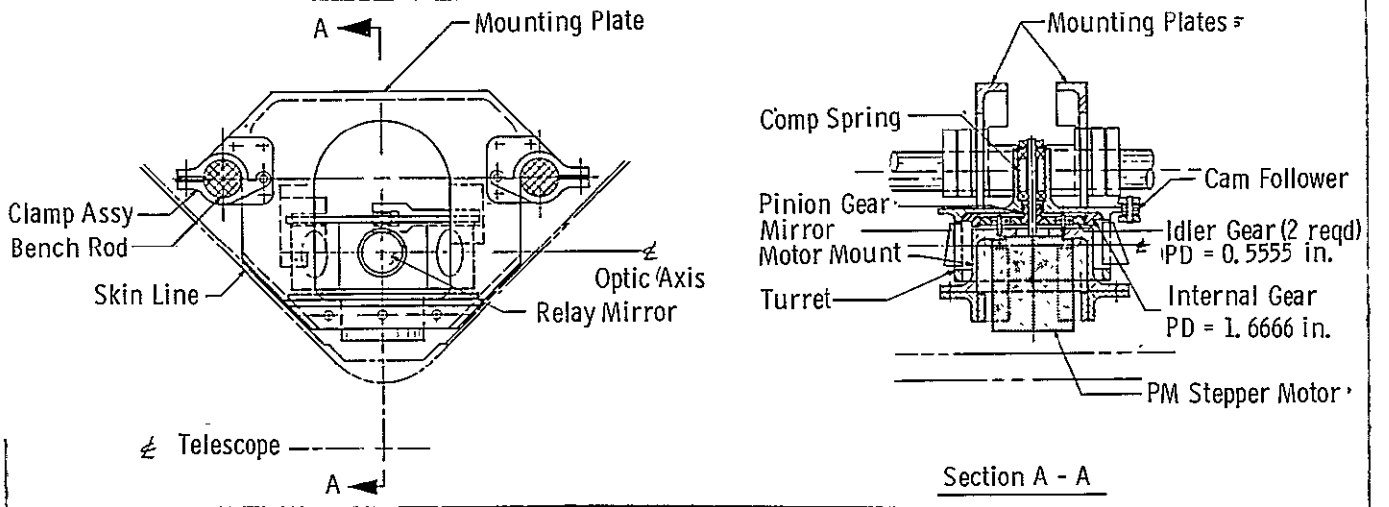

A simplified carousel drive system is shown. A size 15 permanent magnet stepper motor is nested within the hexagonal carousel. The whole drive is more compact than the concept shown in Figure 3.4-7 but a shaft must protrude into the area above the carousel. This places a restraint on location of the area detector but the area detector is now located above and aft of the carousel where it does not interfere with this carousel alternative.

Figure 3.4-7 Mirror Carousel Alternative

Available Text and Illustration Image Area (including titles): 51 elite lines

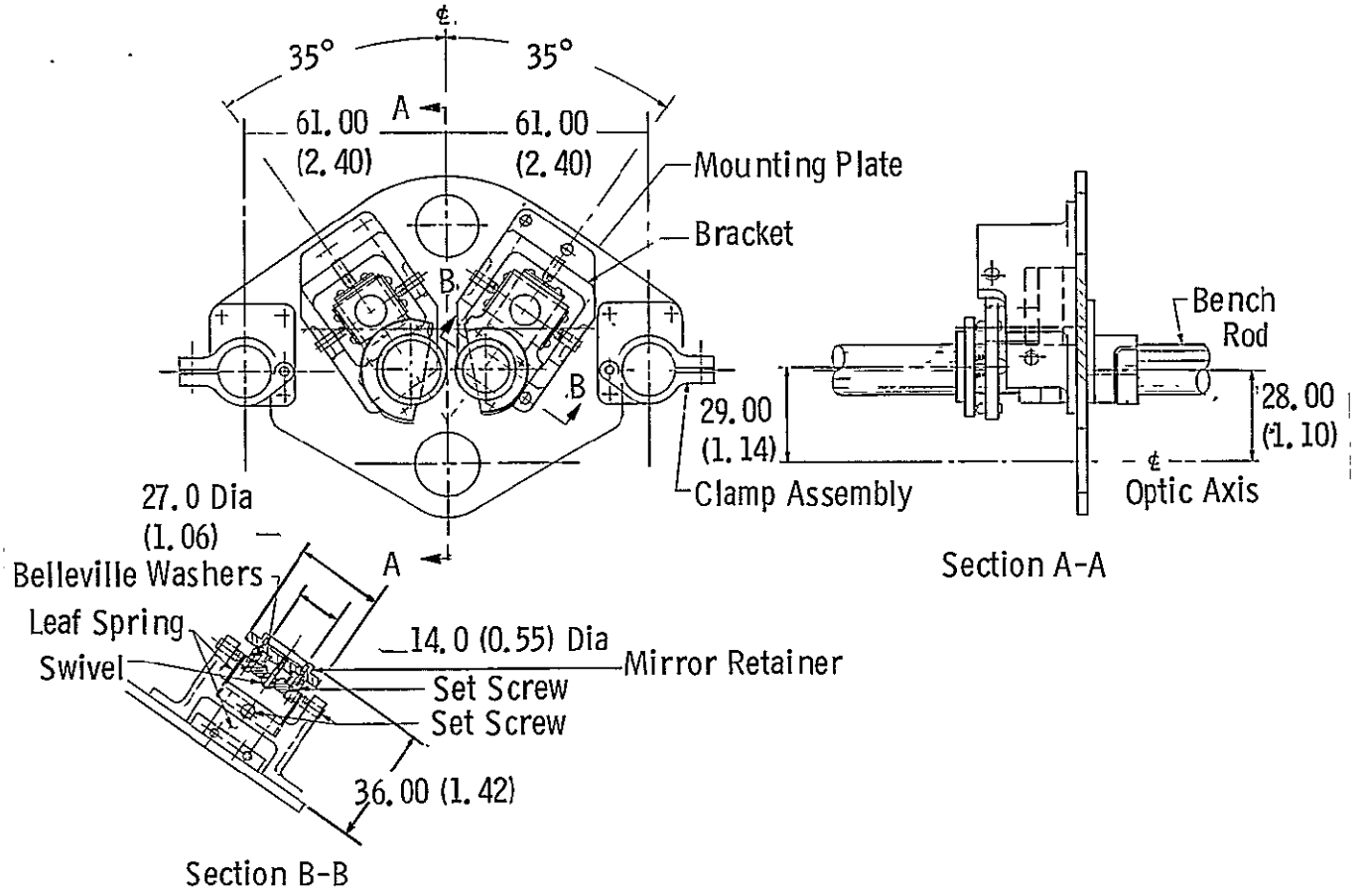

The two secondary relay mirrors for f/24 and f/96 imaging modes are placed immediately aft of the filter wheel assemblies. Initial spacing is set with the clamps on the rods. However, fine adjustment capability must be provided with five degrees of freedom. This is accomplished with the set screw, spring and swivel arrangement that is shown. The sixth degree, roll about the mirror center axis, has relatively little effect on image quality so this will be pre-set and no adjustment capability provided.

Figure 3.4-8 Secondary Mirror Mount Assembly

3.4.7 (Continued)

preload to the mirror mount. In addition each mirror can be rotationally adjusted on a swivel mount by fine adjustment of a spring loaded leveling plate which can be tilted by set screws.

3.4.8 Area Detector (ICCD) Assembly

The area detector mounting assembly is shown in Figure 3.4-9. The selected method of installation is designed to provide a high degree of thermal isolation from the opto-mechanical supporting structure while providing adequate stiffness to protect the sensor from the transient loads experienced during launch and re-entry. The low conductance mount for the area detector is discussed in Section 3.4.9.

The detector package is essentially suspended by equally spaced radial standoffs which attach to ring bands clamped to the forward and aft ends of the detector canister. A pair of triangular shaped frames provides support for the outer ends of the standoffs and are clamped to the optic bench rods with a typical clamp assembly. The apex of each equilateral triangualr shaped frame are tied together with a thin metal strap to provide stabilization.

3.4.9 Venting and Purging

The photometer is equipped with connections for a dry nitrogen purge for prelaunch and postlaunch phases at least when the instrument is not installed in the shuttle orbiter. The purge provides a small positive internal pressure to exclude contaminants. At this time we do not anticipate a gas purge during on-orbit maintenance. The photometer has several vents which allow the instrument to depressurize during launch. The vents also repressurize the instrument during return and must therefore be designed to control contamination carried by the hot and perhaps dirty repressurization gases.

3.4.10 Mechanism Assembly Clamp Concept

The "optical bench rod" concept adopted for this design facilitates installation, alignment and removal of each of the mechanisms and optic mounts. A typical clamping device, as shown in Figure 3.4-10 is attached to mounting plates on each mechanism assembly. The clamp assembly consists of a fixed upper section which is essentially one-half of a cylindrical sleeve. Integrately machined flanges on this section provide for attachment of mounting screws and installation of a pivot shaft, A lower section completes the clamp circle and is attached to the fixed section through clevis lugs to the pivot shaft. Both sections have extended lugs with match drilled holes for inserting bolts which provide clamping force. A special mandrel tool will be used to properly align the clamp assembly to each mechanism mounting plate. When clamp assembly is properly centered, dowel pins will be installed and attachment screws installed. During alignment and checkout of the opto-mechanical assembly the clamp device allows longitudinal adjustment of individual mechanisms. When all adjustments have been made, the clamp is locked to bench rod with set screws or dowel pins.

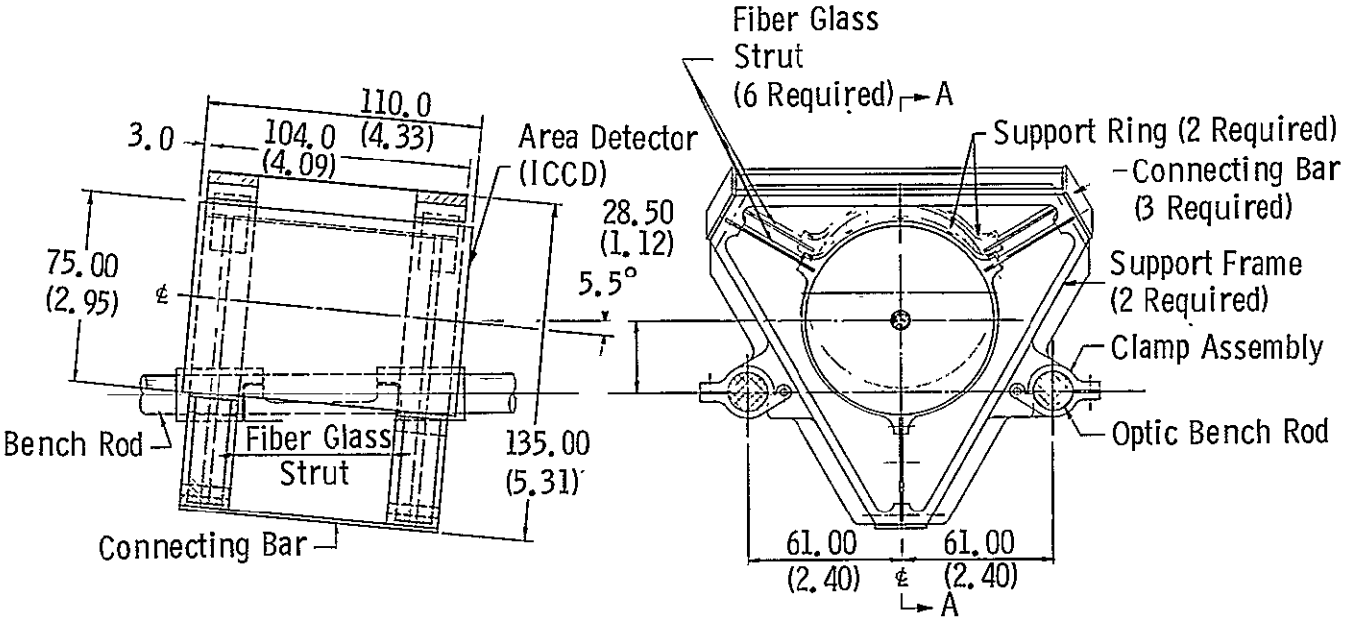

The area detector is clamped to the optical bench rods near the aft end of the opto-mechanical submodule. The area detector is held by two support rings which are in turn held by low thermal conductance fiber glass struts. The strut lengths can be adjusted for final alignment of the area detector.

Figure 3.4-9 Area Detector Mounting

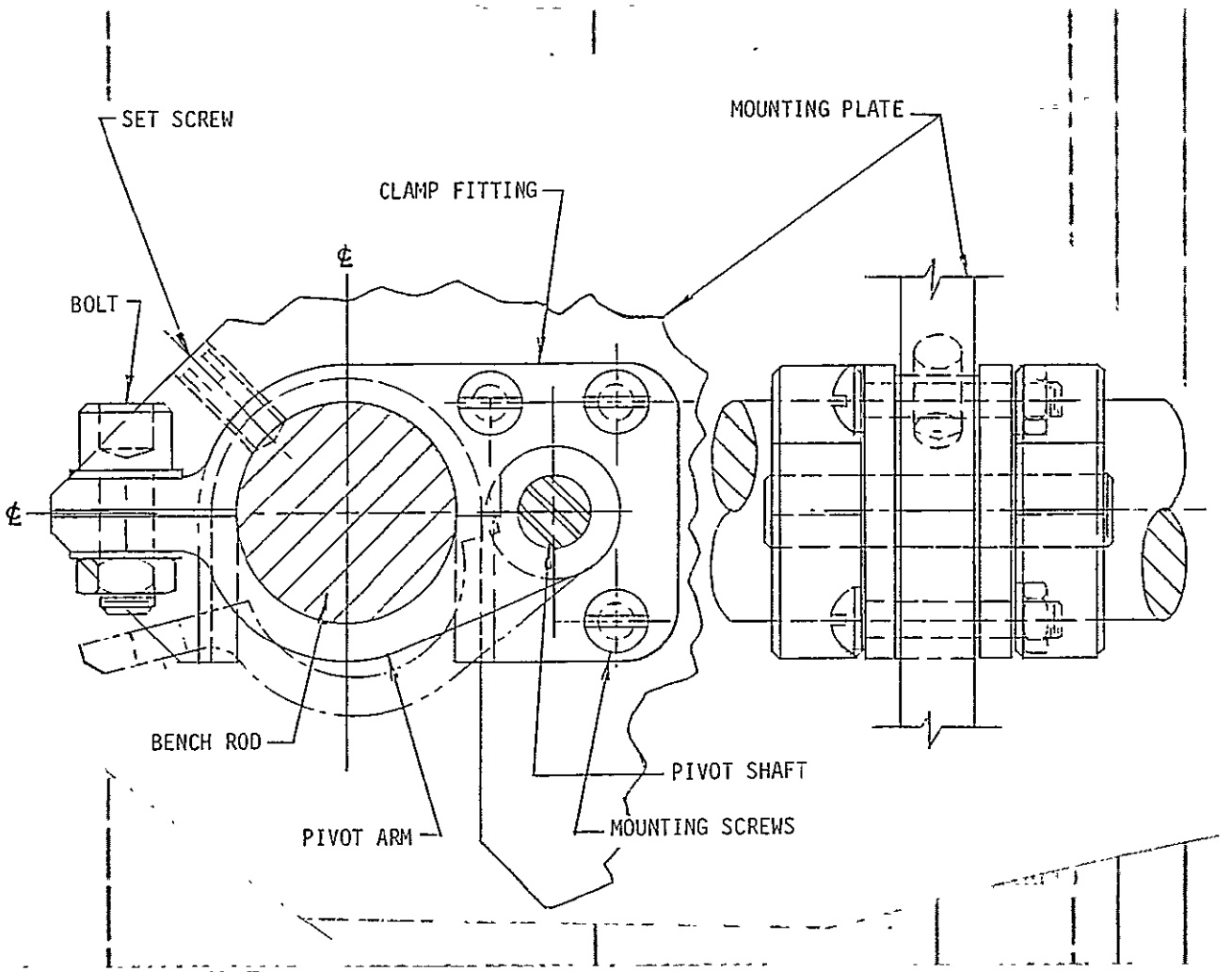

All mechanical and optical components are on carriers which clamp to the optical bench rods. The clamps are two piece fittings which allow components to be moved along the rods during assembly and alignment. The lower half of each clamp assembly is hinged to permit installation. When an assembly has been precisely located the clamp is closed, bolted securely, and then the clamp and rod are either drilled and pinned together or located with a set screw as shown in the figure.

Figure 3.4-10 Bench Clamp Device

3.5 ELECTRONICS

The photometer electronic system supports the operation by providing control, status monitoring, and scientific data handling.

3.5.1 Requirements

The photometer basic performance requirements listed in Section 2.0, require support from the electronics:

a) The speed of the electronics influences the brightest targets which may be viewed. Maximum acceptable target brightness in the photocounting mode is determined by the shortest time interval between distinguishable photocounts. The minimum discernible time interval in turn depends on the sharpness pulse shape from the point detector and the amplifier/discriminator use and fall times. The calculations (Section 3.1.5) indicate that the electronics and PMT's can resolve photon arrivals separated by 10 ns. The minimum required exposure (PMT frame) time is however 0.1 ms.

b) The noise of the point detectors and their preamplifier/discriminator set a limit on the signal-to-noise ratio on faint sources. The largest contributor to dark noise is expected to be the PMT itself--mainly from radiation induced noise. Signal-to-noise ratio is, aside from biases, the reciprocal of the photometric precision. Higher photometric precision necessarily involves high signal-to-noise ratio.

c) Temporal stability of the sensitivity and noise characteristics of the detectors and electronics affects photometric precision. Calibration of sensitivity and noise performance will be done in order to deduce radiances of targets with respect to "standard" sources.

d) Implementation of the "synchronous photometry" mode for observation of rapidly varying periodic sources (pulsars) will not be distinct from simple high speed photon counting with a point detector. The data will not be synchronously detected but rather sampled with precisely controlled intervals. The samples will not generate data in excess of the capacity of the LST data management system, so all synchronous photometry data will be sent directly to the SSM for transmission to the ground without data processing by the Photometer.

e) The minimum exposure duration is 100 μs. The exposure is controlled by gating the high voltage in either point detector or in the ICCD. The gate timing must be controlled to 0.1% by the timing and control function.

f) Choice of the optical elements in the light path is controlled by the Photometer electronics as it executes command sequences which originate outside the instrument.

3.5.1 (Continued)

g) The instrument can accept a set of commands from the S1 computer. A generalized command triggers a standard sequence of operational actions or a string of single commands.

3.5.2 ICCD Characteristics

The ICCD is under development currently and its characteristics are subject to change. The ICCD with its thermoelectric cooler and memory will be Government Furnished. The photometer electronics and other systems must interface with the ICCD which will be integrated into the photometer system.

The ICCD consists of an electrostatically focused intensifier section preceding a solid state silicon charge coupled device which is exposed by the electrons from the intensifier. The CCD format on the photo-cathode is 3.0 x 4.5 mm overall organized as 100 lines of 160 pixels each. The pixels on the photcathode are 25 μm square; they are about 20 μm square on the CCD chip. The light sensitive photocathode is a conventional semi transparen bi-alkali coating on a magnesium fluoride faceplate.

The ICCD tube and some potting (though no shielding) is contained in a can 110 mm long and 75 mm in diameter. Development efforts include a reduction of the required diameter. The potted tube is expected to weigh less than 500 gm (most likely less than 150 gm). Structural support, radiation shielding, and thermal insulation will add some mass, however. The high voltage power supply and post-amplifiers are located external to the tube but in close proximity.

The ICCD requires a high speed buffer memory which is mounted external to the tube and is expected to occupy a volume of approximately 10^4 cm^3 and weigh approximately 5 kg. I/O control and dual 16k word x 16 bit memory sections are included in the volume and weight estimate. Power dissipation is less than 25 watts at 3.0 MHz speeds. 4K RAM (N-MOS) chips are utilized.

Thermoelectric devices will be used to provide cooling and they will be included as an integral part of the tube mounting structure and shield. Cooling of the CCD chip for analog mode is critical. Cooling of the photocathode is less important. A uniform cold soak of the entire tube at 0 to -20°C is planned with additional chip cooling to -40°C. The temperature needs to be controlled only to about $\pm$ 5°C. A two stage thermoelectric device will be required.

For the photon counting imager application, a nominal fixed voltage of -18 kV is applied to the ICCD. A gating voltage of several kilovolts will be employed referenced to the -18 kV. The gating supply shall have transient response of sub-milliseconds driving a 100 pf load. For the acquisition application, the ICCD assumes the proximity diode configuration and requires a nominal 6 kV. Fixed voltages are baselined. Power required for the high voltage supplies is approximately 2 and 5 watts for the 6 and 18 kV supplies respectively.

3.5.2 (Continued)

Readout is fixed by the architecture and chip selection within the memory. TTL logic levels are to be specified for the interface. A second scheme cycles the ICCD four-bit data into four quadrants of the 16K x 16 bit memory in order to achieve the required readout rate. A 14 and 15 bit address control is used in the two schemes, respectively. Somewhat less than 333 ns is to be used to convert the video output; a parallel level sensing scheme is being considered. In both schemes only 1 μs is needed to cycle with the 16 bit memory. Parallel bit organization is assumed. No random access mode is being considered at the present, but in both schemes a zero input at any pixel will inhibit a complete cycle involving the adders for the corresponding memory location. Standard RAM's utilize plus and minus five and plus twelve volts.

The video output is an analog signal which requires analog-to-digital conversion prior to storage in memory. Digitizing to either four bits or ten bits is effected for the "digital" and analog modes respectively.

In the digital mode the output video signal is quantized to 16 levels (that is, four bits A to D). The greatest acceptable signal level in this mode is 16 photoelectron events per picture element. In general the center of the electron image will not fall on the center of a pixel but straddle several pixels. The greatest acceptable light level can thus on the average correspond to somewhat more than 16 photoelectrons per star image.

The ICCD is readout at 3×10^6 pixels per second. Each pixel is represented by a data word of four bits. The digital words are accumulated in a 16k x 4 bit buffer which holds one frame. The four bit data are subsequently added to the 16k x 16 bit deep memory during the next frame (or integration) time of the tube. The frame time is about 12.5 ms.

Synchronous photometry is possible with the area detector provided that the frame rate of the ICCD is significantly smaller than the target period. Although a variable object could be observed with the area detector time variations would be observed in only a few pixels of the sixteen thousand pixels in the format. The variation in those few pixels would be mutually identical because they would correspond to different parts of the image of essentially a point source.

A pentode construction for the electrostatic tube is anticipated: photocathode, focus, accelerator, field corrector, and CCD (at ground potential). The four tube elements will operate at large negative potential with respect to ground; on the order of 10-18 Kilovolts. Fixed voltages, except for the field corrector will be established to achieve optimum performance.

3.5.3 Functional Organization

An interface block diagram for the photometer is shown in Figure 3.5-1. It is assumed that all command and control which originates external to the

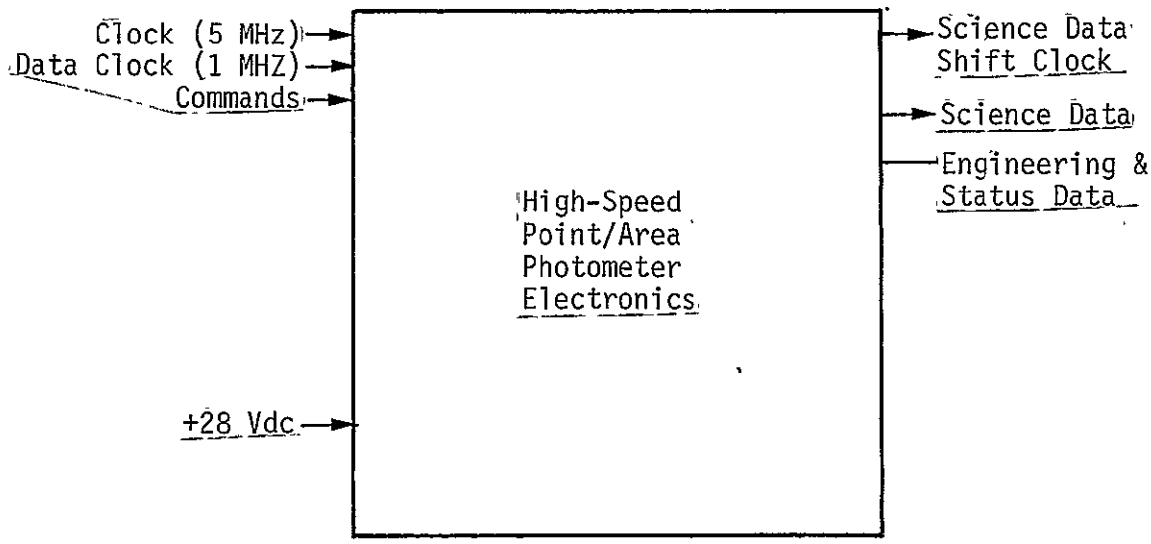

The Photometer interfaces are deliberately made simple to facilitate interchangeability with the other scientific instruments. Inputs are only clocks, commands, and power. Outputs are only science and engineering serial data streams and an associated data clock.

Figure 3.5-1 Interface Block Diagram

3.5.3 (Continued)

photometer is provided via a serial digital command interface line and likewise data are taken from the instrument on a serial digital line. It is further assumed that all engineering status data and all detector (science) data would be formatted within the Photometer system.

A functional block diagram which shows the implementation of the requirements is shown in Figure 3.5-2. It is also assumed that the 256 kilobit memory required for the ICCD would be available for use by the Photometer control electronics to perform whatever data storage is required. This is reasonable because only one detector can operate at a time.

3.5.4 Command and Control

The Photometer is designed to be sufficiently versatile to perform the functions identified so far and other functions which may be defined in the future. Internal instrument operations are controlled by outputs from a timing and control unit through the microprocessor. The timing and control unit can receive and interpret two general kinds of commands across the Photometer interface with the LST (SSM) C&DH system. The commands are called elemental and macro commands. Under most circumstances the Photometer receives macro commands which identify a set of instrument operations to be performed in a specified time sequence. The macro command calls up from a programmable read only memory (PROM) a set of elemental commands which are further decoded into drive signals for motors and so on. The elemental commands can also be sent directly to the Photometer for sequences which were not anticipated or not performed frequently enough to justify storage in the PROM. This approach allows easy implementation of a virtually unlimited number of operational sequences.

Commands which have been identified at this time are listed in Table 3.5-1. The particular structure of the command word has been set up so that these commands could be implemented with a 16-bit word with spare capability for adding additional commands at a later time. In addition a specific coding scheme has been identified to determine the coding capability with the 16-bit word for the number of commands and types of commands required. Other coding schemes should be evaluated and should include error detection and/or correction which is compatible with the SI data handling system for LST.

A master control sequence flow diagram is shown in Figure 3.5-3. A microprocessor is used to handle all timing and control functions. Sequences required for the various operating modes will be stored in programmable read-only-memories thereby giving the flexibility of many and varied sequences. A small buffer RAM will be used to hold special sequences commanded by the command and data handling system (SSM). In addition, as previously discussed the 256 kilobit memory will be attached to the microprocessor providing the ability to more efficiently control this memory.

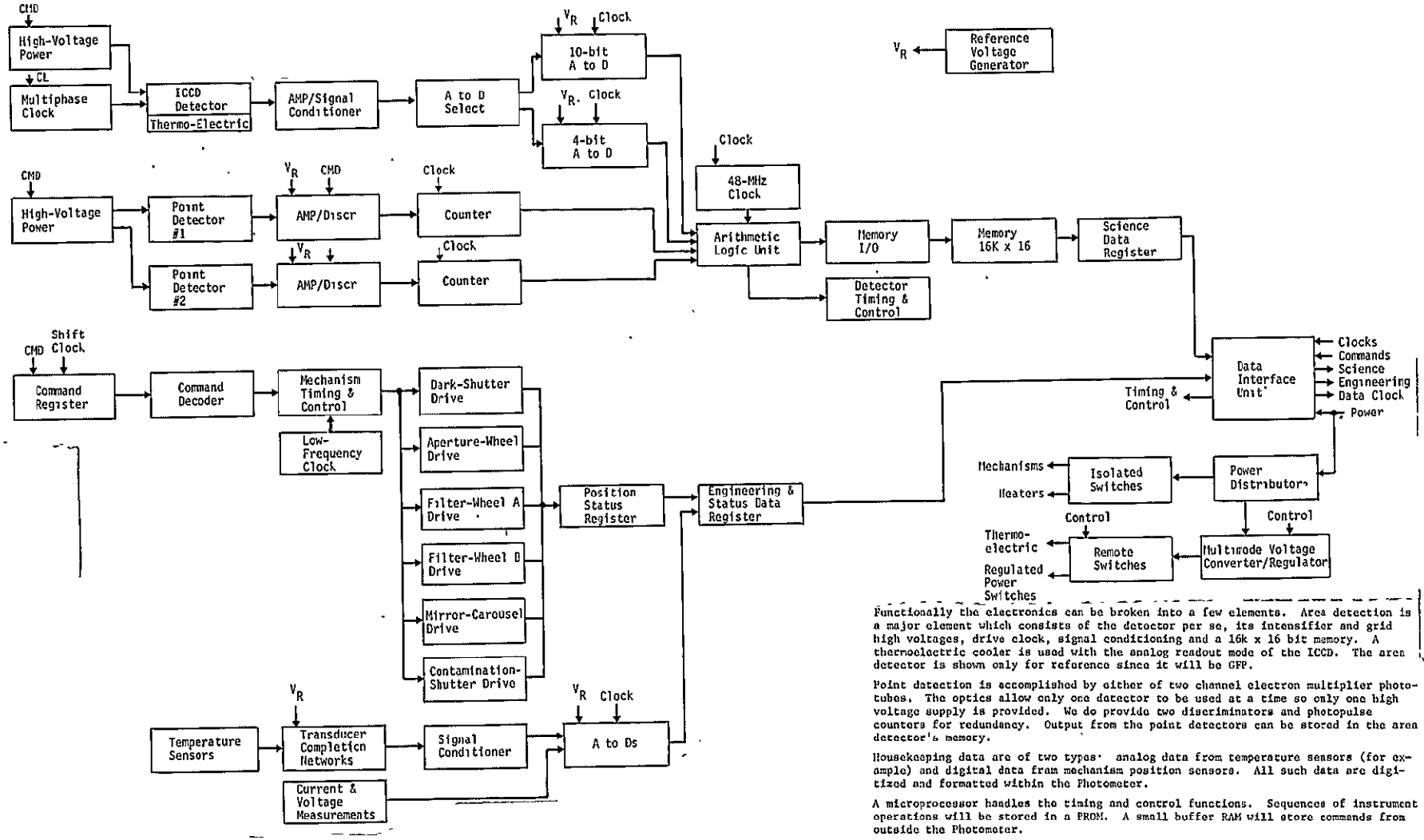

Functionally the electronics can be broken into a few elements. Area detection is a major element which consists of the detector per se, its intensifier and grid high voltages, drive clock, signal conditioning and a 16k x 16 bit memory. A thermoelectric cooler is used with the analog readout mode of the ICCD. The area detector is shown only for reference since it will be GFP.

Point detection is accomplished by either of two channel electron multiplier phototubes. The optics allow only one detector to be used at a time so only one high voltage supply is provided. We do provide two discriminators and photopulse counters for redundancy. Output from the point detectors can be stored in the area detector's memory.

Housekeeping data are of two types: analog data from temperature sensors (for example) and digital data from mechanism position sensors. All such data are digitized and formatted within the Photometer.

A microprocessor handles the timing and control functions. Sequences of instrument operations will be stored in a PROM. A small buffer RAM will store commands from outside the Photometer.

Stepper motors and solenoids are used for mechanism positioning. Positions are sensed with optical encoders and switches to close the loop with the mechanism positioning logic.

Refer to the text for fuller explanation of the electronics functions.

Figure 3.5-2 Electronics Functional Block Diagram

Table 3.5-1 Command List

Number	Command	Command Form
1	Aperture wheel step	12 bits
2	Filter wheel A step	12 bits
3	Filter wheel B step	12 bits
4	Fabry/relay mirror carrousel step	12 bits
5	Spare step	12 bits
6	Spare step	12 bits
7	Point detector high voltage A	8
8	Point detector high voltage B	8
9	Point detector discriminator threshold	8
10	ICCD acceleration high voltage	8
11	ICCD grid high voltage	8
12	Exposure duration (100 s x $2^{N/2}$; N = 14)	14 bits
13	Number of exposures in a frame (M = 256)	8 bits
14	Detector select	3 bits
15	ICCD A/D code (4 or 10 bit)	1 bit
16	Contamination door failure override	1 bit
17	Spare failure Override	1 bit
18	Execute discrete command (each entry represents two commands)	(1, 2) master power (on/off) (3, 4) contamination shutter (open/close) (5, 6) dark count shutter (open/close) (7, 8) heater #1 (on/off) (9, 10) heater #2 (on/off) (11, 12) heater #3 (on/off) (13, 14) heater #4 (on/off) (15, 16) heater #5 (on/off) (17/ 18) thermoelectric cooler (on/off) (19 thru 32) spares
19	Spare	
20 thru 39	Spares	

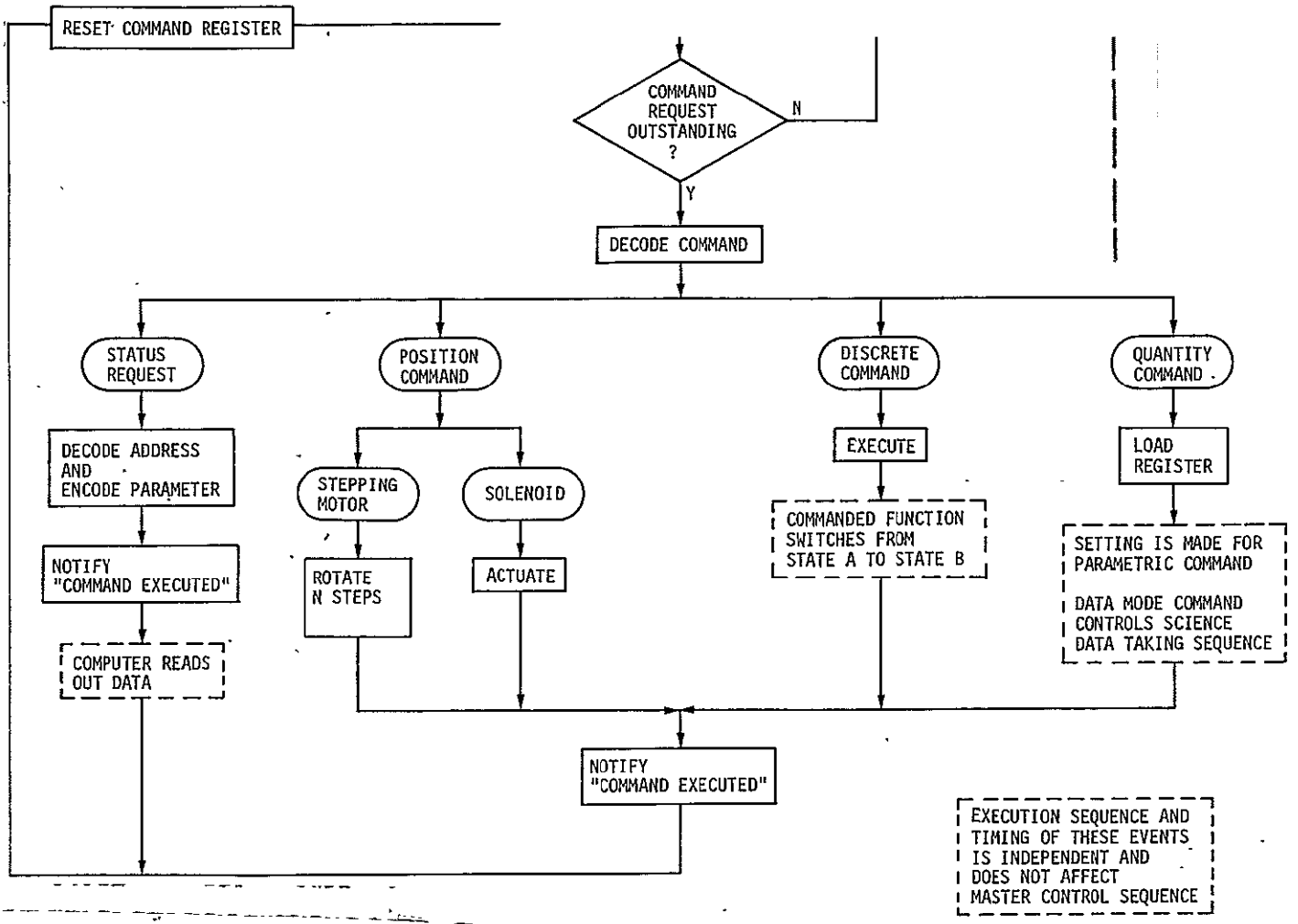

Figure 3.5-3 Master Control Sequence

3.5.4 (Continued)

Timing and control function interfaces directly with the Data Interface Unit (DIU), and is synchronized to the one MHz clock. This clock is divided down in frequency and is used to perform all clocking functions with the exception of that required to operate the Area Detector in the Digital Mode. For this mode a 48 MHz oscillator is required

3.5.4.1 Mechanism Control

Stepper motors and solenoids are used for all mechanism position changes. Appropriate electronics are employed to drive the mechanisms upon receipt of commands.

There are four stepper motors used for the aperture wheel, each of two filter wheels and the mirror carousel. A command to operate a motor consists of selector bits which specify the proper motor and position bits which specify the number of steps. The motor rotation is always counter clockwise. Unidirectional rotation allows reduction of power consumption, greater simplicity of the motor driver electronics and the saving of a discrete command for direction.

Absolute shaft position can be determined although in general only the relative position (number of steps taken) is known. An optical encoder on each shaft generates a pulse for each degree (or other increment) of rotation. The encoder pulses are counted in a nine-bit counter and presented to one side of a comparator. If a non-compare is sensed, a discrete command is sent to the motor controller to step the motor. Motor steps continue until a compare discrete is generated by the comparator. When the motor has stepped to the desired position the nine bit counter contents are read out to the output data formatter as a word of status data. The shaft zero position may be found by stepping to the motor zero position and examining the status data.

There are solenoids used for both the contamination door and the dark shutter. Operation of the solenoid changes the state of the shutter from open to closed or vice versa. Positions of the door and shutter are sensed by switches. The sensed position can be determined by examining the discrete status data.

The electronics used for mechanism positioning are shown in Figure 3.5-4.

Power consumption analysis of the stepper motors is presented in Table 3.5-5.

3.5.5 Data Handling

The data sources for the Photometer consist of Area Detector, the two point detectors, and engineering measurements data. These data can be stored in the instrument until requested by the SI data system or they can be collected and transmitted in real time. The limitation on the amount of data which can be stored is 256 kilobits (the size of the area detector memory), plus the capacity of the buffers. Since there is a redundant 256 kilobit memory, this too could be used for storage if there is a need.

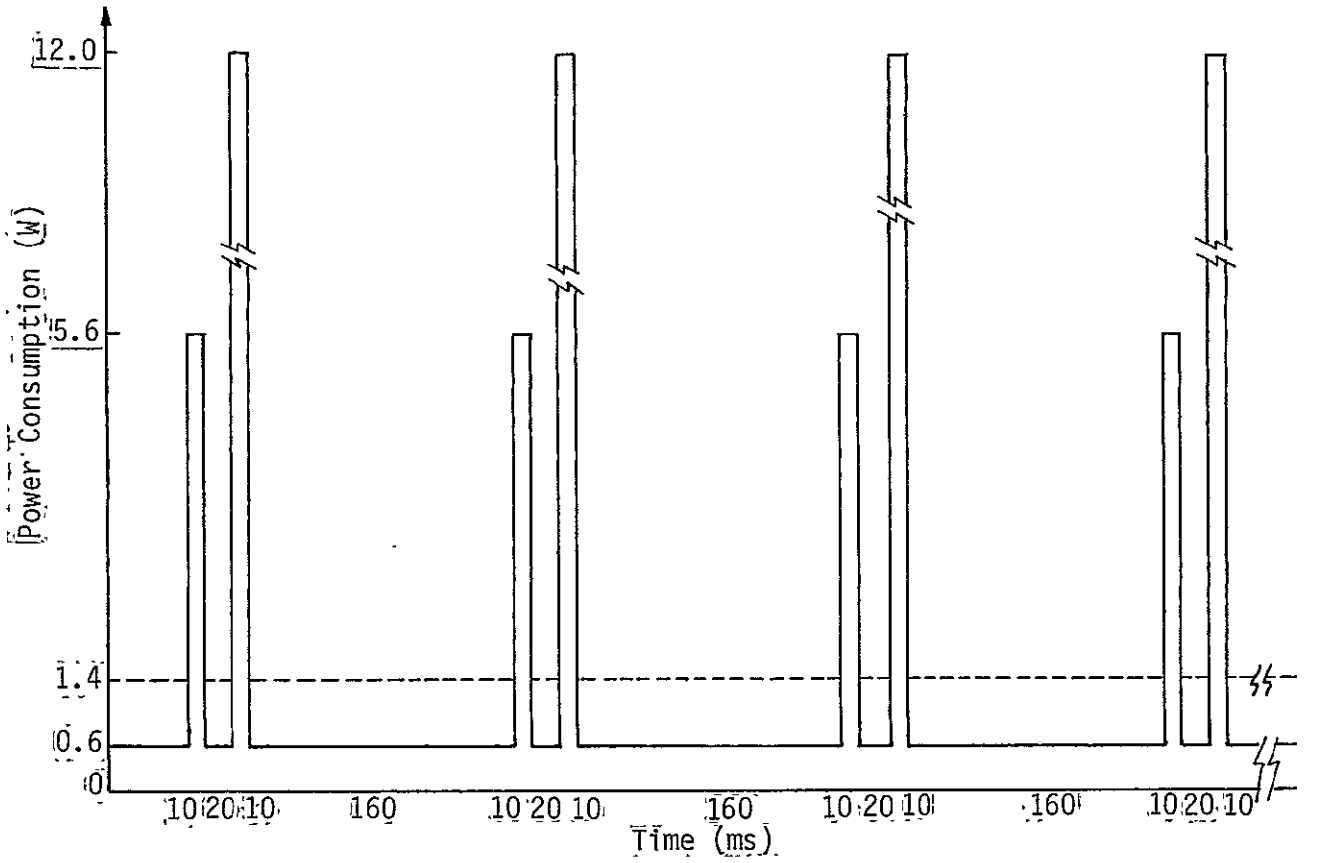

The time line for a hypothetical use of two stepper motors each driven at five steps per second is shown. The motors use 5 and 12 watts for 10 ms when they are energized. The motors are not driven simultaneously to reduce the peak power consumption. The 0.6 W constant load is for the drive electronics for the two motors. The average power consumption is shown as a dashed line at 1.4 W which is indicative of the largest average power consumption during operation of mechanisms.

Figure 3.5-5 Mechanism Drive Motor Power Consumption for Two Motors

Table 3.5-2 Measurement List

Name	Signal Type
Protective shutter open/closed	discrete
Dark count shutter open/closed	discrete
Aperture wheel assembly temperature	analog
Fabry/relay mirror temperature	analog
Point detector #1 temperature	analog
Point detector #2 temperature	analog
Area detector photocathode temperature	analog
Area detector CCD temperature	analog
Area detector cooler hot side temperature	analog
Area detector radiator temperature	analog
Area detector cooler current	analog
Structure position #1 temperature	analog
Structure position #2 temperature	analog
Structure position #3 temperature	analog
Structure position #4 temperature	analog
Reference voltage	analog
Secondary voltage #1	analog
Secondary voltage #2	analog
Secondary voltage #3	analog
Secondary voltage #4	analog
Data mode register contents	digital 12 bits
Motor position register contents	digital 12 bits
Electronics submodule temperature	analog
Structural housing shell position #1 temperature	analog
Structural housing shell position #1 temperature	analog
Overlight sensor	analog
Quartz crystal microbalance	analog
Radiation detector	analog

3.5.5 (Continued)

The need would be based on, as yet undefined, limitations of the LST data management systems to accept the instrument output.

3.5.5.1 Point Detection

The output of a point detector will go directly to a pulse amplifier/discriminator. The discriminator will distinguish most real photo electron events from most noise. The time response will allow counting to a rate of 100k pulses per second. The pulse amplifier/discriminator circuits for the point detectors have a counting rate on the order of 100 kbps. The amplifier is a charge amplifier which uses a high performance FET front end. The gain of the detector is high enough so that no part amplifier is required. This tradeoff is primarily determined by the signal to noise ratio. Filtering and pulse shaping will be provided to sense the voltage changes out of the charge amplifier as the average DC level builds up. The discriminator is a voltage comparator whose threshold level is set depending on the overall system requirements on signal-to-noise level.

A 16 stage counter counts the pulses out of the discriminator. At the end of the programmed counting period the counter contents are stored in a buffer memory. The timing and control unit simply sets the exposure (i.e., counting) duration from 100 ms to as long as desired.

The synchronous photometry mode required by the Final Instrument Definition can be implemented on the ground instead of within the Photometer. The complexity of synchronizing slightly aperiodic sampling to a variable target is avoided by providing only periodic sampling. The data rate from the sampling process is sufficiently low, approximately 100 kbps, that all the samples can be sent to the ground for processing. Doppler correction can also be calculated from the spacecraft ephemeris data and applied on the ground.

3.5.5.2 Area Detection

The area detector is operated in either "analog" or "digital" modes. In digital mode the output video signal is digitized by a four bit A/D converter and in analog mode the signal is digitized by a ten bit A/D converter. The frame times can be significantly different as well. In digital mode exposure times are variable from 30 μs to 300 ms in multiples of $\sqrt{2}$ with a maximum of 250 frames per second. In the analog mode exposure times are variable from 30 ms to 300s. Exposure and readout are in all cases under the control of the timing and control unit.

The primary requirement in the signal conditioning of the Area Detector output will be to handle the analog pulse corresponding to the shortest frame time. The special design of the charge amplifier will be to have a high gain-bandwidth product to process this pulse.

The area detector output is always analog and must therefore be digitized In the "digital" mode a four bit analog-to-digital conversion is performed in

3.5.5.2 (Continued)

250 ns. In the "analog" mode the conversion is to ten bits and is performed in 18 ms.

The ICCD memory could be used not only for the ICCD but also for other Photometer uses. The memory is a 16k word by 16 bit random access memory (RAM) built up of 1024 x 1 N-MOS chips. The memory assembly is designed to operate in a read/write two segment mode. This allows a continuous 18 samples per second at a 3 megaword rate.

The read/write mode of operation consists of first reading data out of memory and adding this data to the four bits from the A/D, then writing the data sum back into the same memory location. During the first cycle the data from the memory is not added to the 4 bit input data, thereby doing a memory initialization. If an overflow indication is detected from the Authentic Logic Unit (ALU), the overflow data sum is not written into the memory. This method of operation lends itself to simplified timing and control functions for the A/D, ALU, and memory assemblies.

The ALU is a full look-ahead adder capable of doing a 16 bit add operation in less than 40 ns.

Two discretes are transmitted. These are Zero Input and Overflow. The first discrete is sent as long as the 4 bit A/D converter output is zero, thus indicating "no" or "low" sensor output from the Photometer assembly. The overflow discrete is sent when an add operation overflows the sixteen bit buffer limit. The overflow discrete should be detected and change the operating mode from ADD OPERATION to DATA DUMP and ADD OPERATION RESTART mode. In this read/write mode of operation a dump memory and restart add operation can take place simultaneously thereby maintaining a high sampling rate efficiency.

The assumed modes of operation are: STANDBY, PWR DOWN, ADD OPERATION, DUMP MEMORY, DUMP MEMORY & RESTART ADD OPERATION, and TEN BIT QUANTIZATION.

Timing and phasing between the Memory Assembly and Photometer Assembly can be maintained by a timing discrete and a master clock for both assemblies, thereby establishing coherent timing and phasing.

It must be noted that by going to a "four quadrant" mode on the RAM and a Photometer sampling rate of 6 MHz; the sampling rate per pixel can be increased to 37 samples per second from 18 samples per second. This increase in sampling rate involves no new technology advances other than those now proposed for the memory assembly.

3.5.5.3 Temperature Sensing

Supporting the evaluation of the detector data will be the temperature sensor data. This supporting data is important from the viewpoint of having a clear understanding of the instrument as it is exposed to varying temperatures specifically in supporting the calibration of the instrument. Another

3.5.5.3 (Continued)

important aspect will be to monitor the "health" of instrument and take whatever precautionary measurements are necessary whenever temperatures exceed certain values. Temperature sensors are platinum wire resistance elements connected to a resistive bridge network to obtain a signal which varies between 0 and 40 millivolts for each sensor. An accurate reference voltage is supplied to the bridge from a voltage generator. Amplifiers are used to condition the signal up to 5 volts prior to being digitized. A multiplexer is used to apply all engineering measurement signals to an A/D converter.

3.5.5.4 Data Formatting and Output

Proper interpretation of science data requires information about the status of various Photometer internal conditions. As an example, the known mean noise counts are subtracted from the observed signal plus noise. The accuracy of the resultant estimate clearly depends on how well the mean noise is known. Since noise generated by the detectors depends, in part, on photocathode temperature, it is necessary to know those temperatures. Of course it is also necessary to know the relationship between temperature and mean noise count rate but without the temperature measurement there is no way to estimate the noise. Temperature sensors are provided at appropriate locations within the Photometer. Critical engineering data, such as appropriate temperatures will be interleaved with the science data to facilitate data reduction. The interleaving is performed by a formatter in the DIU which then transmits the assembled science plus engineering data frame over the output data channel to the SSM. Sets of engineering status requests will be generated in accordance with a program stored in a PROM. The resultant engineering data streams will then be interleaved. This approach will be flexible and accommodate the needs of the investigators.

3.5.6 Power Conditioning and Distribution

Input electrical power to the Photometer is 28 vdc ± 20%. The Photometer provides appropriate regulation and voltage levels as required by electronics, sensors, and mechanisms. The internal power supply consists of two programmable high voltage supplies, 18 kV and 3 kV for sensors and a low voltage converter regulator supply which provides all of the secondary voltages required by the instrument. The converter can process up to 150 watts. The converter design incorporates high and low voltage sensing to insure that a failure in the supply would not cause damage to any parts. Should any voltage go out of tolerance, the converter would be turned off. The low voltage supply is dual redundant.

Both high and low voltage supplies are commandable to accommodate different Photometer operational modes. Table 3.5-4 lists power consumption requirements. There is also a minimal power consumption dormant mode in which the Photometer consumes approximately 3 watts, most of which is the inefficiency of the power supply operating at low power. In this mode the instrument has been powered on and has only those circuits necessary to sense a command to go into an operational mode.

3.5.6.1 Power Consumption Timeline

A list of power consumptions of the various loads is shown in Table 3.5-4. The three detector modes are shown separately because the components constituting the load are different from one to another. These power consumption figures do not incorporate the effect of duty cycle on mechanism power consumption as shown in Figure 3.5-5. The average power consumed by solenoids and stepper motors is quite low because of the duty cycle.

The timeline in Figure 3.5-7 shows how power consumption varies during use of the three detector modes. The durations of the loads depend on the targets being observed and on mission constraints such as passage through the South Atlantic Anomaly. This timeline should be of sufficient accuracy for sizing of the Photometer's power system and predicting power requirements.

3.5.7 Reliability Considerations

To improve the reliability of data handling functions the system uses a concept of partial redundancy. The concept employs a "pilot" and a "co-pilot" set of electronics. The pilot electronics are always on (unless they have failed) and the co-pilot is in a powered off state. Determination of a failure is made on the ground and a command issued to switch to the co-pilot. Except for electronics intimately associated with the detectors, all electronics can be duplicated. This approach is compatible with the dual memory configuration defined to us.

Use of majority vote electronics was considered and rejected because a majority vote system requires three sets of electronics all of which are on all the time that a given function is required. The resultant additional hardware, power consumption and waste heat generation was determined to be unnecessary because the ground operator can detect failure and determine appropriate remedial action. Thus, a "voting" operator can replace voting electronics.

TABLE 3.5-3 Power Consumption

Load	Power Consumption (Watts) Operating Mode		
	Area Analog	Area Digital	Point
ICCD			
Control	3.5	3.5	0
High Voltage Supply	2	5	0
Thermo-electric Cooler	22	0	0
Clock	.5	.5	0
Signal Processor	2	2	0
Memory	0	25	0
Memory Input/Output	0	10	0
Arithmetic Logic Unit	0	2	0
Point Detector			
High Voltage Supply	0	0	2
Signal Processor	0	0	2
Clock	0	0	.5
Timing and Control Logic	10	10	10
DIU's (Total For Two)	8	8	8
Transducers/Housekeeping Sensors	.5	.5	.5
Mechanisms			
Contam. Door Solenoid	15	15	15
Contam. Door Solenoid Controller	.05	.05	.05
Park Count Shutter	15	15	15
Dark Count Shutter Controller	.2	.2	.2
Aperture Wheel	12	12	12
Aperture Wheel Controller	.2	.2	.2
Filter Wheel A	5	5	5
Filter Wheel A Controller	.4	.4	.4
Filter Wheel B	5	5	5
Filter Wheel B Controller	.4	.4	.4
Mirror Carousel	12	12	12
Mirror Carousel Controller	.2	.2	.2
Buffers, Comparator, Storage Register	1	1	1
Thermal Control Heaters (Range 1.5 to 15W)	15	15	15

NOTE: Motor loads are intermittent having a duty cycle of 5% or less.

Figure 3.5-6 Power Consumption in Various Operational Modes.

State or Events	Loads On	Average Power Consumption (Watts)		Duration
Dormant	Heaters	3		
	+ Housekeeping Sensors	.5		
	+ DIU's	8		
	+ Power Supply	3		
			14.5	Indefinite
ICCD Cooldown	Above	14.5		
	+ TE Cooler	22		
			36.5	600s
Initialize Mechanisms	Above	36.5		
	+ Overall Timine & Control Logic	10		
	+ Buffers, Comparator, Storage Register	1		
	+ Drive Mechanisms	1.4		
	+ Power Supply Increment	3.0		
			51.9	60s
Mechanisms in Place	Above	51.9		
	- Drive Mechanisms	-1.4		
	- Power Supply	- .3		
			50.2	Indefinite
Target Acquisition Expose (Area Defector Analog)	Above	50.2		
	+ ICCD Control	3.5		
	+ HVPS	2		
	+ Clock	.5		
	+ Signal Processor	2		
	+ Power Supply Increment	2		
			60.2	30s
Readout to SSM	Above		60.2	16s
Wait for Pointing Correction	Above	[illegible]	60.2	15s
Target Acquisition Expose	Above	6	60.2	30s
Readout to SSM	Above		60.2	16s
Mechanisms	Above	60.2		
	+ Drive Mechanisms	1.4		
	+ Power Supply	0.3		
			61.9	2s

Figure 3.5-6 Power Consumption in Various Operational Modes - Continued

State or Events	Loads On	Average Power Consumption (Watts)		Duration
Target Acquisition	Above	61.9		
Expose	- Drive Mechanisms	-1.4		
	- Power Supply	-0.3		
			60.2	30s
Readout to SSM	Above		60.2	16s
Area Detector Off	Above	60.2		
	- ICCD Control	-3.5		
	- HVPS	-2		
	- Clock	-.5		
	- Signal Processor	-2		
	- Power Supply	-2		
			50.2	Indefinite
Dark Shutter Close	Above	50.2		
	+ Shutter & Power	19.0		
			69.2	10ms
Point Detector On	Above	69.2		
	- Shutter	-15.2		
	+ HVPS	+2		
	+ Signal Processor	+2		
	+ Clock	+.5		
	+ Power Supply	1.1		
			55.8	Indefinite
Dark Count	Above		55.8	30s
Dark Shutter Open	Above	55.8		
	+ Shutter & Power	19		
			74.8	10ms
Point Detector Expose	Above	74.8		
	- Shutter & Power	-19		
			55.8	40s
Change Filter	Above	55.8		
	+ Drive Mechanisms & Power	1.7		
			57.5	5s
Point Detector Expose	Above	57.5		
	- Mechanism & Power	-1.7		
			55.8	100s
Repeat Change Filter and Expose Sequence 10 Times				1050s

Figure 3.5-6 Power Consumption in Various Operational Modes - Concluded

State or Events	Loads On	Average Power Consumption (Watts)	Duration
Dark Shutter Close	Above	55.8	
	+ Shutter & Power	+19	
		74.8	10ms
Dark Count	Above	74.8	
	- Shutter & Power	-19	
		55.8	30s
Slew to Next Target	Above	55.8	120s
Dormant	Heaters	3	
	+ Housekeeping Sensors	.5	
	+ DIU's	8	
	+ Power Supply	3	
		14.5	Indefinite
Initialize Mechanisms	Above	14.5	
	+ Timing and Control Logic	10	
	+ Buffers, Comparator, Storage Register	1	
	+ Drive Mechanisms	1.4	
	+ Power Supply Increment	3.1	
		30.0	60s
Mechanisms in Place	Above	30.0	
	- Drive Mechanisms	-1.4	
	- Power Supply	-0.3	
		28.3	Indefinite
Area Detector Expose	Above	28.3	
	+ ICCD Control	3.5	
	+ HVPS	5	
	+ Clock	.5	
	+ Signal Processor	2	
	+ Memory	25	
	+ Memory I/O	10	
	+ ALU	2	
	+ Power Supply	12	
		88.3	120s
Change Filter	Above	88.3	
	+ Drive Mechanism & Power	1.7	
		90.0	5s

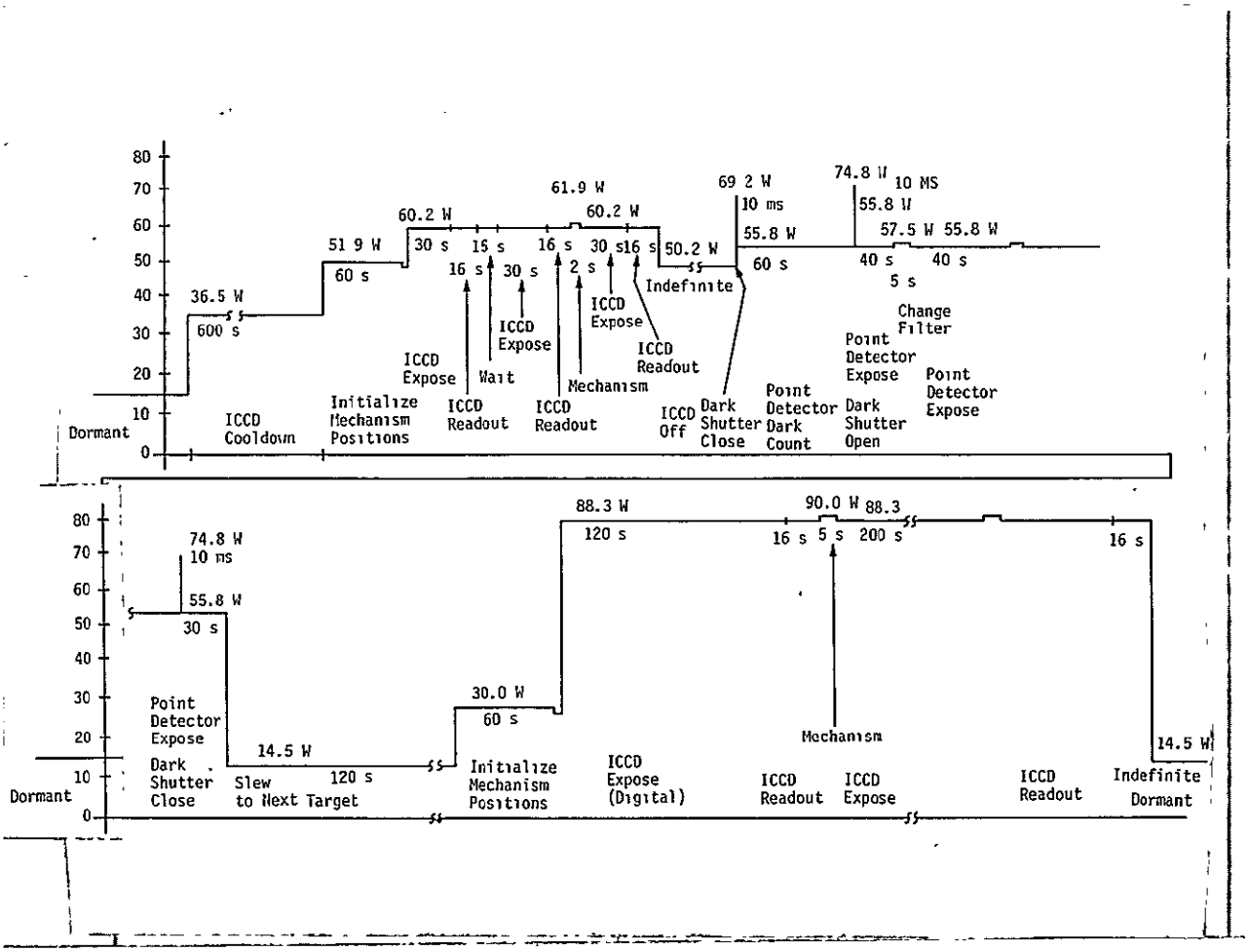

Peak power ever consumed is in the worst case about 115 W. Typical power consumption is about 60 W for both ICCD analog mode and point detection and is about 90 W for the ICCD digital mode. Power consumption of individual loads is presented in Table 3.5-4. Events or instrument states are indicated under the time line. Power consumption and duration of the load are also shown. Exposure times shown are arbitrary and would in practice depend on the observations to be made.

Figure 3.5-7 Timeline for Power Consumption

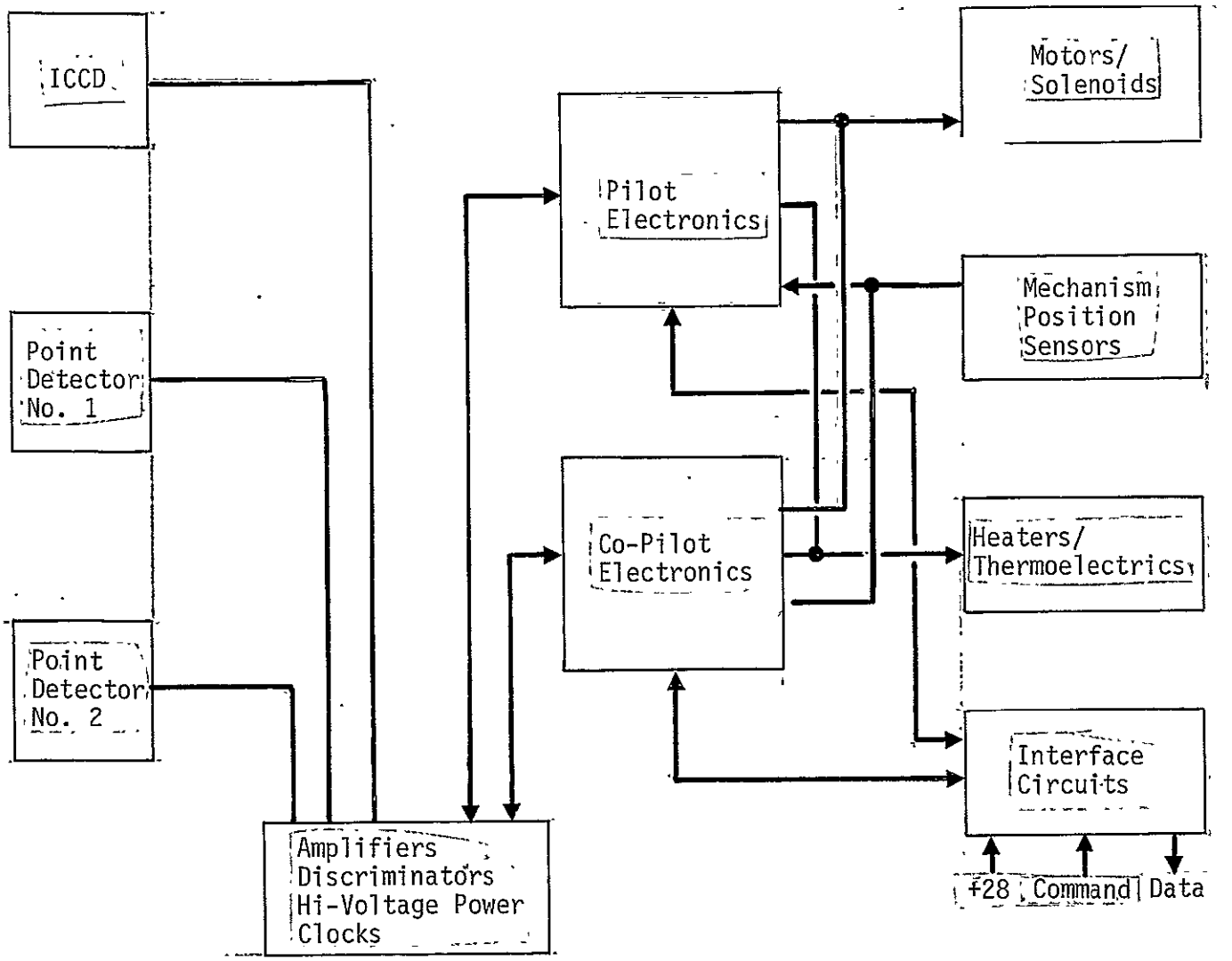

To improve the reliability of data handling functions the system uses a concept of partial redundancy. The concept employs a "pilot" and a "co-pilot" set of electronics. The pilot electronics are always on (unless they have failed) and the co-pilot is in a powered off state. Determination of a failure is made on the ground and a command issued to switch to the co-pilot. Except for electronics intimately associated with the detectors, all electronics can be duplicated. This approach is compatible with the dual memory configuration to be provided with the ICCD.

Figure 3.5-8 Electronics Redundancy Approach

3.5.8 Packaging

The electronics for one system are packaged on eight printed wiring boards whose size is approximately 15.5 x 17.8 cm. Boards up to four layers are used. The redundant system also requires eight boards. The electronics compartment within the instrument provides two cavities each having a useable volume of 7.4 which is adequate to package the electronics.

Electronics are located so that they have a clear radiative path to the outer (curved) surface of the structural housing. The inside of that surface is painted black with a pattern of reflective tape applied as necessary to tailor the overall emissivity. Compactness of the electronics is not needed because the volume of the Photometer is ample. A large electronics surface area facilitates thermal control.

3.5.9 Connectors

The electronics contained in the electronics submodule can be separated mechanically from the structural housing. All leads to the opto-mechanical submodule are routed through a small number of connectors. All leads to the outside world are likewise routed through a small number of connectors. Support equipment cables are provided to facilitate checkout of the Photometer when the submodules are separated from the structural housing. Connectors to the outside are operable by the gloved hand of an astronaut while the LST is on orbit. The connectors will be identical with those of other scientific instruments.

4.0 OPERATIONS

4.1 Operational Modes

The Photometer must operate in distinct ways to various times in response to different environments and functional demands.

4.1.1 Launch and Prelaunch

Launch and prelaunch phases include time that the Photometer is in the Shuttle Orbiter either installed in the LST or installed into a yet-to-be-specified container for an on-orbit maintenance launch. The Photometer will be inactive and will consume no electrical power. The immediate environment of the instrument will have to be maintained within specified tolerable limits with special attention given to protection from contamination. That environment has not yet been defined.

4.1.2 Calibration

Calibration here refers to on-orbit measurement of instrument performance characteristics. The calibration will involve viewing one or more of a set of "standard" stars as well as some internal checks.

Initial calibration is expected to be extensive in order that operators may thoroughly evaluate instrument performance. Subsequent calibrations are expected to be less extensive and serve mainly to monitor possible degradation or other changes with time. In any case calibration sequences are commandable from the ground. Frequently used sequences could be programmed into the Photometer's programmable read only memory just as frequently used observational sequences could be programmed.

A possible set of calibration for an initial calibration sequence could include measurement of the offsets of each of the apertures with respect to the fine guidance sensor primary pointing reference. These data would be required for efficient target acquisition for all future observations. The calibration could be accomplished by stepping the telescope line of sight through small increments and observing the optical power transmitted by each aperture as a function of pointing direction. The apertures involved would be all except the large aperture used only as a stray light stop for area detection. A similar off-set calibration would be performed for the area detector at both f/24 and f/96 although it would not be necessary to increment the line of sight direction.

It might also be desirable to measure the transmittance profiles of the apertures. This measurement cannot be made with extremely high precision for two reasons: the OTA input image is not small compared to many of the aperture sizes and the area detector relays have been designed to form good images of the sky and not of the apertures. Nevertheless, scanning an image over an aperture does yield the convolution of the image intensity with the aperture transmittance. The deconvolution can be done if the image intensity profile is known.

4.1.2 (Continued)

One of the fundamental calibrations needed is the instrument overall sensitivity. That is photon count rate output for stars of known radiances. The calibration needs to be done for each of the four detectors and with each of the spectral filters. If a polarization analysis system were included a calibration of instrument throughput as a function waveplate position would be performed. The instrument sensitivity calibrations are important for at least two reasons: throughput of the entire optical system (OTA plus Photometer) is not easily measured on the ground especially in the extreme ultraviolet and the system photometer accuracy requirement is very stringent.

Spatial resolution calibration of the f/24 and f/96 area detection modes is required. Resolution calibration of the point photometry modes is required only for the two long slits used for double star scanning. In the case of the slits the important calibration is actually of slit profile measured on the ground and line-of-sight drift rate which is measured by some element of the fine guidance system. Resolution calibration of area photometry would be performed by viewing a set of double stars of known separations when imaged in various parts of the area detector field-of-view.

Geometric distortion of area detector images can be calculated from the optical formula, measured in the lab, or checked against known star fields on-orbit. The very high resolution of the Photometer may make star field calibrations impractical because the relative positions of the stars will not be known any better than can be measured with the Photometer itself.

Exposure intervals can be best calibrated electronically rather than by actual star observations. This is especially true for short exposures which accumulate, in general, only a modest number of photons - an observation which suffers from photon rate fluctuations which are intrinsic to the signal and cannot be compensated for.

Frequent calibrations will be made of apparent count rates in the absence of a signal. These dark count calibrations are likely to vary substantially as a function of detector temperatures, radiation environment, exposure history of the detectors and so on. High photometric accuracy requires accurate removal of as much of the dark count rate as possible.

4.1.3 Target Acquisition

Pointing of the LST is under the control of the Fine Guidance System (FGS). The FGS will always use two or three off-set guide stars and not the Photometer target as the pointing reference. A central data processor in the System Support Module will do sequencing and data processing for target acquisition.

The Photometer will, however, participate in acquisition by using the analog area detection mode to obtain a picture of the sky. The image will be transmitted to the ground for interpretation and evaluation either by operations personnel or a computer system or both. The pointing corrections are determined, verified and uplinked to the LST. Real time operation is presumed as the norm.

4.1.3 (Continued)

The SSM data management system will (when used with the Itek FGS) perform the following tasks:

1) Take the programmed target location, in appropriate coordinates, and convert it to pitch, yaw and roll commands for the SSM Pointing Control Programs. A wait will be calculated and initiated while the coarse pointing is complete.

2) Identify guidestar offsets from the target and convert them to eight OTA P&CS grate and optical micrometer settings. These values are transferred to the OTA P&CS. Sensors (image dissectors) then provide error signals to the SSM Pointing Control Programs.

3) Command the SI to acquire an image when the fine guidance acquisition is complete.

4) Receive the image as a digital data stream and transmit it to the ground. This transmission is required for normal data taking, except that the action should be constrained to real time for target acquisition.

5) Receive the uplink commands identifying the pointing increments needed in pitch and yaw. These must be converted to 8 new Fine Guidance System grate and optical micrometer settings (2 grate intersection and 2 micrometer offsets for each of 2 guidestars).

The Photometer itself operates the area detector in a special mode. Preceding the desired time of target acquisition the ICCD cooler is turned on to precool the entire ICCD. The cold soak will reduce the temperature of the entire tube to 0 to -20°C and the CCD chip to -40°C. Cooling is necessary to allow substantial integration times on the CCD chip. The aperture wheel will place the large rectangular aperture in the light path. Presumably no filters will be in the light path for most targets to allow highest possible light levels on the detector. The f/24 relay will be used.

4.2 Operability

4.2.1 Reliability

The design makes unlikely the occurrence of an internal failure which could terminate all science data taking. There are some elements which constitute single point failure locations but they have been given special attention to assure reliability. It is worth noting that despite the theoretical possibility of replacing a disabled photometer it is unlikely that a maintenance mission would be made for the sake of the Photometer alone. Routine maintenance visits can be anticipated at intervals of two to three years. Photometer is, therefore, necessarily a high reliability, long life instrument.

We used an extensive and detailed parts list developed as part of the preliminary design to assess Photometer reliability. Historical experience with motors, gear trains, electronic components and so on was used with a mathematical model. Successive computer runs of the model use statistical failure rates for components to derive failure rates for the entire instrument.

We assumed a duty cycle for the Photometer of 25% because it is only one of the four instruments anticipated. Actually some orbital time is lost because of observational constraints so the duty cycle may be less than 25%. Our model also included the polarization analysis mechanisms which have been deleted. The predicted reliability for one year on-orbit was 0.8435 which is insignificantly less than the required reliability of 0.85.

Table 4.2-1 summarizes failure rates of the components which are currently in the Photometer.

In general single point failure probability has been minimized through design alone. Both the contamination door and dark shutter, however, have fail safe modes. The contamination door has an override device for opening the entrance port even if the normal door drive should fail closed. Probabilities of failure of the aperture wheel, filter wheels, and mirror carousels between acceptable locations were considered to be acceptably low. Furthermore, fail-safe mechanisms for those devices would be complex, difficult to design, expensive, and subject to their own failure. We thus retained some potential single point failures as shown in Table 4.2-2.

4.2.2 Maintenance

We analyzed the Photometer to determine its compatibility with the LST maintenance approach, and to evaluate on-orbit and ground maintainability. Previous analyses using our computer maintenance simulation model resulted in identification of all the scientific instruments as candidates for on-orbit maintenance since each contains both "life limited" and "high failure rate" items. This analysis assumed that the SI's will be replaced on-orbit; however, trade studies and analyses are still being conducted on the total LST to determine the optimum balance between on-orbit and ground maintenance and specifically which items are cost effective to replace on orbit.

4.2.2.1 On-Orbit Maintenance - All SI modules and layout were designed specifically for ease of on-orbit maintenance and instrument updating. The modular approach greatly simplifies on-orbit removal and replacement of instruments since the total instrument complement is contained in four axial modules that can be easily handled by a suited astronaut in zero-g conditions. This common module approach simplifies the instrument interfaces with the Focal Plane Assembly and allows the suited astronaut to maintain critical alignments necessary for the instruments.

The instrument updating can be accomplished by installing the new instrument in one of the common modules and installing it on-orbit in place of the existing instrument. A disadvantage of the modular approach is that the complete instrument must be replaced even though only a single item such as a detector has failed. Replacement of any items within the modules would be difficult with respect to alignment and would create contamination problems for the instrument optics.

The removal and replacement of the Photometer and other instrument modules have been analyzed in detail to determine the specific requirements for handrails, foot restraints, latching mechanisms, electrical connectors, and space to translate the modules in and out of the compartment. The SI modules are provided with a latch mechanism and locating blocks for alignment when the module is installed. All of the latches can be operated easily by a suited astronaut using one hand. Also, the required space for the suited astronaut to translate the modules has been provided in this SI arrangement.

4.2.2.2 Ground Maintenance - Ground maintenance and refurbishment of the Photometersis estimated to occur 3-4 times during the total LST mission. Also, ground maintenance may be performed during the testing and checkout phases prior to installation of the LST in the Shuttle for launch.

The Photometer has been designed primarily for ease of on-orbit installation and removal; however, the large and fairly heavy module is difficult to remove and replace on the ground. Radial access doors are necessary with the LST in either a vertical or horizontal position since a special fixture to aid in removal or replacement of the Photometer through the aft end would be complex and difficult to design.

4.2.2.3 Problems and Recommendations - There are no apparent problems associated with the on-orbit replacement of the Photometer module. The contamination control should not be difficult with the modular concept. It is recommended that the ability to maintain the required alignments during replacement of the modules be verified to ensure proper operation of the latching mechanisms and locating blocks on the Photometer.

4.2.3 Contamination Control

The Photometer will be assembled and tested in clean environments. The assembled instrument will be protected by control of its environment and by its own contamination door. Control of the Photometer environment during transportation will be accomplished by enclosing the instrument in a box which excludes contaminants. During installation on the LST we expect the Photometer to be kept in a dry nitrogen environment.

Table 4.2-1 Reliability Estimate

Subassembly/Part	Quantity	Failure Rate*
Contamination Door Assembly	1	2.00
Shutter Assembly	1	4.00
Aperture Wheel Assembly	1	4.00
Filter Wheel Assembly	1	9.20
Primary Mirror Assembly	1	6.00
Secondary Mirror Assembly	1	0.01
Point Detector Assembly	1	4.00
Area Detector Assembly	1	8.00
Electronics Module	1	10.00
Housing	1	0.05
Total Operating Failure Rate =		= 47.26
Non-operating Failure Rate =		= 9.78

One Year Reliability: 0.8455 for 25% Duty Cycle

*Failures per million hours.

Table 4.2-2 Single Point Failures

Single Point Failure	Method of Elimination or Rationale for Retention
Contamination Door Assembly, Fails Closed	Fail safe device will swing door to the open position.
Shutter Assembly, Fails Closed	Fail safe release mechanism is provided so shutter fails open.
Aperture Wheel Assembly, Jams	Probability very low, fail safe device very complex.
Filter Wheel Assembly, Jams	Probability very low, fail safe device complex.
Mirror Carousel, Jams between Positions.	Probability of failure very low, therefore is acceptable.

The Photometer is equipped with connections for a dry nitrogen purge for prelaunch and postlaunch phases at least when the instrument is not installed in the shuttle orbiter. The purge provides a small positive internal pressure to exclude contaminants. At this time we do not anticipate a gas purge during on-orbit maintenance. The photometer has several vents which allow the instrument to depressurize during launch. The vents also repressurize the instrument during return and therefore are filtered to control contamination carried by the hot and perhaps dirty repressurization gases.

As the name implies the contamination door is an optically opaque closure of the Photometer entrance port. The door is closed except during observations to prevent contaminants from entering the instruments. Even when the door is open the only opening to the interior of the opto-mechanical submodule except for filtered vents is the entrance aperture. The entrance apertures are, of course, very small and thus susceptible to blockage by small particles, but they do keep most contaminants away from the other optics.

4.2.4 Radiation Effects

Data from the Orbiting Astronomical Observatories have shown that the radiation environment in low earth orbit causes considerable dark noise in photomultiplier tubes. The exact mechanism is not known but appears to be primarily emission of light by tube faceplates after exposure to protons. Much of the light emission is delayed and thus corrupts observations made even when the incident proton flux is low.

Radiation effects to be considered and avoided in the design are "browning" of the tube windows by radiation induced crystal inperfections, fluorescence of the windows, and to a lesser extent damage to the photocathodes and other parts of the tubes. Existing data imply that the radiation dosage rather than kind of radiation (electrons, protons, and bremsstrahlung photons) determines the detector dark noise.

Techniques for minimizing noise effects are to use low susceptibility materials such as magnesium fluoride and to reduce the volume of the faceplates. We intend to use magnesium fluoride for its desirable spectral properties anyhow and have chosen a tube with a faceplate volume of only two mm^3. Shielding has not yet been designed but room has been left to install shielding. All the Photometer detectors are near the centerline of the LST and will thus benefit from the radiation protection provided by the LST structure even without deliberate application of shielding.

5.0 TEST

The basic approach to piece part testing has been to specify NASA approved parts per MIL-S-975. We will suggest additions to the approved list where required. The Photometer design has been defined to the piece part level as far as practicable.

We expect to test the delivered flight article to levels sufficient to assure that it will meet its functional performance requirements. Qualification and acceptance of the instrument will be done by the NASA at GSFC.

5.1 Test Requirements

Test requirements have not been supplied by the Final Instrument Definition nor by any NASA document. In accordance with discussions with GSFC personnel, we have assumed that the Photometer flight unit will receive system level qualification and acceptance tests at GSFC with the tests performed by NASA personnel with support from Martin Marietta engineering personnel. The tests performed by Martin Marietta will all be in process tests to assure us (and not necessarily NASA) that the Photometer construction and functioning are in accordance with design requirements.

5.2 Test Operations

The details of the test flow must await further clarification of both the design and the division of testing responsibilities between MMC and NASA. The current best estimate is shown in Figure 5.2-1. Tests will consist basically of electronics subsystem verification, thermal subsystem verification, optical alignment verification, functional verification and alignment verification. All tests will be performed in laboratory ambient conditions except a thermal control system design verification which must be performed in vacuum.

Tests will be performed at the highest practicable assembly level. Component tests will also be performed though none are shown in Figure 5.2-1. The complement of tests will be performed on the prototype Photometer. After testing, workmanship and design faults should be apparent and will be remedied during refurbishment. After the prototype has been refurbished it will be called the flight unit and will be subjected to similar tests again except that the thermal control system will not be verified again. All flight unit tests at MMC will be in laboratory ambient conditions. The cleanliness levels required during assembly and test have not been defined, but it is expected that class 10k will be specified.

Both prototype and flight units will be tested to assure and set optical alignments with the opto-mechanical submodule in the laboratory separate from the structural housing. Access to components for adjustment is only possible with the submodule separate. The attachment of the opto-mechanical submodule has been designed so that no forces can be introduced by the structural housing which would misalign the optics.

ORIGINAL PAGE IS OF POOR QUALITY

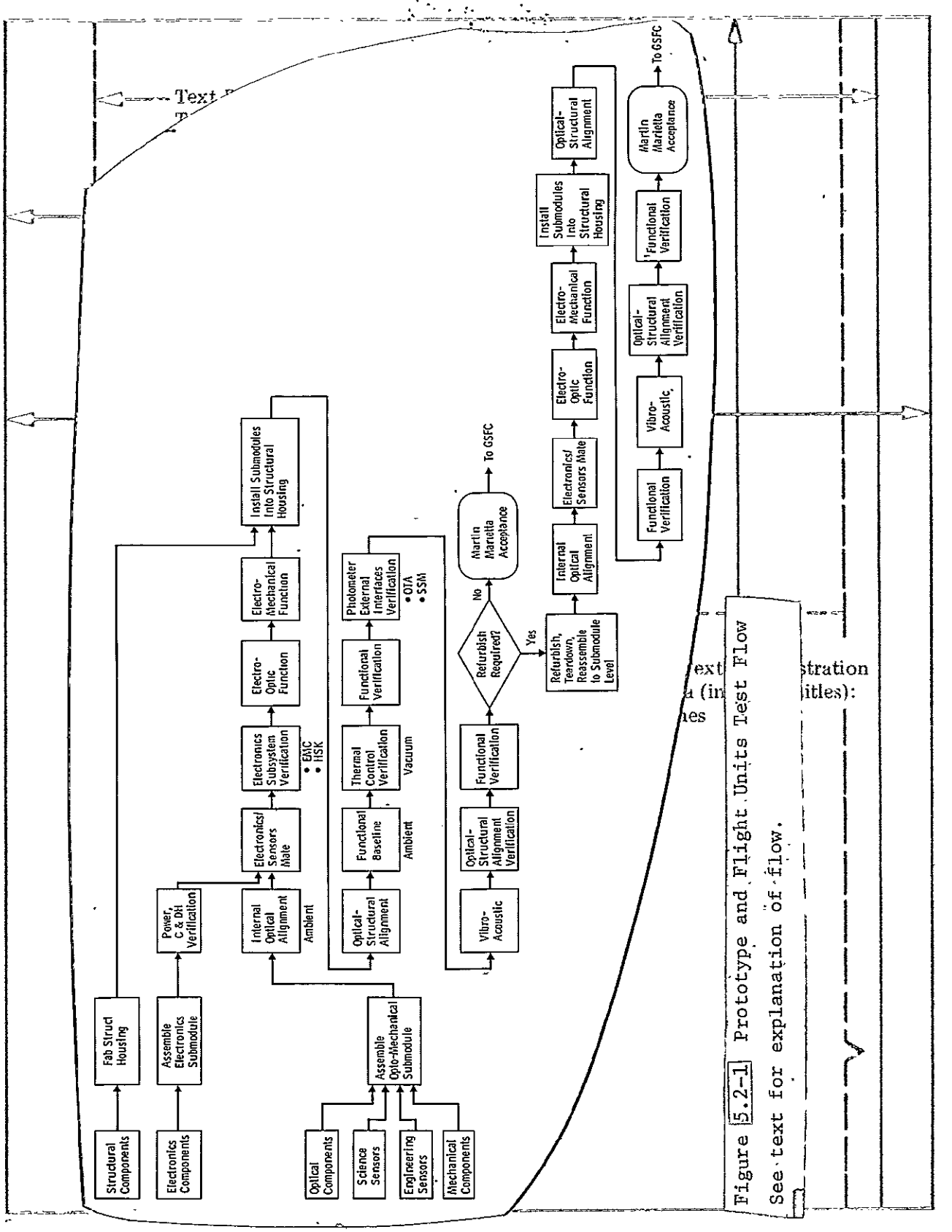

Figure 5.2-1 Prototype and Flight Units Test Flow

See text for explanation of flow.

The electronics submodule can be similarly tested outside of the structural housing. Service cables are provided to connect the opto-mechanical and electronics submodules and to connect with a simulated SSM. The SSM simulator supplies electrical power, commands and a clock and receives both simulated science and engineering data from the Photometer. After connection of the submodules tests are performed to verify compliance with emc requirements, to verify proper functioning of housekeeping and engineering sensors, the electro-optical devices (sensors) and to verify proper functioning of all mechanisms. The power conditioning and data handling systems can be verified by the use of appropriate test gear before mating of the electronics to the opto-mechanical submodule.

Upon completion of those tests the opto-mechanical and electronics modules are both installed into the structural housing. The opto-mechanical optical alignment is then set with respect to the interface pads on the structural housing. Those pads mate to the Focal Plane Assembly. No internal alignment of the opto-mechanical submodule is attempted at this point. Now the Photometer is a complete instrument and is run through a gamut of tests to establish its performance characteristics functional baseline such as mechanism actuation times, electronics noise characteristics and so on.

The functional baseline is followed by the only vacuum test: verification of proper function of the thermal control system throughout the expected range of operating thermal environments. The test results will also be incorporated into the thermal math model of the instrument and potentially into the thermal/mass simulator.

Functional verification is performed again after the thermal vacuum exposure to detect any changes or failures in the instrument. The nominal interfaces with the OTA and SSM are then simulated and compatibility of the Photometer with those interfaces is verified. The interfaces of interest are optical, mechanical alignment, electrical, command and data. The dry gas purge system will also be verified because its performance is related to the mechanical interface of Photometer and OTA structure.

A low level vibro-acoustic test will be performed to expose any defects in workmanship. Acoustic excitation is expected to be the largest part of the launch vibro-acoustic environment so the test will emphasize acoustic disturbance. Following the vibro-acoustic exposure the alignment of the opto-mechanical submodule to the structural housing will be reverified. Functional verification will be performed again and a decision made as to the level of refurbishment of the prototype needed.

In any case the refurbishment will involve partial disassembly of the prototype Photometer to clean all the optics and to replace defective parts. It is possible that inadequate design of some assemblies will be revealed and redesign and fabrication of new assemblies will be required. Upon completion of refurbishment the gamut of tests except thermal control system verification will be repeated. At the conclusion of the flight unit tests MMC will consider the Photometer to be deliverable to the NASA. Photometer level qualification and government acceptance tests will be performed at GSFC with MMC support.

5.3 Test Equipment

Several specialized pieces of equipment will be required to test the Photometer prior to delivery to the NASA. Post-delivery test equipment is not addressed here.

5.3.1 Optical Stimulator

Much of the optical alignment of the Photometer will be performed with ordinary optics lab equipment. There is, however, a need for a special "optical stimulator" which will allow through-the-system tests of Photometer mechanical, electrical and optical functions. The optical stimulator will simulate the behavior of the Optical Telescope Assembly and will provide images to the Photometer which simulate various possible astronomical targets. Special targets can also be provided whose function is purely diagnostic and which are not intended to resemble any celestial source. Multiple star targets for example could be used. Light of arbitrary polarization and spectral content can be provided (within some limits) if desired.

The stimulator is built up from off-the-shelf commercial parts as much as possible. Every attempt will be made to reduce hardware complexity and cost while still making a useful instrument. To control cost we do not intend to design the optical stimulator to work in the extreme ultraviolet so that the instrument may operate in air and employ refractive optics. Interchangeable parts will be moved manually wherever possible to spare the complexity of motor drives except for a waveplate rotator. The waveplate rotator is only required if the Photometer itself has the optional polarization analysis features.

It is possible that other LST scientific instruments would need equipment highly analogous to our optical stimulator. We suggest that a stimulator more universal than the one we identify here deserves investigation.

The overall configuration of the optical stimulator consists of a set of sources, filters, chopper, polarizers, pinhole or other targets, a collimating lens, relay and a mask simulating the OTA exit pupil. All the components are mounted in appropriate carriers which are attached to a common optical bench.

The Photometer spans a very large spectral range. It is, however, prohibitively difficult to cover the whole range with the optical stimulator, particularly the far ultraviolet. We will use two light sources: a tungsten lamp and a xenon arc lamp. Each source has its own housing, condensers, attenuators, cooling blower, power supply and so on. The light from the source fills any of a set of targets with a uniform irradiance. The near uv and visible ranges are covered by the two sources.

A carrier is provided to accept spectral filters. The filters are placed between the light source condenser and the target plane so they are not in the imaging path. The Xe arc lamp has a substantial UV output which may degrade some filters so it may prove desirable to place filters where the flux is lower. A tradeoff with optical imaging quality would have to be made if the filters followed the target plane. A set of narrow hand filters could be used to perform a rough spectral sensitivity

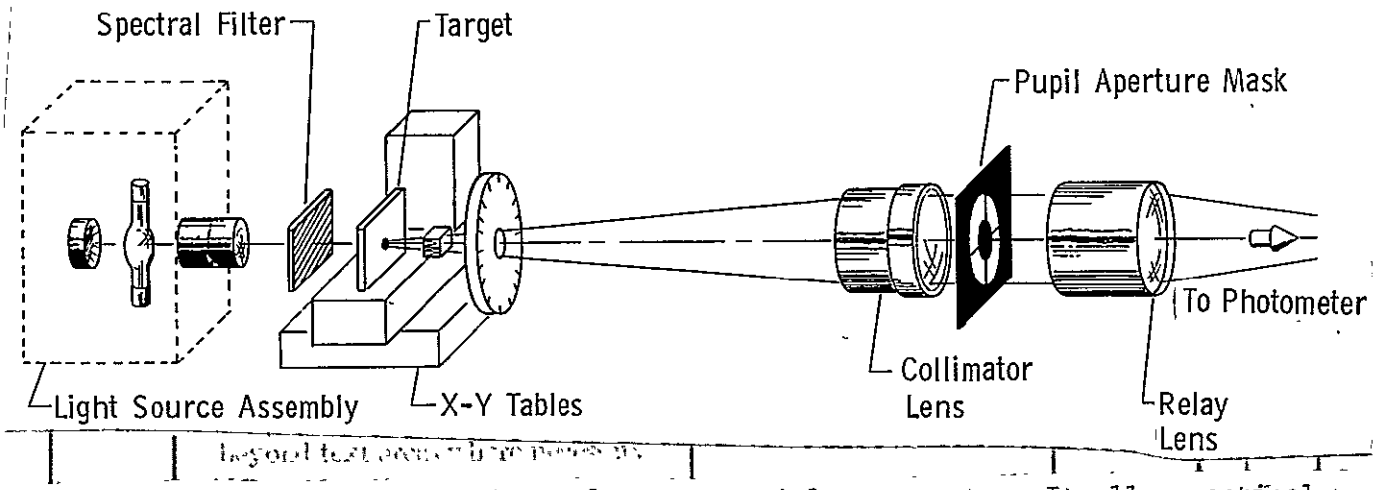

An optical stimulator is built up from commercial components. It allows optical functional checkout of the Photometer with light that is similar to that which will be provided by the OTA.

Figure 6.3-1 Optical Stimulator

calibration of the Photometer without the need for a monochromator. Broad-band filters could be used to modify the lamp spectral distributions to simulate stars of various spectral classes.

A chopper can be placed near the target plane to modulate the irradiance in time. A variable frequency chopper would roughly simulate a pulsar-like source.

A depolarizing wedge is placed near the target plane when pinhole targets are used to eliminate any polarization of the source light. This is important even if the Photometer has no polarization analysis capability because the Photometer optics will introduce their own polarization sensitivity which is undesired but also nearly unavoidable.

The stimulator has a carrier to accept interchangeable targets. The targets include small pinholes to simulate stars, multiple pinholes to simulate multiple stars, and a set of multibar charts. The multibars can, with appropriate calibration and data processing, allow determination of the modulation transfer function of the photometer. Of course, modulation transfer function can be deduced from any target in principle but the bars are relatively easy to use in practice.

The targets are held on an x-y motion stage to allow movement anywhere in the aperture plane within a small distance of the optical axis.

A linear polarizer and a quarter waveplate follow the target plane. Each is held in its own rotatable mounting to allow production of 100% elliptically polarized light of any orientation and ellipticity. Several quarter waveplates or an achromatic quarter waveplate are required to cover the whole spectral region. The waveplate is rotated by a stepper motor, the polarizer is rotated manually.

The light diverging from the target is collimated by a diffraction limited lens. The field of the lens need not be large and the lens need not operate over a wide spectral band at any one time so we hope diffraction limited performance can be achieved without tremendous difficulty.

A mask is placed near the collimator lens to simulate the transmittance of the OTA exit pupil including the secondary mirror and spider obstructions.

A second lens is placed to refocus the collimated light from the collimator onto the entrance apertures of the Photometer and to form a virtual image of the aperture mask 57.6 m (or essentially infinity) in front of the Photometer. The relay lens forms a nearly diffraction limited image of the target on the Photometer entrance aperture. The lens is required to operate at two pairs of conjugates simultaneously so the image of the aperture mask may not be very good but would be adequate.

5.3.2 Other Test Aids

5.3.2.1 Master Alignment Template

We provide positive control of the Photometer/OTA physical interface (i.e., registration pads by use of a master template. The tool will be fabricated from aluminum plate with an anodized finish and equipped with hardened steel reference surfaces. A minimum of two locating pads are provided for accurate registration. Orientation, indexing and locating information would be clearly marked on the template to assure proper utilization.

5.3.2.2 Alignment Gauges

Inspection of precision instrument components during fabrication and assembly requires special alignment verification tools. These tools, as yet undefined, will be used for first order inspection at the detail/sub-assembly level and shall facilitate the making of coarse adjustments. Fine adjustments are made at the top assembly level using special optical equipment to measure tilt, rotation, translation and transverse positions. Some of these same devices can be used to verify alignment of Photometer instrument module to OTA focal plane housing.

5.3.2.3 Vibro-acoustic Fixture

The vibro-acoustic fixture(s) are designed and built to duplicate the transmission characteristics, load paths and preloading forces encountered under actual operational conditions. The Photometer instrument module when mounted to the fixture shall experience the same degrees-of-freedom expected in flight configuration. The strength and stiffness properties of fixture shall consider these characteristics of theoretical OTA focal plane housing supporting structure.

5.3.2.4 Thermal Vacuum Fixture

In order to perform the thermal control system verification test in the thermal vacuum chamber it is necessary to provide a holding fixture for mounting the Photometer instrument module. This fixture duplicates the OTA mounting fixture interface for aligning and locking in place only. This fixture shall be lightweight, portable and clean room compatible.

5.3.3 Electronics Testers

Testers will be built as required to verify proper functioning of various electronics assemblies of a black box level. For example testers will be built for the high voltage supplies, the stepper motor drive electronics and so on. Testers will be built up from off-the-shelf commercial parts and assemblies as much as possible.

An electronics test set will be built and used with system level prototype and flight units to exercise the instrument and to analyze the Photometer's responses. The test set is considered Ground Support Equipment and is discussed in Section 7.1.

6.0 SUPPORT EQUIPMENT

Support equipment here means deliverable items used in testing the Photometer. Support equipment of distinct kinds is needed in space and on the ground.

6.1 Space Support Equipment

Preservation of the cleanliness level of the Photometer module both interior and exterior is of paramount importance. A reusable flight stowage container is required to protect the Photometer instrument from contamination during transport in the shuttle cargo bay. In addition a stowage container prevents inadvertent damage due to activities in cargo bay which might jar or degrade internal optic alignment.

These containers are of seamless aluminum construction insofar as possible. Dessicant breathers shall be installed to maintain a dry atmosphere and to allow venting. Containers are equipped with hinged lids fitted with dust and moisture seals. Over center locking latches are provided to positively seal the lid against metal stops.

Mounting of the Photometer inside the container will consider the "built-in" instrument hard points and utilize these points for rigidly attaching to the container. Shock isolation is provided if required.

The approximate size of the container is 220 cm x 100 cm x 100 cm. Provision will be made to attach the stowage container to the orbiter bay structure utilizing special tie-down fittings.

If on-orbit maintenance plans indicate that the Photometer would be exposed to open space for a substantial length of time, a fabric bag will be provided to protect the instrument from extreme thermal environments associated with exposure to either the sky or to direct sunlight.

6.2 Ground Support Equipment

GSE handling equipment includes those devices required to lift, adjust, mount or temporarily protect the instrument package during assembly, or checkout. The devices include slings, detachable handles, support fixtures for maintaining instrument in any attitude, equipment carts, simulated OTA interface mounting brackets and special tools. All devices shall be clean room compatible.

Reusable shipping containers will be provided to protect Photometer assemblies during shipping and ground storage. These containers are also used for on-site transportation to assure cleanliness levels and to facilitate handling. When the Photometer has been completed it will be hard mounted in the containers by means of the OTA mounting fittings. The shipping container can then be placed in a larger container or crate equipped with fitted foam cushions to provide a high degree of shock attenuation.

The construction of the shipping containers will be similar to the flight stowage containers described in Section 7.1.

An operational support fixture is required to mount and support the Photometer during test operations such as temperature cycling, thermal vacuum and humidity tests. The fixture will have built-in adjustment capability in order to support instrument in any attitude and any height. The support fixture will utilize Photometer hard points for primary support and mounting.

A data rack will be supplied. It is built up from commercial equipment and contains oscilloscopes, tape recorders, programmable signal generators and the like. The data rack will be used for functional checkout of the Photometer.

A manual control box will be supplied to introduce commands to the Photometer to perform functional checkout. The control box will also provide display.

7.0 POLARIMETRY OPTIONS

At this time there is no requirement for polarization analysis capability in the Photometer. In the past such a requirement has existed and we have performed a preliminary design. Designs of mechanisms and optics to accomplish the polarimetry function have been developed to a sufficiently sophisticated level to allow cost estimation.

The existing Photometer modular design can accommodate a polarimetry attachment without major impact. Some additional cabling would be required but there are essentially no other hardware design impacts. In particular there is sufficient space on the optical bench rods to mount the waveplates and polarizers and their associated mechanisms without moving any other components.

7.1 Polarization Optics

A waveplate assembly and a linear polarizer constitute the polarimetry portion of the photometer. They are used to analyze the Stokes parameters of the incoming light. For quasimonochromatic light the Stokes parameters comprise a complete description of the state of polarization. Systematic errors are avoided by placing the waveplates in front of the polarizer which is fixed. Section 14.2 derives the operation of the polarimetry apparatus in exhausting detail. Here it suffices to say that rotation of a waveplate modulates the light reaching the detector. The modulated light is sampled by stepping the waveplate rotation at 22.5^{o} increments. The increments could be increased to 30^{o} if desired although there is no compelling reason to do so. In all cases the light that reaches the detectors is linearly polarized (though of variable intensity) so that the intrinsic polarization of the detector has a constant effect and thus does not bias the measurements. Various weighted combinations of the output signal observed with different waveplate positions allow each Stokes parameter to be determined.

7.1.1 Waveplates

Polarization analysis over the entire spectral range requires a set of four quarter wave retardation plates and a single linear polarizer. The waveplates retard the light by a nominal quarter wavelength but any retardation other than half a wave is acceptable. The exact retardation as a function of wavelength must be known by calibration to allow the observations to be reduced properly.

Three waveplates are used exclusively in the ultraviolet. The fourth waveplate is "achromatic" over the spectral range from 320 nm to 650 nm. The waveplates are retained in a wheel which has six circular holes. Four holes hold the complement of waveplates while two holes are open positions. The waveplates can also be rotated around the optical axis. The waveplates are made as thin as possible to minimize their optical path length and absorption. The waveplates are also made plane parallel and smooth so that even when they are rotated they do not deviate the ray bundle and thus cause spurious signal modulation. The waveplates are sized to preclude vignetting

of the light in even the worst case of largest aperture and maximum allowable decentration. Waveplates have clear apertures on the order of 10 mm. The open holes are as large as possible to increase the probability that a waveplate wheel drive failure will not block the light beam.

In the far ultraviolet the only transmitting and birefringent material is crystaline magnesium fluoride. The waveplates are thus made of magnesium fluoride except for the achromatic plate which is made of a cemented sandwich of magnesium fluoride and crystaline quartz. The plates made entirely of MgF_2 consist of two crystals with their optic axes (in the crystal optics sense) crossed. The optical thickness of the waveplates is on the order of 0.15 mm.

The waveplate assembly is clamped to the optics bench about 100 mm behind the entrance aperture and a similar distance in front of the filter wheels.

The individual waveplates are mounted in a rotatable housing which is press fitted into a hubless spur gear. The waveplate housing is mounted in precision bearings of ABEC 9 precision quality. Basic positioning of any waveplate is accomplished by a Geneva mechanism as shown in Figure 7.1-1. The Geneva mechanism consisting of a 6-tooth Geneva gear, cam driver and stepper motor was selected for its simplicity, considering that precise positioning is not required. The mechanism shown has been designed to satisfy the requirements of waveplate positioning in the light path and rotation around the chief ray when in position.

When the Geneva driver is positioning a waveplate by indexing the Geneva gear, the individual waveplate housings are caused to rotate about a central sun gear which is fixed directly to a separate stepper motor (nonenergized during positioning phase). The 2:1 gear ratio between the sun gear and the planetary gears surrounding the waveplate housing are such that a 60° (or any multiple of 60°) rotation of the Geneva wheel results in a 180° rotation of all waveplates with respect to their initial position. Since the transmission characteristics of a waveplate repeat with every 180° of rotation, the waveplates will always end up at the proper reference (starting) position.

The Geneva wheel is positioned by a size 15 permanent magnet stepper gear motor with a 60:1 internal gear ratio. The cam driver is pinned directly to the motor shaft. The central, sun-gear driver is a side mounted permanent magnet stepper/gear motor with a 45:1 internal ratio which transmits rotary motion through a 1:1 bevel gear set. This motor is mounted in this manner for clearance purposes.

Two optical encoders are employed: one for waveplate position indication where the disc is mounted directly to Geneva wheel cam, and one for waveplate rotation indication where the disc is rigidly attached to the sun-gear hub which is pinned to motor shaft.

7.1.2 Polarizer (Analyzer)

The second essential element is polarization analysis is the linear polarizer or analyzer. The analyzer is, at present, a development item similar in principal to a three-piece prism described in the literature. The proposed

A mechanical concept for a polarization analysis device is shown. The Photometer's other features require no modifications to accept the assembly which fits on the bench rods between the entrance aperture assembly and the filter wheel assembly.

Figure 7.1-1 Waveplate Changer/Rotator and Polarizer Assembly

Photometer analyzer is a Rochon multiprism consisting of about twenty-five magnesium fluoride prisms optically contacted together. The clear aperture is about 11 x 11 mm and the thickness is about 4 mm. The extraordinary beams (two of them) are refracted some 6^{o} and are intercepted by the filter wheels or by an internal bulkhead which also serves as a baffle. The optical thickness of the multiprism is on the order of 1.1 mm. The polarization analysis system altogether has an optical thickness of about 1.25 mm. The shift in the apparent aperture position due to the polarization system is of such slight consequence (2.3 mm) that an additional lens is not required to correct the focal length of the system for the polarizer thickness.

The polarizer assembly is mechanically part of the waveplate assembly as shown in Figure 7.1-11. The multiprism assembly is hard mounted in an aluminum housing which is pivoted in and out of the light path by a 45^{o} permanent magnet stepper motor with magnetic detents. The housing surface slides in close contact to the forward mounting plate of the waveplate assembly. Positive mechanical stops are provided at the extreme limits of housing travel, which in conjunction with plunger type microswitches sense the open or closed condition.

A single point failure override device is used on the polarizer pivoting arms The device is essentially the same as the device used on the contamination door discussed in Section 3.4.2. The failure override acts only one time and permanently removes the polarizer from the light path in the event that the primary mechanism should fail.

7.2 Principle of the Analysis Technique

Sometimes the state of polarization of light from an astronomical body is known because the physics of the emission process is known. Usually, however, we want to measure the state of polarization to deduce information about the physical nature of the source.

The state of polarization of light is always described completely by four numbers called Stokes parameters. The function of polarimetry is to measure the Stokes parameters. Certain particular values of the Stokes parameters are associated with linear, circular, elliptical and unpolarized light..

There are many ways to measure the Stokes parameters but we will be concerned with one technique that exhibits simplicity and relative freedom from the disturbing effects known to experimenters. In this section we derive the expressions which show how the Stokes parameters may be derived from observations.

Our polarimeter consists of two optical elements: a waveplate and a linear polarizer. Actually several waveplates are used to cover the wide spectral range of the instrument. The waveplates rotate in 22.5° steps while the linear polarizer is fixed. The light coming from the linear polarizer is always linearly polarized but its radiance depends on the state of polarization of the source light and on the angular orientation of the waveplate. The relationship between the observed irradiance and the waveplate angle yields the Stokes parameters after some fairly simple mathematical manipulation.

We will compute how input linearly polarized light is transmitted by our system of waveplate and linear polarizer. First let the input be linearly polarized along the y-axis as shown in Figure 7.2-1. The input light vector is denoted as L.

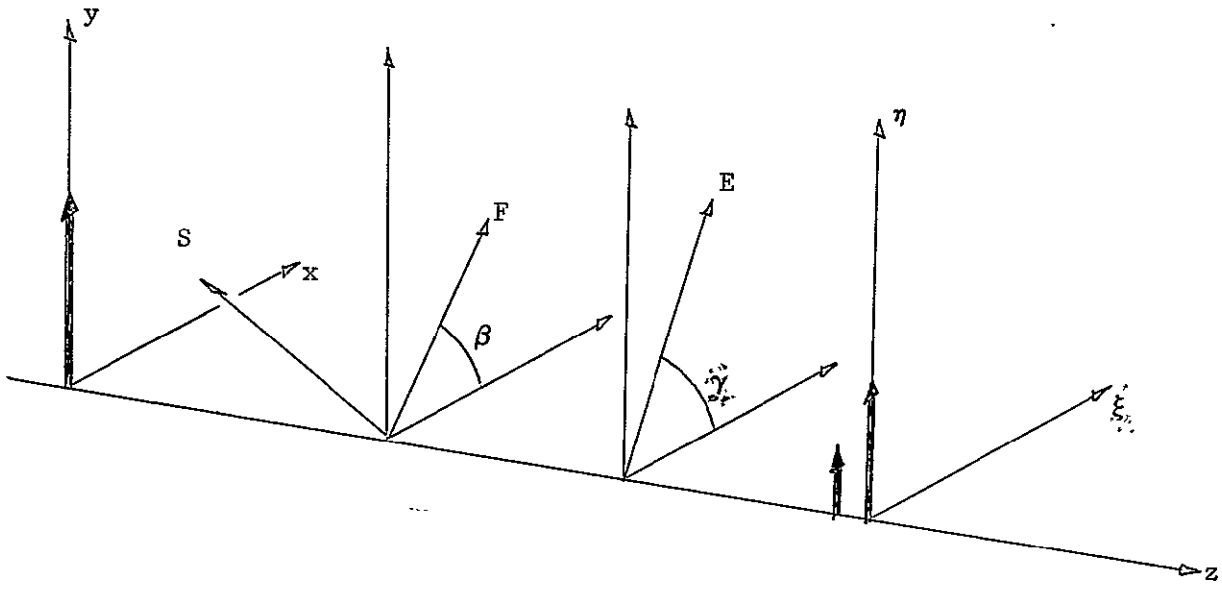

Figure 7.2-1 Orientations of Waveplate Fast (F) Axis and Polarizer Transmission (E) Axis

The waveplate is denoted by its fast axis F at an angle β with the x-axis Light vector components polarized along the fast axis are transmitted without alteration. Light vector components polarized perpendicular to the fast axis (i.e. parallel to the slow axis)suffer a phase retardation by an amount characteristic of the waveplate. So-called quarter wave plates cause a retardation of a quarter of a wavelength or in effect add a quarter wavelength of optical path length to the light vector component along the slow axis.

The light exitting the waveplate can be represented as L $\sin\beta$ exp $i\ell$ along the fast axis and as L $\cos\beta$ exp $i(\ell+\epsilon)$ along the slow axis. ϵ is the retardation divided by two pi. A quarter waveplate would have an ϵ of $\pi/2$. The light is now elliptically polarized. ℓ is the number of wavelengths from the input to the waveplate. It is actual value is of no importance.

The light next encounters a linear polarizer whose transmission is unity along axis E and zero perpendicular to that axis. The fast and slow components from the waveplate are decomposed into components parallel to and perpendicular to the polarizer E axis. Only the parallel component of each is transmitted.

The light exitting from the linear polarizer is then L $\sin\beta\cos(\gamma-\beta)$ exp $[i(\ell+\epsilon)]$ and L $\cos\beta\sin(\beta-\gamma)$ exp $[i(\ell'+\epsilon)]$. ℓ' is the number of wavelengths from the input to the polarizer. The output from the polarizer can be further analyzed into components along ξ and η axes which are parallel to the input x and y axes respectively. The output is then

$$\text{L out}_\xi = \text{L exp}(i\ell')\,(\sin\beta\cos(\gamma-\beta) + \cos\beta\cos(\beta-\gamma)\exp(i\varepsilon))\cos\gamma$$

$$\text{L out}_\eta = \text{L exp}(i\ell')\,(\sin\beta\cos(\gamma-\beta) + \cos\beta\cos(\beta-\gamma)\exp(i\varepsilon))\sin\gamma$$

An input of linearly polarized light of amplitude M along the x-axis can be propagated through the same system of waveplate and polarizer. The results are analogous

$$\text{M out}_\xi = \text{M exp}(i\ell')\,(\cos\beta\cos(\gamma-\beta) + \sin\beta\sin(\beta-\gamma)\exp(i\varepsilon))\cos\gamma$$

$$\text{M out}_\eta = \text{M exp}(i\ell')\,(\cos\beta\cos(\gamma-\beta) + \sin\beta\sin(\beta-\gamma)\exp(i\varepsilon))\sin\gamma$$

A set of transfer functions from input to output can be defined as

$$T_{\xi x} = \text{M out}_\xi/\text{M} = (\cos\beta\cos(\gamma-\beta) + \sin\beta\sin(\beta-\gamma)\exp(i\varepsilon))\cos\gamma\exp(i\epsilon\ell')$$

$$T_{\xi y} = \text{L out}_\xi\text{S/L} = (\sin\beta\cos(\gamma-\beta) + \cos\beta\cos(\beta-\gamma)\exp(i\varepsilon))\cos\gamma\exp(i\epsilon\ell')$$

$$T_{\eta x} = \text{M out}_\eta/\text{M} = (\cos\beta\cos(\gamma-\beta) + \sin\beta\sin(\beta-\gamma)\exp(i\varepsilon))\sin\gamma\exp(i\varepsilon\ell')$$

$$T_{\eta y} = \text{L out}_\eta/\text{L} = (\sin\beta\cos(\gamma-\beta) + \cos\beta\cos(\beta-\gamma)\exp(i\varepsilon))\sin\gamma\exp(i\varepsilon\ell')$$

It can be shown (see J M Stone, Radiation and Optics McGraw-Hill New York 1963) that the irradiance at the output of the polarimetry system H is given by

$$H = \tfrac{1}{2}(|T_{\xi x}|^2 + |T_{\eta x}|^2)\ (I + Q)$$
$$+\tfrac{1}{2}(|T_{\xi y}|^2 + |T_{\eta y}|^2)\ (I - Q)$$
$$+ \mathrm{Re}\ (T_{\xi x} T_{\xi y}^* + T_{\eta x} T_{\eta y}^*)\ (U + iV)$$

where the stars indicate complex conjugates and Re [ ] indicates real part. I, Q, U, and V are the Stokes parameters of the incoming light. We can substitute our expressions for the transfer functions T as follows

$$|T_{\xi x}|^2 = T_{\xi x} T_{\xi x}^*$$
$$= (\cos^2\beta \cos^2(\gamma-\beta) + \cos\beta\cos(\beta-\gamma)\sin\beta\sin(\beta-\gamma)\exp(i\varepsilon)$$
$$+ \sin^2\beta \sin^2(\gamma-\beta) + \cos\beta\cos(\beta-\gamma)\sin\beta\sin(\beta-\gamma)\exp(-i\varepsilon))\cos^2\gamma$$
$$|T_{\xi x}|^2 = (\cos^2\beta\cos^2(\gamma-\beta) + \sin^2\beta\sin^2(\beta-\gamma) + \tfrac{2}{4}\sin\beta\sin 2(\gamma-\beta)\cos\varepsilon)\cos^2\gamma$$

Similarily

$$|T_{\eta x}|^2 = (\cos^2\beta\cos^2(\gamma-\beta) + \sin^2\beta\sin^2(\beta-\gamma) + \frac{1}{2}\sin^2\beta\sin^2(\gamma-\beta)\cos\varepsilon)\sin^2\gamma$$

and

$$|T_{\xi y}|^2 = (\sin^2\beta\cos^2(\gamma-\beta) + \cos^2\beta\sin^2(\beta-\gamma) + \frac{1}{2}\sin^2\beta\sin^2(\gamma-\beta)\cos\varepsilon)\cos^2\gamma$$

and

$$|T_{\eta y}|^2 = (\sin^2\beta\cos^2(\gamma-\beta) + \cos^2\beta\sin^2(\beta-\gamma) + \frac{1}{2}\sin^2\beta\sin^2(\gamma-\beta)\cos\varepsilon)\sin^2\gamma$$

$$T_{\xi x} T_{\xi y}^* = (\cos\beta\sin\beta\cos^2(\gamma-\beta) + \sin^2\beta\sin(\beta-\gamma)\cos(\gamma-\beta)\exp(i\varepsilon)$$
$$+ \sin\beta\cos\beta\sin^2(\beta-\gamma) + \cos^2\beta\cos(\gamma-\beta)\sin(\beta-\gamma)\exp(-i\varepsilon))\cos^2\gamma$$
$$T_{\xi x} T_{\xi y}^* = (\tfrac{1}{2}\sin 2\beta + \tfrac{1}{2}\sin 2(\beta-\gamma)(\sin^2\beta\exp(i\varepsilon) + \cos^2\beta\exp(-i\varepsilon)))\cos^2\gamma$$

and

$$T_{\eta x} T_{\eta y}^* = (\tfrac{1}{2}\sin 2\beta + \tfrac{1}{2}\sin 2(\beta-\gamma)(\sin^2\beta\exp(i\varepsilon) + \cos^2\beta\exp(-i\varepsilon)))\sin^2\gamma$$

so that

$$T_{\xi x} T_{\xi y}^* + T_{\eta x} T_{\eta y}^* = \tfrac{1}{2}\sin 2\beta + \tfrac{1}{2}\sin 2(\beta-\gamma)(\sin^2\beta\exp(i\varepsilon) + \cos^2\beta\exp(-i\varepsilon)).$$

The orientation of the linear polarizer is actually arbitrary so that we can set the angle γ to zero without loss of generality and then have

$$|T_{\xi x}|^2 + |T_{\eta x}|^2 = \cos^2\beta\cos^2\beta + \sin^2\beta\sin^2\beta + \tfrac{1}{2}\sin 2\beta\sin 2\beta\cos\varepsilon$$

and likewise

$$|T_{\xi y}|^2 + |T_{\eta y}|^2 = \sin^2\beta \cos^2\beta + \cos^2\beta \sin^2\beta + \tfrac{1}{2}\sin 2\beta \sin 2\beta \cos\epsilon$$

and

$$T_{\xi x} T_{\xi y}^* + T_{\eta x} T_{\eta y}^* = \tfrac{1}{2}\sin 2\beta \tfrac{1}{2}\sin 2\beta (\sin^2\beta \exp(i\epsilon) + \cos^2\beta \exp(-i\epsilon))$$

Now we can substitute into the expression for output irradiance H to get

$$H = (\cos^2\beta \cos^2\beta + \sin^2\beta \sin^2\beta + \tfrac{1}{2}\sin^2 2\beta \cos\epsilon)(I + Q)$$
$$+ (\cos^2\beta \sin^2\beta + \cos^2\beta \sin^2\beta + \tfrac{1}{2}\sin^2 2\beta \cos\epsilon)(I - Q)$$
$$+ \mathrm{Re}\left[\tfrac{1}{2}\sin 2\beta (1 + \sin^2\beta \exp(i\epsilon) + \cos^2 \exp(-i\epsilon))(U + iV)\right]$$

$$H = (\cos^2\beta \cos^2\beta + \sin^2\beta \sin^2\beta + \tfrac{1}{2}\sin^2 2\beta \cos\epsilon$$
$$+ \cos^2\beta \sin^2\beta + \cos^2\beta \sin^2\beta + \tfrac{1}{2}\sin^2 2\beta \cos\epsilon) I$$
$$+ (\cos^2\beta \cos^2\beta + \sin^2\beta \sin^2\beta + \tfrac{1}{2}\sin^2 2\beta \cos\epsilon$$
$$- \cos^2\beta \sin^2\beta - \cos^2\beta \sin^2\beta = \tfrac{1}{2}\sin^2 2\beta \cos\varepsilon) Q$$
$$+ \mathrm{Re}\left[\tfrac{1}{2}\sin 2\beta (1 + \sin^2\beta (\cos\varepsilon + i \sin\varepsilon) + \cos^2\beta (\cos\varepsilon - i \sin\varepsilon))(U + iV)\right]$$

$$H = (\cos^2\beta + \sin^2\beta + \sin^2 2\beta \cos\varepsilon)$$
$$+ (\cos^2\beta (\cos^2\beta - \sin^2\beta) + \sin^2\beta (\sin^2\beta - \cos^2\beta)) Q$$
$$+ \mathrm{Re}\left[\tfrac{1}{2}\sin 2\beta (1 + \cos\varepsilon + i \sin\varepsilon (\sin^2\beta - \cos^2\beta))(U + iV)\right]$$

$$H = (1 + \sin^2 2\beta \cos\varepsilon) I$$
$$+ (\cos^2 2\beta) Q$$
$$+ \mathrm{Re}\left[\tfrac{1}{2}\sin 2\beta (1 + \cos\varepsilon - i \sin\varepsilon \cos 2\beta)(U + iV)\right]$$

$$H = (1 + \sin^2 2\beta \cos\epsilon)\, I + (\cos^2 2\beta)\, Q + \tfrac{1}{2} \sin 2\beta (1 + \cos\epsilon)\, U + (\tfrac{1}{2} \sin 2\beta \cos 2\beta \sin\epsilon)\, V$$

$$H = (1 + \sin^2 2\beta \cos\epsilon)\, I + (\cos^2 2\beta)\, Q + \tfrac{1}{2} \sin 2\beta (1 + \cos\epsilon)\, U + (\tfrac{1}{4} \sin 4\beta \sin\epsilon)\, V$$

Now we note that

$$\sin^2 x = \tfrac{1}{2} (1 - \cos 2x)$$

$$\cos^2 x = \tfrac{1}{2} (1 + \cos 2x)$$

So that

$$H = (1 + \tfrac{1}{2} (1 - \cos 4\beta) \cos\epsilon)\, I + \tfrac{1}{2}(1 + \cos 4\beta)\, Q + \tfrac{1}{2} \sin 2\beta (1 + \cos\epsilon)\, U + (\tfrac{1}{4} \sin 4\beta \sin\epsilon)\, V$$

The waveplate is rotated in increments of 22.5° ($\pi/8$ radians) so we can tabulate how H varies as a function of

	H			
0	$I + Q$	$+ Q$	$+ 0$	$+ 0$
$\pi/8$	$(1 + \frac{1}{2} \cos\epsilon)\, I$	$+ \frac{1}{2} Q$	$+ \frac{1}{2}\sqrt{\frac{1}{2}} (1 + \cos\epsilon)\, U$	$+ \frac{1}{2} \sin\epsilon\, V$
$\pi/4$	$(1 + \cos\epsilon)\, I$	$+ 0$	$+ \frac{1}{2} (1 + \cos\epsilon)\, U$	$+ 0$
$3\pi/8$	$(1 + \frac{1}{2} \cos\epsilon)\, I$	$+ \frac{1}{2} Q$	$+ \frac{1}{2}\sqrt{\frac{1}{2}} (1 + \cos\epsilon)\, U$	$- \frac{1}{4} \sin\epsilon\, V$
$\pi/2$	I	$+ Q$	$+ 0$	$+ 0$
$5\pi/8$	$(1 + \frac{1}{2}\cos\epsilon)\, I$	$- \frac{1}{2} Q$	$+ -\frac{1}{2}\sqrt{\frac{1}{2}} (1 + \cos\epsilon)\, U$	$+ \frac{1}{4} \sin\epsilon\, V$
$3\pi/4$	$(1 + \cos\epsilon)\, I$	$+ 0$	$+ -\frac{1}{2} (1 + \cos\epsilon)\, U$	$+ 0$
$7\pi/8$	$(1 + \frac{1}{2} \cos\epsilon)\, I$	$+ \frac{1}{2} Q$	$+ -\frac{1}{2}\sqrt{\frac{1}{2}} (1 + \cos\epsilon)\, U$	$- \frac{1}{4} \sin\epsilon\, V$
π	I	$+ Q$	$+ 0$	$+ 0$

To show the above results graphically let us take Q, U, and V all equal to one. Because $I^2 = Q^2 + U^2 + V^2$, $I = \sqrt{3}$. Let us also take ϵ to be $\pi/2$ (corresponding to a quarter waveplate) so that $\cos\epsilon = 0$

Of course we would like to be able to take observations of output irradiance H of several waveplate orientations and then deduce the values of I, Q, U, and V separately. This can be done.

$$I = \frac{H]_{3\pi/8} + H]_{5\pi/8} - H]_{o}}{2(1 + \frac{1}{2}\cos\epsilon) - 1}$$

$$I = \frac{H]_{3\pi/8} + H]_{5\pi/8} - H]_{o}}{\cos\epsilon + 1}$$

$$Q = \frac{H]_{3\pi/8} + H]_{5\pi/8} - 2(1 + \frac{1}{2}\cos\epsilon)\, H]_{o}}{1 - 2(1 + \frac{1}{2}\cos\epsilon)}$$

$$Q = \frac{H]_{3\pi/8} + H]_{5\pi/8} - (2 + \cos\epsilon)\, H]_{o}}{-(\cos\epsilon + 1)}$$

$$U = \frac{H]_{\pi/4} - H]_{3\pi/4}}{\cos\epsilon + 1}$$

$$V = \frac{H]_{\pi/8} - H]_{3\pi/8}}{\frac{1}{2}\sin\epsilon}$$

Notice that ϵ can take any value except multiples of π (i.e. multiples of 90^{o}). In particular a half wave plate causes all the expressions above to be undefined.

By knowing the amount of retardation of the waveplate and thus the observed value of H at several waveplate angles the individual Stokes parameters can be deduced by simple additions and multiplifications.

It is interesting to note that rotation increments of the waveplate can be multiples of $\pi/6$ (30^{o}) rather than $\pi/8$ (22.5^{o}). If $\pi/6$ increments are chosen fewer steps are required and five of the six distinct resultant output irradiances readings are used as opposed to five of eight readings for the $\pi/8$ increments.

	H			
0	I +	Q +	0	+0
$\pi/6$	$(1+\frac{1}{4}\cos\epsilon)$I +	$\frac{1}{4}$ Q +	$\frac{\sqrt{3}}{2}(1+\cos\epsilon)$ U	$+\frac{\sqrt{3}}{4}\sin\epsilon$ V
$\pi/3$	$(1+\frac{1}{4}\cos\epsilon)$I +	$\frac{1}{4}$ Q +	$\frac{\sqrt{3}}{2}(1+\cos\epsilon)$ U	$-\frac{\sqrt{3}}{4}\sin\epsilon$ V
$\pi/2$	I +	Q +	0	+ 0
$2\pi/3$	$(1+\frac{1}{4}\cos\epsilon)$I +	$\frac{1}{4}$Q -	$\frac{\sqrt{3}}{2}(1+\cos\epsilon)$ U	$+\frac{\sqrt{3}}{4}\sin\epsilon$ V

$\pi/6$	$(1+\frac{1}{4}\cos\epsilon)\ I +$	$\frac{1}{4}\ Q -$	$\frac{\sqrt{3}}{2}(1+\cos\epsilon)\ U$	$-\frac{\sqrt{3}}{4}\sin\epsilon\ V$
π	$I +$	$Q +$	0	$+\ 0$

From which the Stokes parameters can be deduced after some manipulation as

$$I = \frac{2}{3+\cos\epsilon}\left(H\right]_{/6} + H\right]_{5\pi/6}) - \frac{1}{3+\cos\epsilon}\left(H\right]_{o})$$

$$Q = \frac{1}{3+\cos\epsilon}\left(H\right]_{\pi/6} + H\right]_{\pi/6}) - \frac{4+\cos\epsilon}{3+\cos\epsilon}\left(H\right]_{o})$$

$$U = \frac{1}{\frac{\sqrt{3}}{2}(1+\cos\epsilon)}\left(H\right]_{\pi/6} - H\right]_{2\pi/6} - H\right]_{2\pi/3})$$

$$V = \frac{1}{\frac{\sqrt{3}}{4}\sin\epsilon}\left(H\right]_{\pi/6} - H\right]_{\pi/3})$$

Notice that as before ϵ can take on any value except a multiple of π. A half wave plate would not allow either U or V to be determined.

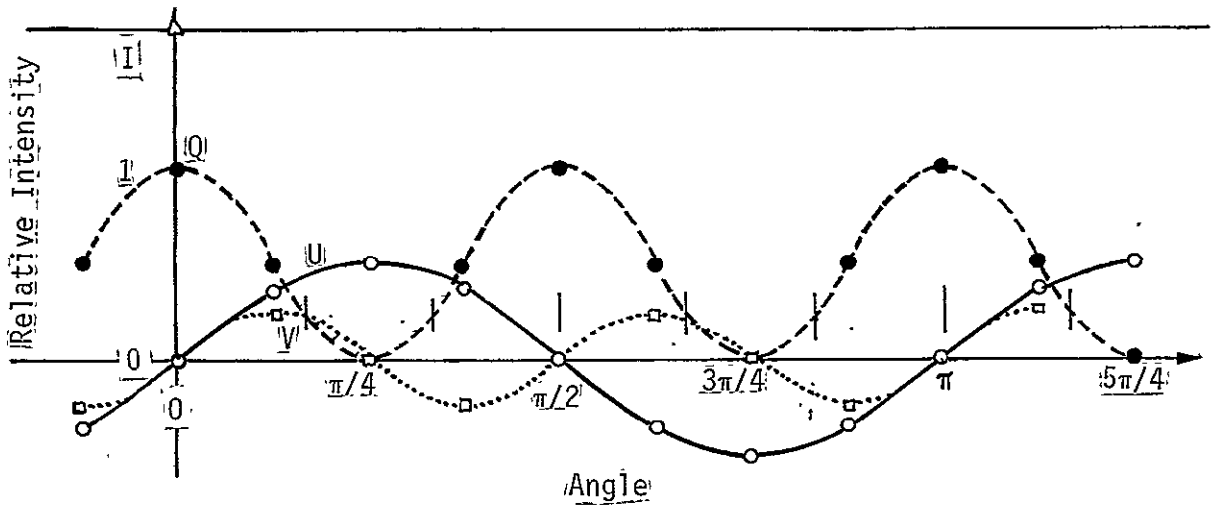

Figure 7.2-2 Stokes Parameter Variation with Waveplate Angle